AD-A058 426 IBM THOMAS J WATSON RESEARCH CENTER YORKTOWN HEIGHTS N Y F/G 20/12
ELECTRONIC STRUCTURE AND PROPERTIES OF THE OXIDES OF THE TETRAH--ETC(U)
JUL 78 S T PANTELIDES N00014-76-C-0934
UNCLASSIFIED NL

1 OF 2
ADA
058426

ELECTRONIC STRUCTURE AND PROPERTIES OF THE OXIDES OF THE TETRAHEDRAL SEMICONDUCTORS AND THEIR INTERFACES

Sokrates T. Pantelides

IBM Thomas J. Watson Research Center

P. O. Box 218, Yorktown Heights, New York 10598

July 31, 1978

Final Report for Period 1 June 1976 - 31 May 1978

Contract N00014-76-C-0934

Sponsored by Office of Naval Research

ELECTRONIC STRUCTURE AND PROPERTIES OF THE OXIDES OF THE TETRAHEDRAL SEMICONDUCTORS AND THEIR INTERFACES

Sokrates T. Pantelides

IBM Thomas J. Watson Research Center

P. O. Box 218, Yorktown Heights, New York 10598

July 31, 1978

Final Report for Period 1 June 1976 - 31 May 1978

Contract N00014-76-C-0934

Sponsored by Office of Naval Research

UNCLASSIFIED

SECURITY CLASSIFICATION OF THIS PAGE (When Data Entered)

REPORT DOCUMENTATION PAGE

READ INSTRUCTIONS BEFORE COMPLETING FORM

1. REPORT NUMBER	2. GOVT ACCESSION NO.
3. RECIPIENT'S CATALOG NUMBER (9)	
4. TITLE (and Subtitle) (6) ELECTRONIC STRUCTURE AND PROPERTIES OF THE OXIDES OF THE TETRAHEDRAL SEMICONDUCTORS AND THEIR INTERFACES.	5. TYPE OF REPORT & PERIOD COVERED Final Report, 1 June 1976-31 May 1978,
	6. PERFORMING ORG. REPORT NUMBER
7. AUTHOR(s) (10) Sokrates T. Pantelides	8. CONTRACT OR GRANT NUMBER(s) (15) N00014-76-C-0934
9. PERFORMING ORGANIZATION NAME AND ADDRESS IBM T. J. Watson Research Center P.O.Box 218 Yorktown Heights, NY 10598	10. PROGRAM ELEMENT, PROJECT, TASK AREA & WORK UNIT NUMBERS
11. CONTROLLING OFFICE NAME AND ADDRESS Office of Naval Research 800 N. Quincy Street Arlington, Virginia 22217 (11) 31	12. REPORT DATE Jul 1978
	13. NUMBER OF PAGES (12) 145p.
14. MONITORING AGENCY NAME & ADDRESS(if different from Controlling Office)	15. SECURITY CLASS. (of this report) UNCLASSIFIED
	15a. DECLASSIFICATION/DOWNGRADING SCHEDULE

16. DISTRIBUTION STATEMENT (of this Report)

Approved for public release;
distribution unlimited.

17. DISTRIBUTION STATEMENT (of the abstract entered in Block 20, if different from Report)

18. SUPPLEMENTARY NOTES

19. KEY WORDS (Continue on reverse side if necessary and identify by block number)

SiO_2; GeO_2; $GaAsO_4$; Si-SiO_2 interface; MOS;
Si-SiO_2 traps and electronic structure.

20. ABSTRACT (Continue on reverse side if necessary and identify by block number)

We have developed a simple but general model is developed in terms of which the electronic structure and spectra of SiO_2, GeO_2 and the ABO_4-type oxides are studied in a systematic way. Methods have also been developed in terms of which ~~we calculate~~ are calculated the energy levels of impurities in bulk SiO_2 and at the Si-SiO_2 interface, and the electronic structure of free surfaces and interfaces between crystalline materials. The main objectives of the work reported here →

DD FORM 1 JAN 73 1473 EDITION OF 1 NOV 65 IS OBSOLETE

349250

UNCLASSIFIED

SECURITY CLASSIFICATION OF THIS PAGE (When Data Entered)

20. ABSTRACT (continued)

were to obtain a theoretical description of the electronic structure and properties of the oxides of the tetrahedral semiconductors (in particular, SiO_2, GeO_2, and the ABO_4-type oxides, where AB is a tetrahedral semiconductor) and their interfaces with other materials and vacuum. The results of the work are summarized below. Details are contained in Appendices A-J.

ELECTRONIC STRUCTURE AND PROPERTIES OF THE OXIDES OF THE TETRAHEDRAL SEMICONDUCTORS AND THEIR INTERFACES

FINAL REPORT

by

Sokrates T. Pantelides

Principal Investigator for Contract No. N00014-76-C-0934

ABSTRACT

We have developed a simple but general model in terms of which the electronic structure and spectra of SiO_2, GeO_2 and the ABO_4-type oxides are studied in a systematic way. Methods have also been developed in terms of which we calculate the energy levels of impurities in bulk SiO_2 and at the Si-SiO_2 interface, and the electronic structure of free surfaces and interfaces between crystalline materials. The main objectives of the work reported here were to obtain a theoretical description of the electronic structure and properties of the oxides of the tetrahedral semiconductors (in particular, SiO_2, GeO_2, and the ABO_4-type oxides, where AB is a tetrahedral semiconductor) and their interfaces with other materials and vacuum. The results of the work are summarized below. Details are contained in Appendices A-J.

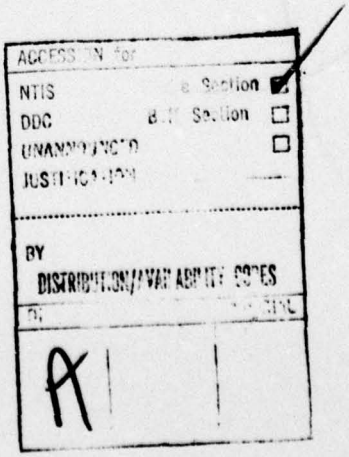

1. BULK ELECTRONIC PROPERTIES

We have developed a simple tight-binding model, based on ideas previously developed and tested for the simple tetrahedral semiconductors,[1-3] in terms of which three distinct kinds of properties were studied: (a) Average Properties: These are properties which correspond to an average over all the one-electron states. Examples are effective charges on atoms, dielectric constants, cohesive energies, etc. (b) Dispersive Properties: These are properties which depend on the details of the distribution of one-electron states. Examples are energy bands, densities of states, photoemission spectra, X-ray emission spectra, etc. (c) Local Properties, such as impurity and defect levels and excitons.

The main achievements of our work using this model are the following: The first sets of energy bands for SiO_2, GeO_2 and the ABO_4-type oxides were obtained (Ref. 3 and Appendix A). The photoemission spectrum and the X-ray emission spectra of SiO_2 were calculated explicitly for the first time and compared with experiment, as opposed to previous work which arrived at *interpretations* of the spectra in terms of electronic transitions (Appendix A). The photoemission spectra of $Si_xGe_{1-x}O_2$ alloys were also calculated and found to agree well with experimental data (Appendix B). Two different complementary model calculations of the optical absorption spectrum of SiO_2 were carried out which established that the observed peaks are excitonic in nature (Appendix C). Finally, by calculating the dielectric constant of SiO_2 explicitly as a function of the Si-O-Si angle, it was possible to deduce information about the structure of various polymorphs (Appendices A and D).

2. IMPURITIES IN BULK SiO_2

The above model for the bulk properties of SiO_2 has been extended to provide a description for substitutional impurities in the bulk material. In particular, we have studied P and As at an O site and predicted their energy levels in the band gap. By using these results we were able to interpret experimental data on ion-implanted SiO_2 and identify the observed centers as substitutional P and As at O sites (Appendix E).

3. THE STOICHIOMETRY OF THE Si-SiO_2 INTERFACE

A large number of experiments have been carried out which have attempted to determine whether there exists an SiO_x ($0 < x < 2$) layer at the Si-SiO_2 interface, and, if so, determine its width. In our study (Appendix F), we pointed out that the definition of a width is not unique and suggested several possibilities that would give different numbers. We also constructed continuous-random-network (CRN) models for the (100) interface and obtained the following: (a) It is possible to construct models with a totally abrupt interface which have distortions that are visually comparable to distortions present in models with a finite SiO_x layer. (b) A simple force model was used to perform computer calculations which showed that the net strain energy was reduced as the finite SiO_x layer was gradually reduced in width, suggesting that an abrupt interface may in fact be preferred. (See Appendix F for details.)

4. SURFACES AND INTERFACES

In this work the main goal was to develop efficient methods to calculate the electronic structure of surfaces and interfaces. At this stage, the work was restricted to crystalline materials for which two-dimensional periodicity could be exploited. We made use of the Koster-Slater[4] idea for localized perturbations which was first introduced for point defects[4] and was later extended to surfaces by Koutecky[5] and others. The advantage of the method is that it builds in the properties of the perfect bulk crystal from the start and then directly calculates changes in the electronic structure produced by the perturbation. In contrast, alternative methods, such as cluster and slab methods,[6] rely on a finite number of atoms or layers of atoms to give an adequate description of both bulk properties (e.g., bandwidths, bandgaps) and localized states. In the case of surfaces, we made use of empirical tight-binding Hamiltonians and introduced a novel way to define the perturbation that creates free surfaces. Instead of "cutting bonds" to divide an infinite solid into two decoupled semi-infinite solids, we "remove" layers of atoms by setting their on-site Hamiltonian matrix elements to infinity, a procedure first used to describe a single vacancy.[7]. This choice of perturbation makes the

calculations straightforward and fast. Calculations have been carried out for test purposes and for cubic SiO_2. The details of the method and the results are discussed in Appendix G.

We also extended the Koster-Slater approach to describe interfaces between crystalline materials by assuming the unperturbed system to consist of two noninteracting infinite solids and then constructing an appropriate perturbation matrix. Calculations so far have only been done on the Ge-GaAs and Ge-ZnSe systems for which other theoretical work is also available. The method and results are discussed in Appendix H.

The perturbation matrices for free surfaces and for interfaces may be combined so that calculations can be performed for monolayers or multiple layers of a given material on a crystalline substrate. This technique is therefore capable of providing information about gradual oxidation of materials.

5. IMPURITIES AT INTERFACES

Theoretical work has been done in two different areas:

(a) It has been observed[8] that some of the traps introduced into SiO_2 near a Si interface by ionizing radiation and by electron-beam irradiation (procedures used in the fabrication of some devices) do not anneal out. There are two types of such traps, one with a cross section of about 10^{-17} cm^2, and the other with a cross section of about 10^{-15} cm^2. The latter was not produced in samples irradiated at intensities below 200 W/cm^2 at any temperature. The rate of production of the former was suppressed by lowering the irradiation temperature down to 90K. These data have been explained in terms of two different processes, namely the formation of point-defect bound complexes by recombination-enhanced diffusion and by dislocation migration. Details are given in Appendix I.

(b) We have developed a method to calculate binding energies of shallow impurities at or near the Si-SiO_2 interface. The method is based on effective-mass theory, which is adapted for the cylindrical symmetry of the interface problem. Results and comparison with experimental data are contained in Appendix J.

REFERENCES

1. W. A. Harrison, Phys. Rev. B **8**, 4487 (1973); W. A. Harrison and S. Ciraci, Phys. Rev. B **10**, 1516 (1974).

2. S. T. Pantelides and W. A. Harrison, Phys. Rev. B **11**, 3006 (1975); *ibid.*, 4049 (1975).

3. S. T. Pantelides and W. A. Harrison, Phys. Rev. B **13**, 2667 (1976).

4. G. F. Koster and J. C. Slater, Phys. Rev. **95**, 467 (1954).

5. J. Koutecky, Adv. in Chem. Phys. **9**, 85 (1965).

6. K. C. Pandey and J. C. Phillips, Phys. Rev. Lett. **32**, 1433 (1974); M. Schlüter, J. R. Chelikowsky, S. G. Louie and M. L. Cohen, Phys. Rev. B **12**, 4200 (1975).

7. J. Bernholc and S. T. Pantelides, Phys. Rev. B. (August 15, 1978).

8. J. M. Aitken and D. R. Young, J. Appl. Phys. **47**, 1196 (1976).

LIST OF APPENDICES

Appendix A — "Some Properties of the Oxides of the Tetrahedral Semiconductors and the Oxide-semiconductor Interfaces", by S. T. Pantelides, J. Vac. Sci. Technol. **14**, 965 (1977).

Appendix B — "The Electronic Structure of SiO_2, GeO_2 and Intermediate $Si_xGe_{1-x}O_2$ Compositions: Experiment and Theory", by S. T. Pantelides, B. Fischer, R. A. Pollak, and T. H. DiStefano, Solid State Comm. **21**, 1003 (1977).

Appendix C — "The Optical Absorption Spectrum of SiO_2", by S. T. Pantelides, RC 7119 (1978); International Topical Conf. on the Physics of SiO_2, Yorktown Heights, N.Y., March 22-24, 1978, to be published in Proceedings (Pergamon Press, Elmsford, N.Y., 1978).

Appendix D — "Recent Advances in the Theory of Electronic Structure of SiO_2", by S. T. Pantelides, Comments Solid State Phys. **8**, 55 (1977).

Appendix E — "Photodepopulation of Electrons Trapped in SiO_2 on Sites Related to As and P Implantation", by R. F. DeKeersmaecker, D. J. DiMaria, and S. T. Pantelides, *RC 7102 (1978)*.

Appendix F — "Continuous-Random-Network Models for the Si-SiO_2 Interface", by S. T. Pantelides and M. Long, RC 7161 (1978).

Appendix G — "Scattering-Theoretic Approach to the Electronic Structure of Semiconductor Surfaces - The (100) Surface of Tetrahedral Semiconductors and SiO_2", by J. Pollman and S. T. Pantelides, RC 7163 (1978).

Appendix H — "New Method for the Electronic Structure of Heterojunctions - Application to the (100) Ge-GaAs Interfaces", by S. T. Pantelides and J. Pollmann, RC 7200 (1978).

Appendix I — "Temperature and Intensity Dependence of Rate of Introduction of Neutral Traps in SiO_2 by e-Beam Irradiation", by J. A. Van Vechten, C. M. Serrano, and J. M. Aitken, ECS Spring Meeting, Seattle, Wash., Electrochemical Society Extended Abstracts, Vol. 78-1, p. 331 (1978).

Appendix J — "Electronic States of Impurities Located at or near Semiconductor-Insulator Interfaces", by N. O. Lipari, J. Vac. Sci. Tech., in press (Aug. 1978).

Some properties of the oxides of the tetrahedral semiconductors and the oxide–semiconductor interfaces[a)]

Sokrates T. Pantelides

IBM Thomas J. Watson Research Center, Yorktown Heights, New York 10598

(Received 10 February 1977; accepted 4 April 1977)

Continuous-random-network models have been constructed for the Si–SiO_2 interface. It is found that an abrupt interface with no SiO_x layer is posible. A simple tight-binding model is described that is applicable for the calculation of the electronic properties of the bulk oxides and the oxide–semiconductor interfaces. Results are given only for selected bulk properties, namely the photoemission and x-ray emission spectra, and the dielectric constants of SiO_2, GeO_2, and various ABO_4-type oxides.

PACS numbers: 71.45.Nt, 79.60.Eq, 73.40.Qv, 71.20.+c

I. INTRODUCTION

In order to develop a theory for the electronic properties of a given material, it is essential that the stoichiometry and the atomic arrangement be known. In this paper, a step is taken toward understanding the stoichiometry, atomic arrangement, and electronic properties of the native oxides of the tetrahedral semiconductors and the oxide–semiconductor interfaces.

II. STOICHIOMETRY AND ATOMIC ARRANGEMENT OF INTERFACES

The native oxide of silicon, SiO_2, exists in a variety of crystalline forms (quartz, tridymite, etc.[1]), but the films grown thermally on Si for the manufacture of devices are amorphous. As for the Si–SiO_2 interface, the situation is complicated even more by the question whether an SiO_x layer, with $x \neq 2$, exists between Si and SiO_2. Answers to this question have been sought by various experimental techniques,[2–6] but evidence thus far is inconclusive. Estimates of the width of the SiO_x layer include values of essentially zero[2] (abrupt interface), about 4 Å (Ref. 3), 12–15 Å (Ref. 4), and even more.[5,6] In an attempt to obtain some insight into this question, a number of continuous-random-network (CRN) models have been built. Details of the construction will be given elsewhere.[7] The main idea, however, was to start with a crystalline Si substrate, expose a well-defined surface, and then attempt to build up an amorphous oxide layer bond by bond.[8] Clearly, an SiO_x-type interface layer of arbitrary width can be built before full SiO_2 coordination is reached, and therefore the aim was to strive for a *minimum interface width*. The first models that were built indicated that a finite minimum width existed, but finally a model was constructed with zero interface width (abrupt interface). No dangling bonds were allowed and the local distortions are comparable to those present in bulk amorphous CRN models. This model is shown in Fig. 1.

The construction of the model indicates that an atomically sharp interface may in fact be energetically possible, but does not rule out the possibility that some real interfaces have an SiO_x layer of finite width, which may be a function of the growth conditions. An attempt is now under way to quantify the amount of local distortions in the various models in order to extract preferred configurations. Work is also in progress to calculate the electronic properties of the Si–SiO_2 interface, assuming the atomic arrangements of these models. The na-

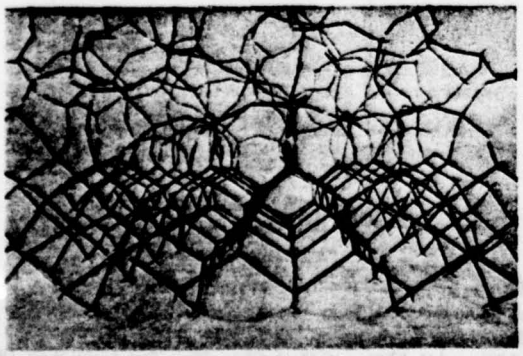

FIG. 1. Photograph of the CRN model described in the text.

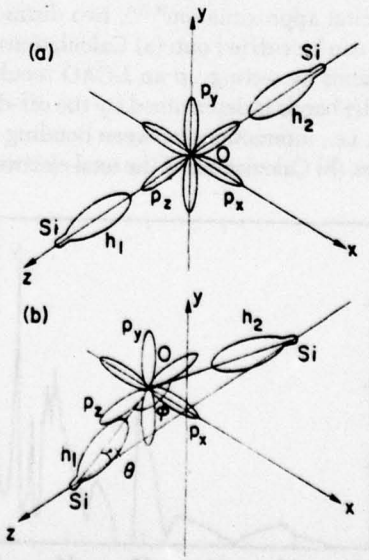

FIG. 2. The basis orbitals for the model described in the text. (a) orbitals used in the ideal cubic (β-cristobalite) structure; (b) orbitals used for the more general case. The Si–O–Si angle is 144°.

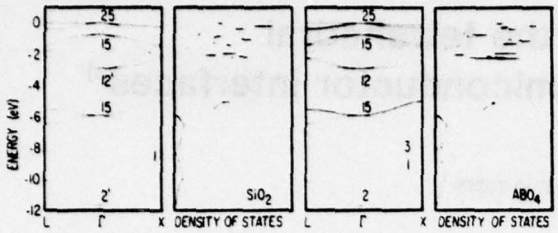

FIG. 3. The valence energy bands and DOS of cubic SiO_2 and typical ABO_4-type oxide.

ture of interface states may suggest preferred configurations. The basic aspects of the model used in this calculations and results on bulk properties are described in the next section.

It should be noted that the CRN models described above apply to the compound semiconductors as well, assuming that the native oxide is of the ABO_4 type. Other possibilities, of course, exist. For example, any of three oxides may be formed on GaAs, namely Ga_2O_3, Al_2O_5, and $GaAsO_4$.

III. BULK ELECTRONIC PROPERTIES

SiO_2 and GeO_2 are special cases of the general ABO_4-type oxide, where AB is a tetrahedral semiconductor, with A = Si and A = B = Ge, respectively. The properties of all these materials can therefore be described in a systematic manner. A simple parametrized tight-binding model has previously[9] been introduced for SiO_2 and GeO_2 and has now been extended to treat the ABO_4-type oxides. The model is similar to that used for the tetrahedral semiconductors.[10] In this paper, the model will be discussed briefly and a few new applications will be given.

Central to the understanding of the model is the concept of a *bonding unit*. In the case of the tetrahedral semiconductors, one constructs the familiar sp^3 hybrids on each atom. A bonding unit is then defined to consist of two hybrids, h_A and h_B, on nearest neighbors, directed toward each other. One then constructs bonding and antibonding orbitals in each bonding unit. By focusing on the bonding orbitals alone (bond-orbital approximation[9,10]), two distinct kinds of calculations can be carried out: (a) Calculations of the valence energy bands by setting up an LCAO secular matrix. The form of the bands is determined by the off-diagonal matrix elements, i.e., interactions between bonding orbitals on different sites. (b) Calculations of the total electronic energy both

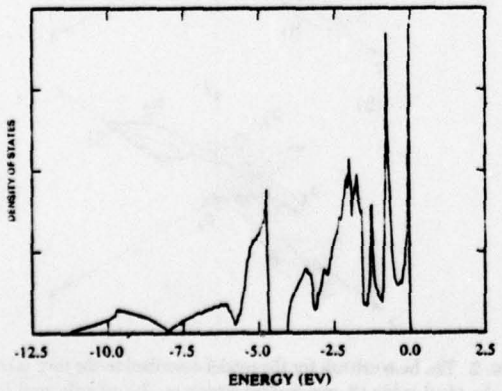

FIG. 4. The DOS for the simulated amorphous SiO_2. See text.

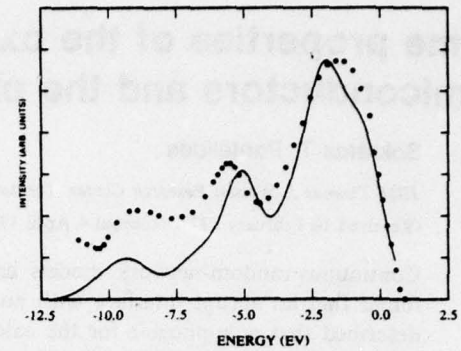

FIG. 5. The UPS spectrum of SiO_2 (dotted curve) compared with the broadened DOS (solid curve). The experimental curve is from B. Fischer, R. A. Pollak, T. H. DiStefano, and W. D. Grobman, Phys. Rev. B 15, 3193 (1977).

in the absence and presence of external perturbations and thus of explicit analytical expressions for response functions. For this kind of calculation, one needs only the diagonal matrix elements and no matrix diagonalization or Brillouin zone sums are necessary.

The bonding unit in an ABO_4-type oxide is an sp^3 hybrid on an A atom, and sp^3 hybrid on a B atom and oxygen orbitals on the oxygen atom in between. For valence-band and total-energy studies the oxygen 2*p* orbitals are adequate. The important point is that an A–O or B–O bond is not a well-defined entity and one must construct A–O–B bonding orbitals, which will be referred to as *extended bonding orbitals* (*EBO's*).

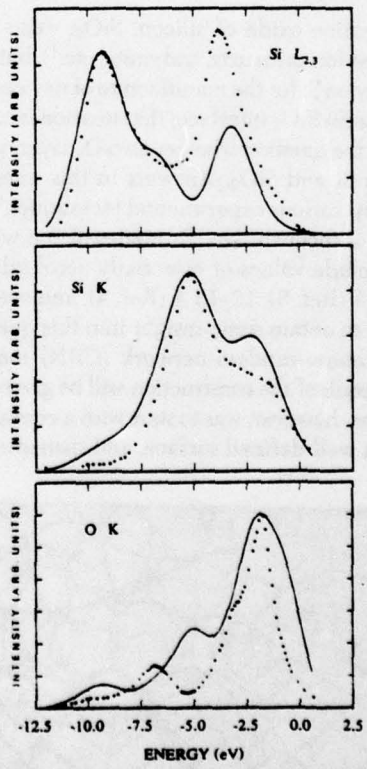

FIG. 6. Theoretical (solid curves) and experimental (dotted curves) x-ray emission spectra of SiO_2. The experimental curves are from G. Wiech, in *Soft-X-Ray Band Spectra*, edited by D. J. Fabian (Academic, New York, 1968), and G. Klein and H. U. Chun, Phys. Stat. Solidi B 49, 167 (1972).

TABLE I. Theoretical and experimental values for the electronic (high-frequency) dielectric constants of SiO_2, GeO_2, and various ABO_4-type oxides.

Material	A–O–B angle (°)	ϵ(th.)	ϵ(exp[a])
SiO_2 (α-quartz)	144[b]	2.4	2.4
SiO_2 (β-quartz)	144[b]	2.3	2.3
SiO_2 (α-cristobalite)	144[b]	2.3	2.2
SiO_2 (β-cristobalite)	180[b]	2.7	2.2
SiO_2 (β-cristobalite)	144[c]	2.2	2.2
SiO_2 (coesite)	120[b]	2.0	2.6
SiO_2 (coesite)	144[c]	2.6	2.6
SiO_2 (vitreous)	144[d]	2.1	2.1
GeO_2 (quartzlike)	130[b]	2.9	2.9
BPO_4	135[b]	2.0	2.6
$BAsO_4$	125[b]	2.3	2.8
$AlPO_4$	145[b]	2.4	2.3
$AlAsO_4$	146[b]	2.9	...
$GaPO_4$	135[b]	2.6	...

[a] Landolt-Börnstein, *Zahlenwerte und Funktionen* (Springer, Berlin, 1962), Vol. 2, pt. 8.
[b] Reference 1.
[c] See text.
[d] Assumed.

The internal structure of the EBO's is rather intriguing. Let h_A and h_B denote the hybrids in a bonding unit and p_x, p_y, p_z, the p orbitals on the oxygen (Fig. 2). Instead of h_A and h_B, are given elsewhere.[9,12] In this paper a few new results will be given to demonstrate the power of the method. Figure 3 shows the valence energy bands and densities of states (DOS) one can work with their linear combinations $b = h_A + h_B$ and $a = h_A - h_B$. Note that these would be the bonding and antibonding orbitals, respectively in an elemental semiconductor like Si. In SiO_2, the main EBO is formed from p_z and the *antibonding* combination, a, so that it is odd about the midpoint between the two Si's. The structure of some of the valence-band orbitals of SiO_2 is thus similar to the structure of the conduction-band orbitals of Si and vice-versa.

In constructing the EBO's for SiO_2, two quantities, β_{px} and β_{pz}, enter, which describe the charge transfer between the oxygen and its two neighboring Si's. In constructing the EBO's for a typical ABO_4-type oxide, b and a defined above are not adequate, just as they are not adequate for the description of zinc-blende-type compounds.[10] For the latter, modified b's and a's are introduced, given by $b = (1 + \alpha_p)^{1/2}h_A + (1 - \alpha_p)^{1/2}h_B$ and $a = (1 - \alpha_p)^{1/2}h_A - (1 + \alpha_p)^{1/2}h_B$, where α_p, the polarity, describes the charge transfer between atom A and B. Similar quantities enter the construction of the EBO's for the ABO_4-type oxides. They are denoted by α_{px} and α_{pz} and are referred to as external polarities. The quantities β_{px} and β_{pz} are referred to as internal polarities.

Mathematical detail and the method of parametrization for the ideal cubic form of SiO_2 and a typical ABO_4-type oxide. Note the opening of an additional gap in ABO_4, which is analogous to the so-called antisymmetric gap in the bands of the AB-type semiconductors.[10] Figure 4 shows the DOS for a more general SiO_2 structure, which is a simulation[9] of amorphous SiO_2 and has the Si–O–Si angle to be the observed 144° instead of the ideal 180°. Figure 5 shows the same DOS broadened by 0.8 eV and compares it with the measured ultraviolet photoemission spectrum (UPS). The agreement between theory and experiment is substantially better than that obtained previously[11] with only 0.5 eV of broadening. Figure 6 shows the calculated and experimental x-ray-emission spectra of SiO_2. This is the first such calculation of these spectra and the agreement with experiment is seen to be very satisfactory. Comparable spectra have been calculated for ABO_4-type oxides but no experiments are available. One of the response functions that can be calculated without needing the energy bands, as mentioned earlier, is the electronic (high-frequency) dielectric constant ϵ, for which an explicit analytical expression is obtained.[9,12] It turns out that, in addition to the density of electrons, ϵ depends on the angle at the oxygen atom in an important way. In Table I, a number of theoretical and experimental values of ϵ are given. In the case of the β-cristobalite and coesite forms of SiO_2, ϵ was calculated with the Si–O–Si angles listed by Wyckoff[1] and *also* with the quartz value of 144°. The 180° value for β-cristobalite has been questioned by many authors. The comparison seems to suggest that the two extreme angles may in fact be unrealistic and that all forms of SiO_2 have angles in the neighborhood of 144°. The values of ϵ listed for the boron compounds are not very reliable due to complications with first-row elements.[10] A more extensive treatment of this and other questions is given in Ref. 12.

[a] Work supported in part by the Office of Naval Research under contract No. N00014-76-C-0934.

[1] R. W. G. Wyckoff, *Crystal Structures* (Interscience, New York, 1965), and original references therein.
[2] J. Maserjian, J. Vac. Sci. Technol. 11, 996 (1974).
[3] T. H. DiStefano, J. Vac. Sci. Technol. 13, 856 (1976).
[4] S. I. Raider and R. Flitsch, J. Vac. Sci. Technol. 13, 58 (1976).
[5] W. L. Harrington, R. E. Honig, A. M. Goodman, and R. Williams, Appl. Phys. Lett. 27, 644 (1975).
[6] J. S. Johanessen, W. E. Spicer, and Y. E. Strausser, J. Appl. Phys. 47, 3028 (1976).
[7] S. T. Pantelides and M. Long, (to be published).
[8] CRN models for bulk amorphous SiO_2 have previously been built by others. See, e.g., R. J. Bell and P. Dean, Philos. Mag. 25, 1381 (1972).
[9] S. T. Pantelides and W. A. Harrison, Phys. Rev. B 13, 2667 (1976).
[10] W. A. Harrison and S. Ciraci, Phys. Rev. B 10, 1516 (1974); S. T. Pantelides and W. A. Harrison, Phys. Rev. B 11, 3006 (1975).
[11] S. T. Pantelides, B. Fischer, R. A. Pollak, and T. H. DiStefano, Solid State Comm. 21, 1003 (1977).
[12] S. T. Pantelides, Phys. Rev. B, (to be published).

Solid State Communications, Vol. 21, pp. 1003-1006, 1977. Pergamon Press. Printed in Great Britain

THE ELECTRONIC STRUCTURE OF SiO_2, GeO_2 AND INTERMEDIATE $Si_xGe_{1-x}O_2$ COMPOSITIONS: EXPERIMENT AND THEORY*

Sokrates T. Pantelides, Bernhard Fischer,† Roger A. Pollak, and Thomas H. Di Stefano

IBM Thomas J. Watson Research Center, Yorktown Heights, New York 10598, USA

(Received 27 December 1976 by E. Burstein)

Theoretical calculations are reported for SiO_2, GeO_2 and the intermediate composition $Si_3Ge_3O_2$ which reproduce the main observed features and trends in experimental photoemission spectra. The agreement between the two establishes the importance of band theory in understanding the electronic structure of these materials, and demonstrates that detailed quantitative predictions are feasible for such complex materials in terms of the empirical tight-binding method. The calculations further establish that the structure in the valence bands is determined mainly by nearest-neighbor oxygen-oxygen interactions.

The electronic structure of SiO_2 and GeO_2 has been the subject of considerable attention in the literature. Most attempts have, however, mainly focused on *interpreting* experimental data (optical absorption, x-ray absorption, x-ray emission, photoemission, etc.) in terms of simple "molecular-orbital" energy levels. Such assignments have worked well for certain experimental spectra, but at the same time were incompatible with other spectra.[1,2] Furthermore, several assignment schemes, based on similar ideas, differ substantially from each other. One difficulty arises from the fact that the crystal structures of these materials are complex, with low symmetry and many atoms in a primitive unit cell. This complexity has inhibited the successful application of band-theoretic techniques which have in the past proven very powerful for simpler materials. Recently, Pantelides and Harrison[2] (PH) and Schneider and Fowler[3] (SF) performed energy band calculations for SiO_2 and independently pointed out the importance of energy-band theory for a systematic interpretation of the data. PH went beyond SF in calculating densities of states (DOS) but both used the band results only as *guides* to interprete the data, leaving a host of questions unresolved. The nature of the electronic states in these materials has not therefore thus far been conclusively determined due to the inability of theory to directly and unambiguously reproduce the observed spectra.

In the present paper we present theoretical calculations of the photoemission spectra of SiO_2, GeO_2, and the intermediate composition $Si_3Ge_3O_2$, which reproduce the important features and trends in the observed spectra. The results show that a molecular-orbital picture about a single oxygen atom is inadequate. They also establish the importance of band theory for these materials and show that quantitative predictions are feasible for materials of such high complexity and low symmetry. Finally, they establish that the bandwidth and much of the internal structure are largely determined by the nearest-neighbor oxygen-oxygen p-orbital interactions, a factor which should be central in understanding the electronic propeties of all the silicate glasses.

The ultraviolet photoemission spectroscopy (UPS) measurements were performed using a cylindrical mirror electrostatic-deflection type electron energy analyzer (resolution 0.25 eV) and 40.8 eV photons from a He-discharge lamp. The x-ray photoemission spectroscopy (XPS) measurements were performed with a Hewlett-Packard x-ray photoelectron spectrometer which has a monochromatic Al $K\alpha_{1,2}$ x-ray source (1486.6 eV) and a resolution of 0.6 eV. First, Si_xGe_{1-x} films several thousand Ångstroms thick were deposited on sapphire substrates by DC sputtering from targets formed by melting high-purity polycrystalline silicon and germanium onto a molybdenun substrate. The $Si_xGe_{1-x}O_2$ films which were studied with UPS were oxidized *in situ* in the spectrometer by heating to 450° C for 15 minutes in 10^{-5} torr of oxygen. The films studied with XPS were oxidized by heating in oxygen to 650° C for two hours in a tube furnace and then immediately transferred to the spectrometer vacuum. The compositions of the films used in the UPS experiments were determined by electron microprobe analysis and the compositions of the films used in the XPS experiments were estimated from the relative intensities of XPS spectra from the Ge 3d, Si 2p, and O 1s core levels. The oxide films were thicker than the escape depth of the photoelectrons, as evidenced by the absence of unoxidized Si or Ge core levels in the spectra. More experimental details are given in Ref. 4. The experimental spectra are shown in Fig. 1.

The theoretical calculations were carried out in terms of the empirical tight-binding model employed by PH. The basis orbitals are the tetrahedrally-oriented sp^3

* Work supported in part by the Office of Naval Research, Washington D.C. under contract No. N 00014-76-C-0934 and in part by the Advanced Research Product Agency and monitored by AFCRL under contract No. F19628-76-C-0249

† Present address: Max-Planck Institut fur Festkorperforschung, Stuttgart, West Germany.

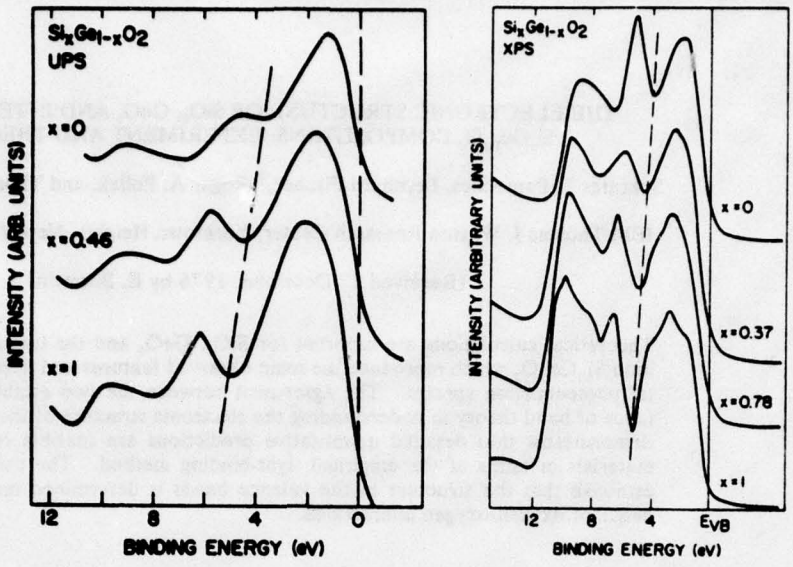

Fig. 1. Experimental UPS and XPS spectra for $Si_xGe_{1-x}O_2$ films.

hybrids on the Si/Ge atoms and the p orbitals on the oxygens. These orbitals (Fig. 2) are allowed to interact, giving rise to five types of orbitals: (1) a bonding orbital B_z comprized of p_z and the odd combination of the hybrids, (2) an orbital B_x comprized of p_x and the even combination of the hybrids ($B_x=p_x$ for the ideal cubic structure, Fig. 2a), (3) a non-bonding orbital $B_y=p_y$, and (4,5) two corresponding antibonding orbitals A_z and A_x. The B's are occupied, giving rise to the valence bands while the A's are empty, giving rise to the conduction bands. For the intermediate $Si_3Ge_3O_2$ composition, the main additional[5] effect is a mixing between B_x and B_z.

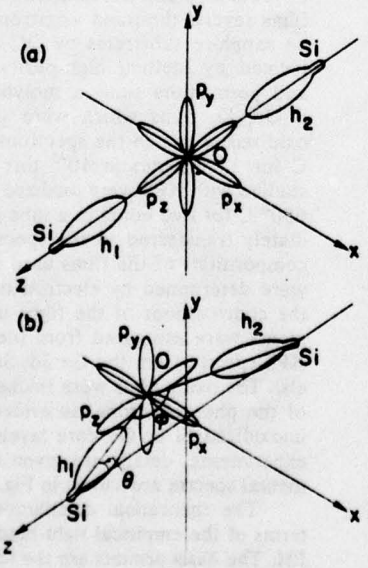

Fig. 2. The tight-binding orbitals employed in the calculations. (a) For the ideal cubic structure, and (b) for the general case.

The precise composition of the various A's and B's, as well as their energy positions are entirely determined in terms of two parameters, the hybrid--p-orbital interaction W_2 and the hybrid--p-orbital energy separation W_3. These have been fixed by making use of the optical spectrum of SiO_2 (see Ref. 2). The parameters for GeO_2 and the intermediate compositions are then determined by making use of the relative hybrid energies of Si and Ge and the d^{-2} rule, where d is the bond length.[2] With the basis orbitals just defined, a tight-binding energy band calculation is carried out by retaining only nearest-neighbor interactions. This introduces two new parameters, a hybrid-hybrid interaction V_1 (carried over from previous work on the tetrahedral semiconductors) and the oxygen-oxygen ppσ interaction V_p. The latter is adjusted to the observed total width of the valence bands of SiO_2. For GeO_2 and the intermediate compositions V_p is scaled with the d^{-2} rule. The valence bands obtained for cubic SiO_2 with these choices are in very good accord with the first-principles bands of SF. We are now in position, however, to bend the Si-O-Si chains to the observed angles (144°) and repeat the calculations and obtain the valence bands and corresponding DOS for the various cases of interest. The latter are then broadened by convoluting with a gaussian of width 0.5 eV. This broadening turns out to be extremely important as it eliminates most of the sharp spiked structures in the DOS (see Fig. 3) which precluded PH from carrying out more than a qualitative analysis of the observed spectra.

The final broadened DOS curves for SiO_2, GeO_2 and $Si_{0.5}Ge_{0.5}O_2$ (or $SiGeO_4$), are shown in Fig. 4 for direct comparison with Fig. 1. In view of the fact that the calculation did not include photoemission matrix elements, the comparison must be limited to the overall trends among the various compositions and to the positions of dips and peaks in the individual spectra. No comparison can be made of the relative heights of peaks.

It is seen that the overall trends present in the data are reproduced by the theory. In particular, the total

width decreases as one goes from SiO_2 to GeO_2. Also the main dip at about 4 eV fills up slowly and moves to higher energies in both the experimental and theoretical curves, as shown by the dashed lines in Figs. 1 and 4.

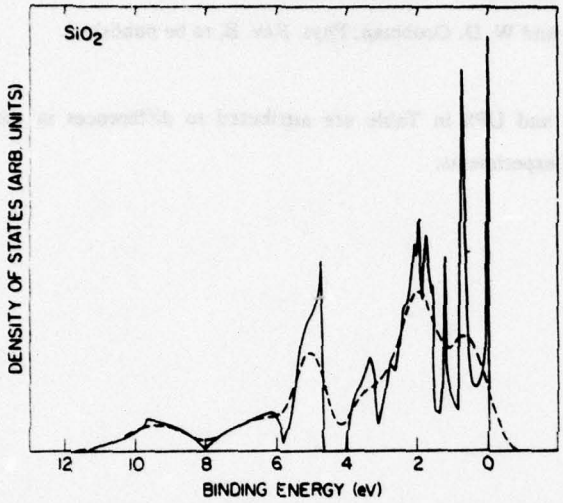

Fig. 3. Density of States (DOS) and broadened DOS for the valence bands of SiO_2.

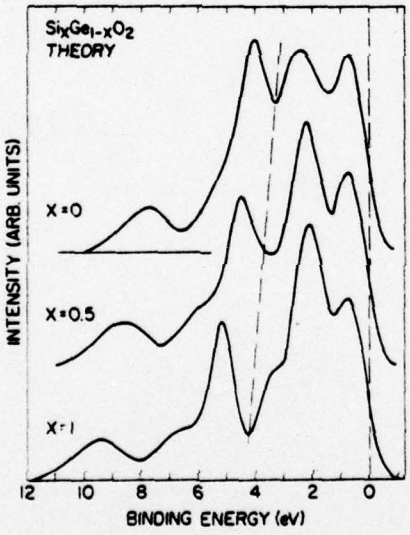

Fig. 4. Theoretical photoemission spectra for $Si_xGe_{1-x}O_2$ films. Compare with Fig. 1.

For more detail comparison between theory and experiment, the positions of the peaks and dips in the theoretical and experimental curves of SiO_2 and GeO_2 are listed in Table I. For the purposes of this Table, the zero of energy in the theoretical curves was redefined by the technique employed in obtaining the zero of energy in the experimental spectra, namely by linear extrapolation of the descending curve. The main discrepancy in both materials is peak 1 which appears as a double peak in the theoretical curves. The agreement between experiment[6] and theory for the remaining features is better than 15%.

TABLE I

Experimental and theoretical positions (in eV) of peaks and dips in the photoemission spectra of SiO_2 and GeO_2. The numbering refers to Fig. 1 in order of increasing binding energy.

Feature	XPS	UPS	Theory
SiO_2			
dip 1	5.3	5.3	4.7
dip 2	7.6	8.1	8.5
peak 1	2.8	2.6	1.2,2.5
peak 2	6.5	6.4	5.7
peak 3	9.8	9.8	9.9
total width	11.5	11.2	11.7
GeO_2			
dip 1	4.0	4.0	3.7
dip 2	6.6	6.9	7.0
peak 1	1.9	1.8	1.2,2.9
peak 2	5.1	5.0	4.5
peak 3	8.7	9.3	8.3
total width	10.4	10.1	10.0

The empirical tight-binding method employed in the calculations presented above allows a detailed analysis of the results in terms of simple physical concepts. For example, it has long been suggested that the top of the valence bands, in particular the broad feature from 0 to about 4 eV, arises from the non-bonding oxygen p orbitals, whereas the remainder of the bands arises from the bonding orbitals. The present calculations show this separation to be an oversimplification of reality. First note that the Si-O interaction (W_2) is responsible for the formation of the bonding orbitals. It is the O-O interaction V_p alone that causes the banding of the non-bonding orbitals, and it is V_p together with V_1 that cause the banding of the bonding orbitals. The same V_p, however, is also responsible for the admixture between the bonding and non-bonding orbitals, the net result being a strong hybridization between the bonding and non-bonding bands. The nature of the hybridization is particularly interesting. If it is turned off, the pure non-bonding bands overlap considerably with the pure bonding ones. When the hybridization is turned on, the two sets of bands push strongly on each other, opening up a gap at 4 eV (Fig.3). This is opposite to what a molecular-orbital picture would suggest, since the presence of a gap between two levels would be viewd as a consequence of hybridization.

In conclusion, we have presented new experimental spectra which help establish the electronic structure of SiO_2 and GeO_2. Theoretical calculations in terms of the empirical tight-binding method (ETBM) have proved successful in reproducing the experimental spectra and establishing the validity of the band picture for these rather complex materials. It should be emphasized that only the total width of the bands of SiO_2 was used as an input in performing the calculations. The internal structure in the spectrum of SiO_2, as well as the other spectra in their entirety, were *predicted* and found to be in good agreement with experiment. This demonstrates the capability of the ETBM to yield quantitative predictions for materials for which other methods may not be too convenient to apply due to low symmetry and complicated lattices.

REFERENCES

1. See e.g. recent review by A. R. Ruffa, J. Non-Cryst. Solids 13, 37 (1973/74).

2. S. T. Pantelides and W. A. Harrison, Phys. Rev. B 13, 2667 (1976); and references therein.

3. P. M. Schneider and W. B. Fowler, Phys. Rev. Lett. 36, 425 (1976).

4. B. Fischer, R. A. Pollak, T. H. DiStefano and W. D. Grobman, Phys. Rev. B, to be published.

5. S. T. Pantelides, to be published.

6. The small discrepancies between XPS and UPS in Table are attributed to differences in the intrinsic broadening of the curves in the two types of experiments.

RC 7119 (#30460) 5/5/78
Solid State Physics 5 pages

Research Report

THE OPTICAL ABSORPTION SPECTRUM OF SiO_2‡

Sokrates T. Pantelides

IBM T. J. Watson Research Center, Yorktown Heights, NY 10598

IBM Research Division
San Jose · Yorktown · Zurich

RC 7119 (#30460) 5/5/78
Solid State Physics 5 pages

THE OPTICAL ABSORPTION SPECTRUM OF SiO_2[‡]

Sokrates T. Pantelides

IBM T. J. Watson Research Center, Yorktown Heights, NY 10598

ABSTRACT: We show that inclusion of electron-hole interactions not only produces an exciton at 10.4 eV, but also modify the interband continuum in a substantial way. The result is a spectrum consisting of three excitonic peaks, in good agreement with the observed spectrum. These peaks are identified in terms of the bond-orbital model as members of a crystal-field split Frenkel-type exciton corresponding to the free oxygen atom $2p \rightarrow 3s$ transitions.

[‡]Supported in part by the Office of Naval Research under Contract No. N00014-76-C-0934.

LIMITED DISTRIBUTION NOTICE

This report has been submitted for publication elsewhere and has been issued as a Research Report for early dissemination of its contents. As a courtesy to the intended publisher, it should not be widely distributed until after the date of outside publication.

Copies may be requested from:
IBM Thomas J. Watson Research Center
Post Office Box 218
Yorktown Heights, New York 10598

INTRODUCTION

The optical absorption spectrum of SiO_2, shown[1] in Figs. 1a and 2, has been the subject of considerable interest and controversy[2]. Following early attempts to interpret the spectrum,[2,3] DiStefano and Eastman[4] concluded from a series of photoconductivity and internal photoemission measurements on Si-SiO_2 structures that the band gap is about 9 eV. These results raised the question why no strong excitons appear in the absorption spectrum below the band edge as is the case in other ionic wide-gap materials, such as the alkali halides. The observed peaks thus became the subject of conflicting interpretations in terms of excitons, interband transitions and various combinations thereof (see e.g. Fig. 6 in Ref 2 for summary). More recently, Schneider and Fowler[5] calculated a band structure for cubic SiO_2 and suggested that excitons are *not* formed because of a symmetry-forbidden edge. Chelikowsky and Schlüter (CS)[6] actually calculated an interband spectrum (Fig. 1c) and found an indirect bandgap of 9.2 eV, which is consistent with the measurements of Ref. 4. They also found that matrix elements suppress absorption below ~10.4 eV. They therefore suggested that the first observed peak corresponds to an exciton, as previously proposed by others,[2,3] while the rest of the spectrum is due to interband transitions. In support of the latter assignment, they displayed the experimental spectrum shifted by 0.7 eV and noted the resulting good agreement between theory

‡Supported in part by the Office of Naval Research under Contract No. N00014-76-C-0934.

and experiment (Fig. 1b and 1c). More recently, Mott[7] investigated the subject and suggested that there exists an allowed exciton at 9 eV which has a dispersion of ~2.4 eV due to hopping, resulting in the 10.4 eV peak (see also the paper by Mott in these Proceedings).

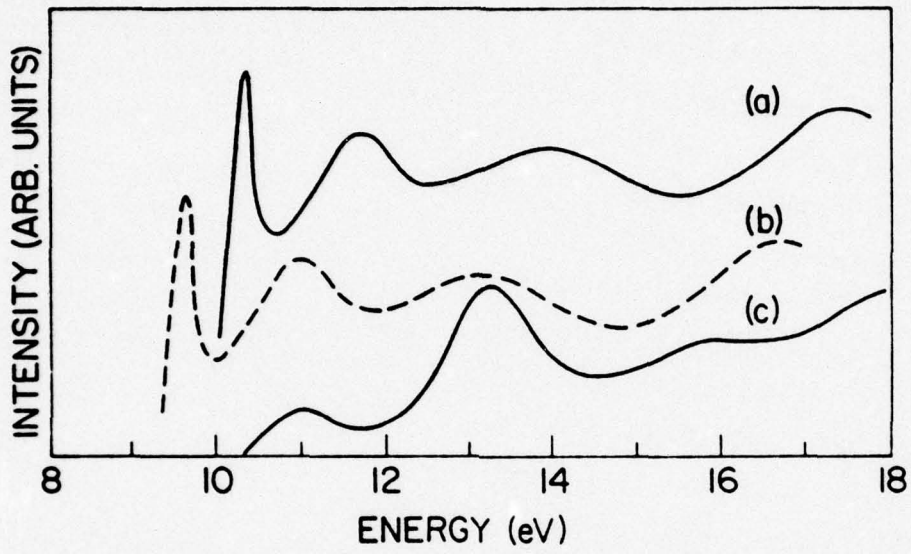

Fig. 1 (a) The optical absorption spectrum of SiO_2 measured by Klein and Chun [Ref. 1; the spectrum shown is actually $E^2\varepsilon_2(E)$]. (b) The same spectrum shifted by 0.7 eV in Ref. 4 in order to align it with the theoretical interband spectrum, curve (c).

In this paper we present two completely independent treatments of electron-hole (e-h) interactions and conclude that the observed peaks are a series of excitonic resonances. This interpretation is consistent with but goes beyond a band-theoretic approach and is also consistent with the known data.

BAND-THEORETIC APPROACH AND THE EFFECT OF E-H INTERACTIONS

In most semiconductors which have large dielectric constants, e-h interactions tend to be weak and produce excitons with very small binding energies and oscillator strengths. As a result, the interband spectrum remains essentially unmodified and is in general well reproduced by band-structure calculations. In the case of wide-gap insulators, however, dielectric constants are small, making e-h interactions very strong. The resulting excitons are then localized and carry considerable oscillator strength. This oscillator strength is pulled out of the interband continuum (the total oscillator strength remains constant) in such a way that the final spectrum is substantially different from the independent-particle spectrum. This assertion has been

supported by theoretical calculations[8,9] and by a study of 39 x-ray absorption spectra of alkali halides.[10]

In this section we start with the interband spectrum of SiO_2 calculated by CS[6], which indicated that the 10.4-eV peak should not be attributed to interband transitions. We will then incorporate e-h interactions by means of a model calculation, which indicates that e-h interactions strong enough to produce an excitonic peak at 10.4 eV also modify the interband spectrum very strongly, so that all the observed peaks are excitonic in nature.

The model calculation we intend to carry out is similar to that done previously[9] for LiF. We start with the interband spectrum calculated by CS and assume it can be simulated by a two-band model and momentum-independent transition matrix elements. In such a model, the absorption coefficient for interband transitions is given by the imaginary part of a two-particle Green's function G^o describing independently propagating electrons and holes. We therefore construct an analytical form for $G^o(E)$ as in Ref. 9, chosen so that its imaginary part, when broadened by 0.5 eV, reproduces CS's interband spectrum. E-h interactions are then introduced in the contact approximation,[8,9] i.e. as a single on-site matrix element V in the Wannier representation. The new absorption spectrum is given by the imaginary part of the new Green's function G, which satisfies Dyson's equation:

$$G = G^o + G^oVG. \tag{1}$$

Eq. (1) is solved directly to yield

$$G(E) = G^o(E)/[1 - G^o(E)V] \tag{2}$$

so that a bound state occurs when $G^o(E) = 1/V$. The value of V was chosen to yield a bound state at 10.4 eV.

The results of the calculation are shown in Fig. 2. The dashed curve is $-\mathrm{Im}\ G^o(E)$, with E having a 0.5 eV imaginary part for broadening, and corresponds to CS's interband spectrum (cf. with Fig. 1c). The solid curve marked theory is $-\mathrm{Im}\ G(E)$, also broadened by 0.5 eV. These results clearly show that if the 10.4-eV peak is indeed an exciton, e-h interactions also modify the interband spectrum strongly, so that the final spectrum is excitonic in nature, i.e. consists of a series of excitonic resonances (sometimes called metastable excitons). Note that whereas the two peaks in the interband spectrum are separated by ~2.3 eV, the two peaks in the final spectrum are separated by 1.4 eV, in excellent agreement with experiment. The spectrum at higher energies is not reproduced very well as one might expect, since oscillator strength at those energies would have to be brought down by e-h interactions from even higher energies, which are left out by the present model. Neverthe-

less, the calculated peak at 15 eV compares rather well with the observed peak at 14 eV.

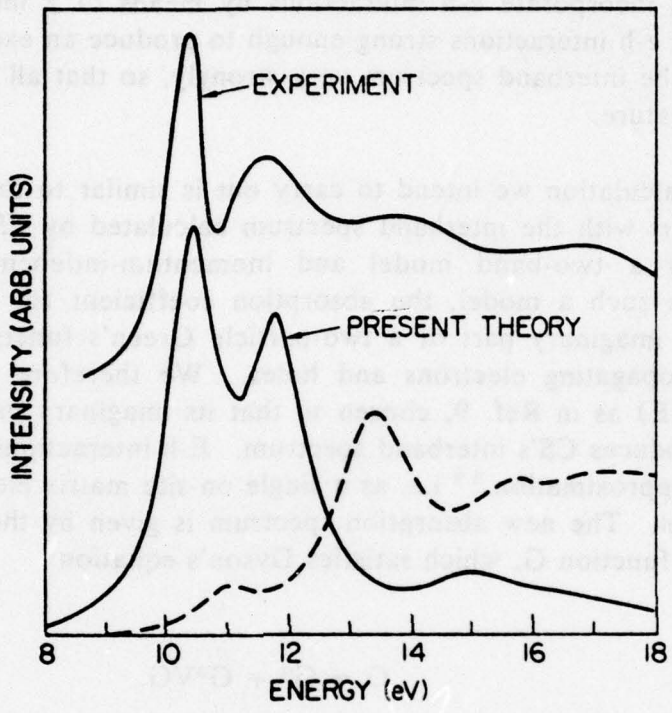

Fig. 2 Theoretical absorption spectrum compared with the optical absorption spectrum [$\epsilon_2(E)$] measured by Philipp (Ref. 1). The dashed line is interband spectrum before e-h interactions. See text.

Apart from the success of the above model calculation in predicting the energy separations and relative heights of the peaks in the optical spectrum, the main conclusion is that in wide-gap insulators one cannot ignore the effect of e-h interactions on interband transitions, as done in semiconductors. In contrast, e-h interactions have a rather pervasive effect, so that excitonic peaks dominate the entire spectrum. One should not, therefore, hope to extract a band gap from such a spectrum.

BOND-ORBITAL APPROACH

The above calculation indicates that the absorption spectrum of SiO_2 can be interpreted as a series of excitonic peaks arising from localized excitations, but does not provide information about the nature of states contributing to the two observed peaks. As was the case for alkali halides,[10] an atomistic point of view can be complementary and useful. For this purpose, we make use of the tight-binding

bond-orbital model[11] for SiO_2, according to which the valence band states arise from three different bond orbitals, associated with a Si-O-Si bonding unit: B_y, which is a pure O *2p* orbital perpendicular to the Si-O-Si plane (lone-pair or non-bonding *p* orbital); B_x, which is ~85% an O *2p* orbital in the Si-O-Si plane perpendicular to the Si-Si axis and ~15% Si sp^3 hybrid (partially bonding orbital); and B_z, which is ~65% an O *2p* orbital along the Si-Si axis and ~35% Si sp^3 hybrid (bonding orbital). These three orbitals at each bonding unit have been found adequate for a calculation of the valence bands and the related photoemission and x-ray-emission spectra.[11]

According to the same bond-orbital scheme, the lowest unoccupied band states arise from a bond orbital denoted in Ref. 10 by A_+, consisting mainly of O *3s* and Si hybrid admixtures. We suggest that during photoabsorption the electron and the hole do not occupy propagating band states. Instead, e-h interactions tend to localize the electron and the hole in the same bonding unit, so that excitonic peaks are expected at the $B_y \rightarrow A_+$, $B_x \rightarrow A_+$, and $B_z \rightarrow A_+$ energies, in that order. Note that these transitions are essentially localized on an O atom and correspond to the atomic transition *2p* → *3s*. In the free atom the transition energy is about 9.2 eV. In the solid, B_y, B_x, and B_z may be viewed as the "crystal-field" split members of the O *2p* orbital, resulting in a "crystal-field" split Frenkel-type exciton with peaks at 10.4 eV, 11.7 eV, and ~14 eV. These energies cannot be predicted by some simple quantitative calculation, but the interpretation may be further supported by a variety of arguments. First, CS's calculation showed that the 10.4-eV should not be attributed to interband transitions. Second, the calculation of the previous section demonstrated that if the 10.4-eV peak is indeed an exciton, the other peaks are also predominantly excitonic in nature. Third, using the identification presented above, one can infer that the three peaks ought to be successively shorter, because of the smaller weight of O *2p* in each successive B, and also broader, because of the shorter lifetime of a hole in each succesive B. Both these observations are in agreement with experiment and consistent with the calculation of the previous section.

REFERENCES

1. H. R. Philipp, **Solid State Comm. 44**, 73 (1966); G. Klein and H. U. Chun, **Phys. Stat. Sol. B 49**, 167 (1972).
2. See recent review by D. L. Griscom, **J. Non-Cryst. Sol. 24**, 155 (1977).
3. A. R. Ruffa, **J. Non-Cryst. Solids 13**, 37 (1973/74).
4. T. H. DiStefano and D. E. Eastman, **Solid State Comm. 99**, 2259 (1971).
5. P. M. Schneider and W. B. Fowler, **Phys. Rev. Lett. 36**, 425 (1976)
6. J. R. Chelikowsky and M. Schlüter, **Phys. Rev. B 15**, 4020 (1977).
7. N. F. Mott, **Adv. in Phys. 26**, 363 (1977).
8. J. Hermanson, **Phys. Rev. 166** 893 (1968).
9. S. T. Pantelides, R. M. Martin and P. N. Sen, Proc. IV Intern. Conf. on VUV Rad. Phys., E. E. Koch, ed., (Pergamon/Vieweg, 1974).
10. S. T. Pantelides, **Phys. Rev. B 11**, 2391 (1975).
11. S. T. Pantelides and W. A. Harrison, **Phys. Rev. B 13**, 2667 (1976); S. T. Pantelides, **J. Vac. Sci. Technol. 14**, 965 (1977).

Recent Advances in the Theory of Electronic Structure of SiO_2

Silicon dioxide (SiO_2) is a material that has attracted the attention of scientists for a long time. It is available in nature in a variety of forms and has been used extensively by the construction industry, by the glass industry, and, during the last fifteen years, in technological applications, in particular the manufacture of metal-oxide semiconductor (MOS) devices. There exists a vast experimental and theoretical literature on its physical, chemical, electronic, optical, thermal, transport, magnetic and other properties.

Theoretical understanding of the electronic properties of SiO_2 began with qualitative molecular-orbital pictures aimed at the interpretation of particular experimental spectra, such as the optical absorption spectra, the x-ray emission spectra, etc. These early models were reviewed by Ruffa,[1] who identified their relative merits and shortcomings. New insights were gained by subsequent work by several workers[2] who quantified such studies with self-consistent calculations on small clusters, but the ambiguities clouding the connection between the discrete energy levels of the cluster with the continuous excitation spectra of the solid were a persistent problem. In particular, clusters of increasing size were not found to yield a converging picture of level densities. Furthermore, clusters centred about different atoms (Si or O) were needed to interpret the x-ray emission spectra associated with core levels on different atoms, so that a consistent and universal level scheme was elusive.

During the last two years several advances have been made in our understanding of the electronic properties of SiO_2, in particular from applications of band theory. In view of the technological importance of SiO_2, it is rather surprising that band calculations have been lacking. It is therefore interesting first to explore the reasons for this. We will then examine the recent accomplishments of band theory and assess the current and future objectives of theoretical work in SiO_2.

The reasons why energy band calculations have not been available for SiO_2 lie in its crystal structure, or, rather crystal structures. SiO_2 exists in nature in a variety of crystalline forms, called polymorphs, all of which have low symmetry

Comments Solid State Phys.
1977, Vol. 8, No. 3, pp. 55–60

Printed in Great Britain

and large unit cells. For example, α-quartz, the best known polymorph, has nine atoms in the primitive unit cell. By comparison, some of the materials that are studied most often have one or two atoms per unit cell (simple and transition metals, alkali halides, tetrahedral semiconductors, etc.). The consequence of many atoms in the primitive unit cell is that many more bands are needed for a complete description. For example, α-quartz has 24 valence bands, compared with 1, 3 or 4 in the materials mentioned above. The large number of bands calls for very large basis sets for proper convergence, which might strain even large computers or computer budgets. Apart from the problem of computer time, other hurdles have also been present. For example, the construction of a potential for wide-gap insulators, especially compounds involving a first-row element, such as oxides, nitrides, fluorides, etc., is known to involve large uncertainties. Calculations on such materials using local-density approximations to the exchange and correlation potentials in general produce bandwidths and bandgaps which are too narrow; pure Hartree–Fock calculations give the opposite; on the other hand, local-density approximations have been quite successful for the less ionic compound tetrahedral semiconductors so that SiO_2 might be thought to be a borderline material.

How were these problems circumvented? The first two calculations[3a,4a] were done on the ideal cubic form of SiO_2, which has, in the past, been thought to be the structure of the polymorph known as β-cristobalite. This structure has six atoms per primitive unit cell, but the symmetry is rather high, namely the same as that of diamond (space group O_h^7). The atomic arrangement is actually quite interesting, in that the Si's form a diamond lattice (just like Si itself, except for a somewhat larger lattice spacing), and the oxygens lie at the mid-points of the lines connecting nearest-neighbor Si's, the so-called bond sites. Thus, each Si is surrounded by four oxygen atoms in tetrahedral directions, and each oxygen has two Si nearest neighbors, just like in most real forms of SiO_2. The only exception is that the Si–O–Si angle is 180° instead of the observed 140°–150°. Parenthetically, we may note that the α-cristobalite structure can be arrived at by starting with the cubic structure just described and bending the Si–O–Si chains in a systematic way. A tetragonal distortion then occurs. In a similar fashion, the structure of tridymite can be arrived at by starting with a wurtzite lattice of Si's (instead of a diamond lattice of Si's) and then inserting the oxygens between the Si's and bending the Si–O–Si chains.

The first band calculation was done[3] for β-cristobalite in the 'empirical tight-binding method' (ETBM) which employs a tight-binding basis set and treats the matrix elements as parameters. This technique resembles the often used procedure of obtaining a tight-binding *fit* to energy bands calculated by a sophisticated first-principles method. The fundamental difference is that in the ETBM one proceeds in the absence of any band calculation whatever, and determines the values of the parameters by scaling parameters from other materials and/or

experimental data for the material of interest. It is thus analogous to the empirical pseudopotential method (EPM) which is also occasionally used as an interpolation scheme. A particular virtue of both the EPM and the ETBM is that they are tests of the single-particle model to interpret the excitation spectra of solids without depending upon the ability of contemporary theory to construct from first-principles the one-electron Hamiltonian, in particular the self-energy operator which describes the complicated electron-electron interaction. On the other hand, a serious drawback of the ETBM is that it produces only valence bands. Later, more laborious calculations, using first-principles potentials, by Schneider and Fowler[5] and by Ciraci and Batra[6] produced similar valence bands which confirmed the validity of the assumptions made in the ETBM.[3] The latter calculations were more complete in that they also produced conduction bands. Calculations on cubic SiO_2, however, do not necessarily relate directly with experimental data because all the real polymorphs of SiO_2 have bent Si-O-Si chains, with angle at the O atoms about 144°, compared with the 180° for cubic SiO_2. Nevertheless, the energy bands of cubic SiO_2 help draw interesting analogies with the well-known bands of Si,[3] and suggest qualitative interpretations[4,6] of the spectra[4,6] of SiO_2.

Experimental optical spectra available for amorphous SiO_2 and for crystalline quartz were known to be identical,[7] which led to the conclusion that the local coordination determined all the structure, with long-range order being immaterial. Pantelides and Harrison[3] then assumed bent Si-O-Si chains in a hypothetical diamond lattice, a model which simulates the local topology of *amorphous* SiO_2, and obtained valence bands and density of states. Pantelides[3c,3d] later extended this to the calculation of the various x-ray emission spectra. After appropriate broadening was included, the calculated photoemission and x-ray emission spectra agreed in a quantitative way with experiment. Similar calculation also reproduced the trends in the experimental spectra of $Si_xGe_{1-x}O_2$ alloys.[8]

More recently, Schluter and Chelikowsky[5] (SC) and Calabrese and Fowler[4] (CF) reported energy band calculations for α-quartz. SC employed parametrized pseudopotentials for the core potentials and carried out a self-consistent calculation for the valence electrons in a plane-wave representation. CF used a superposition of atomic potentials and a mixed basis set. Similar results were obtained, but only SC were able to calculate enough points in the Brillouin zone to obtain explicit spectra

Schluter and Chelikowsky calculated detailed photoemission and x-ray emission spectra that agreed very well with experiment. Furthermore, they obtained detailed charge density plots which confirmed the basic assumptions made earlier[1,3] about the nature of the bonding and non-bonding orbitals. For the first time, however, SC also calculated a theoretical absorption spectrum for SiO_2. The calculation was limited to interband transitions, but it immediately revealed that, even though absorption begins at the indirect gap of about 9.2 eV,

it remains essentially zero for about 1 eV and finally peaks at 11 eV and then again at 13.3 eV. SC identified the first experimental peak at 10.4 eV as an exciton, in agreement with previous assignments, and attributed the structure at higher energies to interband transitions. The interpretation was suggested by the separation of the theoretical peaks being the same as the separation of the experimental peaks at 11.7 and 14.0 eV. One-to-one correspondence between the experimental and theoretical spectra was obtained by shifting the two spectra relative to each other by 0.7 eV.

Another property that has recently been calculated in addition to the spectra mentioned above is the dielectric constant. This was done by Pantelides and Harrison[3] who obtained a rather simple analytical expression, which depended explicitly on the value of the Si-O-Si angle and other known quantities. A new unknown parameter of order unity was introduced, but once its value was fixed for α-quartz, the dielectric constants for the other SiO_2 polymorphs could be predicted, and agreement with experiment was good. The most interesting result[3d] was for β-cristobalite: if the ideal (cubic) value of 180° for the Si-O-Si angle was used, the calculated dielectric constant ϵ was *too large* by 22%. When an angle of 144° (the α-quartz angle) was used, ϵ became identical to the experimental value. Similarly, for coesite, if the value of 120° was used (as listed by Wyckoff[10]), ϵ was *too small* by 25%. Again, use of 144° brought ϵ in line with experiment. Since β-cristobalite and coesite are the only polymorphs thought to have angles significantly different from 144°, these results suggest that all SiO_2 polymorphs may have Si-O-Si angles of about 144°. These results also reveal the amount of detailed information that can be extracted from a parametrized method. Studies of the dependence of spectra and properties on the Si-O-Si angle would otherwise be very involved calculations.

What then have band structure calculations accomplished? For the first time, a consistent picture of bonding in SiO_2 has been obtained. It has been shown that the details of the photoemission spectra and the various x-ray emission spectra can be systematically reproduced *only* via an energy band calculation, and throught the calculation of densities of states with and without matrix elements, a procedure that requires knowledge of the bands at many points in the Brillouin zone. It has also been shown that dielectric constants can be understood in detail. Finally, progress has been made in elucidating the optical absorption spectrum of SiO_2, but that has been limited by the fact that electron-hole interactions cannot yet be conveniently included.

Where do we go from here? Well, much remains to be done. To begin with, the available energy bands don't agree with each other in detail. For example, Calabrese and Fowler obtained a direct gap for α-quartz, whereas Schluter and Chelikowsky find an indirect gap. Furthermore, effective masses have not been calculated accurately. (Schluter and Chelikowsky obtain $0.3m_0$ for the conduction band mass, whereas Schneider and Fowler estimated $0.5m_0$.) These

quantities, as well as the interaction of electrons and holes with the lattice for the formation of polarons, are important in theories of transport properties and tunneling, which are still not very well understood.

Puzzling questions still remain about the optical spectra. What is the nature of the 10.4 eV exciton, in view of the fact that it is *above* the threshold for interband transitions? Is it possible that the formation of a strong exciton leaves the interband spectrum unchanged in its overall shape, as suggested by SC's analysis? Similar suggestions have been made previously in the case of core excitons in alkali halides, but subsequent analysis[9] showed that electron-hole interactions in materials with low dielectric constants not only give rise to highly localized excitons, but also perturb the interband spectrum in a substantial way.

Some uncertainties also still remain in the photoemission and X-ray emission spectra. Both Schluter and Chelikowsky[5] and the present author[3d] do very well for the Si K spectrum. Schluter and Chelikowsky also do very well for the O K spectrum but fail to reproduce one of the two peaks in the Si $L_{2,3}$ spectrum, which they attribute to possible sample contamination. The present author, on the other hand, obtains a good Si $L_{2,3}$ spectrum but a less satisfactory O K spectrum. As for the x-ray absorption spectra, they are virtually not understood at all. Similarly, theories of defect and impurity states are in primitive stages.[11]

Detailed understanding of SiO_2 can also lead to understanding of a large class of materials for which SiO_2 is a prototype. We recall that the structure of SiO_2 may be understood by starting with a lattice of Si atoms and inserting oxygen atoms. One could also insert oxygens in a zince-blende-type lattice, such as GaAs or GaP. The result is then $GaAsO_4$, $GaPO_4$, etc. This class of materials may be described by the general formula ABO_4, where AB is a zince-blende-type semiconductor. SiO_2 is then a special case of the ABO_4-type oxides with A = B = Si ($SiO_2 = SiSiO_4$, or silicon silicate!) and is the prototype of the whole class, just as Si is the prototype of the tetrahedral AB-type semiconductors.[3e]

Finally, an area where detailed theoretical calculations are needed is the interface between SiO_2 and Si, as well as the interfaces between SiO_2 and various metals. The properties of these interfaces are crucial to the behaviour of MOS devices and have long been studied by experimental techniques. One of the outstanding problems is the thickness of such interfaces. For example, the question whether an $SiO_x (0 < x < 2)$ layer exists between Si and SiO_2 has attracted considerable attention. Experimental estimates of the thickness of the SiO_x layer range from less than 4 Å to 15-20 Å.[12] Pantelides and Long[13] recently constructed a continuous random network model which shows that a zero-width interface is possible for the (100) Si-SiO_2 interface, but the question still remains open. This uncertainty complicates even further the difficult task of performing calculations of interface state. Thus far, only qualitative models

have been developed.[14] Some quantitative calculations were recently reported by Ciraci and Batra,[15] but the field is wide open, and all indications are that rigorous calculations should become possible in the immediate future.

In conclusion, considerable progress has been achieved in our understanding of the electronic properties of SiO_2. Band-theoretic techniques have now been applied and have already resolved many outstanding problems. Continued work along the same lines ought to supply even more answers. Finally, more specialized techniques are still needed for the understanding of the electronic properties of the interfaces of SiO_2. The future looks promising for this important material.

SOKRATES T. PANTELIDES
IBM Thomas J. Watson Research Center
Yorktown Heights, New York 10598

Acknowledgement

Work supported in part by the Office of Naval Research under Contract No. N00014-76-C-093.

References

1. A. F. Ruffa, J. Non-Cryst. Sol. 13, 37 (1973/74); see also more recent review by D. L. Griscom, J. Non-Cryst. Sol., in press.
2. A. J. Bennett and L. M. Roth, J. Phys. Chem. Sol. 32, 1251 (1971). T. L. Gilbert, W. J. Stevens, H. Schrenk, M. Yoshimine, and P. S. Bagus, Phys. Rev. B8, 5988 (1973); T. A. Tossell, D. J. Vaughn, and K. H. Johnson, Chem. Phys. Lett. 20, 329 (1973); K. L. Yip and W. B. Fowler, Phys. Rev. B10, 1400 (1974).
3. (a) S. T. Pantelides, Phys. Lett. 54A, 401 (1975).
   (b) S. T. Pantelides and W. A. Harrison, Phys. Rev. B13, 2667 (1976).
   (c) S. T. Pantelides, Proc. 13th Intern. Conf. on the Phys. of Semiconductors, F. G. Fumi, ed. (Tipografia Marves, Rome, 1976), p. 686.
   (d) S. T. Pantelides, J. Vac. Sci. Technol., in press.
4. (a) P. M. Schneider and W. B. Fowler, Phys. Rev. Lett. 36, 425 (1976).
   (b) E. Calabrese and W. B. Fowler, to be published.
5. M. Schluter and J. R. Chelikowsky, Solid State Commun. 21, 381 (1977).
6. S. Ciraci and I. P. Batra, Phys. Rev. B, to be published.
7. H. R. Phillip, Solid State Commun. 4, 73 (1966).
8. S. T. Pantelides, B. Fischer, R. A. Pollak and T. H. DiStefano, Solid State Commun., 21, 1003 (1977).
9. See S. T. Pantelides, Phys. Rev. B11, 2391 (1975). Also S. T. Pantelides, R. M. Martin and P. N. Sen, Proc. IV Intern. Conf. on VUV Rad. Physics, E. E. Koch, R. Haensel and C. Kunz, eds. (Pergamon-Vieweg, Braunschweig, 1974), p. 387.
10. R. W. G. Wyckoff, *Crystal Structures* (Interscience, New York, 1964).
11. See, e.g., J. A. Weil, Rad. Effects 26, 261 (1975).
12. J. Maserjian, J. Vac. Sci. Technol. 11, 996 (1974); J. S. Johanessen, W. E. Spicer and Y. E. Strausser, J. Appl. Phys. 47, 3028 (1976); W. L. Harrington, R. E. Honig, A. M. Goodman and R. Williams, Appl. Phys. Lett. 27, 644 (1975); S. I. Raider and R. Flitsch, J. Vac. Sci. Technol. 13, 58 (1976); T. H. DiStefano, J. Vac. Sci. Technol. 13, 856 (1976).
13. S. T. Pantelides and M. Long, to be published; see also Ref. 3(d).
14. See, e.g., C. T. Sah, IEEE Trans. on Nucl. Sci. (Dec. 1976); also B. E. Deal, J. Electrochem. Soc. 121, 198c (1974).
15. S. Ciraci and I. P. Batra, Bull. Am. Phys. Soc. 22, 293 (1977).

RC 7102 (#30337) 4/21/78
Solid State Physics 9 pages

Research Report

PHOTODEPOPULATION OF ELECTRONS TRAPPED IN SiO_2 ON SITES RELATED TO AS AND P IMPLANTATION*

R. F. DeKeersmaecker
D. J. DiMaria
S. T. Pantelides

IBM T. J. Watson Research Center
Yorktown Heights, NY 10598

Typed by: Kathlyn C. Murray

IBM Research Division
San Jose Yorktown Zurich

RC 7102 (#30337) 4/21/78
Solid State Physics 9 pages

PHOTODEPOPULATION OF ELECTRONS TRAPPED IN SiO_2 ON SITES RELATED TO AS AND P IMPLANTATION*

R. F. DeKeersmaecker
D. J. DiMaria
S. T. Pantelides

IBM T. J. Watson Research Center
Yorktown Heights, NY 10598

Typed by: Kathlyn C. Murray

ABSTRACT

Ion implantation has been used to incorporate As and P into the thermally grown SiO_2 layer of metal-silicon dioxide-silicon structures. These impurities increase the electron trap density in the oxide layer proportionally to the ion fluence (1-3 x 10^{13} cm^{-2}). Avalanche injection from the silicon substrate was used to populate the electron trapping sites. It is shown that the negative charge is removable from the trapping centers under illumination with photons between 3 and 5.6 eV. From the detrapping experiments, we determined a photoionization threshold of $\approx$ 4 eV both for As and P related centers, and a spectrally resolved *effective photoionization cross section*; the latter quantity is defined as the convolution of the photoionization cross section with the optically accessible trap distribution in the energy gap of the SiO_2. A simple model is presented which suggests that the observed detrapping originates from levels corresponding to substitutional P and As at O sites in the SiO_2.

*This work was supported in part by the Defense Advanced Research Projects Agency, and monitored by the Deputy for Electronic Technology (RADC) under contract No. F19628-76-C-0249 and by the Office of Naval Research under contract No. N00014-76-C-0934.

LIMITED DISTRIBUTION NOTICE

This report has been submitted for publication elsewhere and has been issued as a Research Report for early dissemination of its contents. As a courtesy to the intended publisher, it should not be widely distributed until after the date of outside publication.

Copies may be requested from:
IBM Thomas J. Watson Research Center
Post Office Box 218
Yorktown Heights, New York 10598

INTRODUCTION

Photodepopulation spectroscopy in metal-insulator-semiconductor (MIS) structures has recently been used to study both the spatial and energy distribution of optically accessible charges in the insulator film [1]. Several variations of the technique exist, all relying upon the optical stimulation of electrons, trapped in deep levels in the insulator, into cqnducting states from which they drift towards an electrode.

For MIS structures with SiO_2 as the insulator, literature is available on a 2.4-2.5 eV deep electron trap, possibly related to sodium incorporated at elevated temperatures in an immobile configuration in the oxide film [2]. Few studies, however, have been carried out to characterize other charge trapping centers. Several ions such as phosphorus and arsenic were recently demonstrated to exhibit electron trapping characteristics when implanted into the SiO_2 layer [3]. It was determined that P implantation results in a dominant electron trap with a capture cross section of 3×10^{-17} cm^2 [3], whereas for As related centers the dominant trap has a capture cross section of $\approx 10^{-15}$ cm^2 [4]. The trapping sites are in a net neutral state before electron capture. In both cases, the integrated trap density increases with the ion fluence. Good agreement was found between the trapped electron distribution centroid and both theoretical predictions and experimental observations of the ion distribution centroid [3].

In this work, we report on spectrally resolved detrapping measurements for charged MOS structures, from which a photoionization threshold and an effective photoionization cross section spectrum were determined. We also present a simple theoretical model which suggests that the observed levels are those of substitutional P and As at O sites.

EXPERIMENTAL

Sample Fabrication

The starting material was p-type <100> silicon with a resistivity of 0.1-0.2 Ωcm. The wafers were oxidized at 1000°C in a "dry" oxygen ambient to oxide thicknesses ranging from 560 to 1430 Å as determined by ellipsometry. Then P^+ or As^+ implantation was performed at room temperature with energies of 20 to 80 keV and fluences of 1 to 3 x 10^{13} cm^{-2}. The ion current at target during implantation was of the order of 1 x 10^{-6} A. All wafers were then cleaned and annealed in nitrogen at 1000°C for 30 min. Using a shadow mask, semitransparent aluminum electrodes (100-150 Å thick) with an area of 0.0052 cm^2 were deposited to form MOS capacitors. Finally, all devices were given a post-metallization annealing treatment at 400°C in forming gas for 20 min.

Electron Trapping and Photodetrapping

The oxide traps were charged by avalanche injection of hot electrons from the silicon substrate driven into deep depletion [5]. The amplitude of the 50 kHz ramp wave used for this purpose was constantly adjusted in order to keep the average dc injection current constant. The currents ranged from 5 x 10^{-10} to 3 x 10^{-9} A. Some of the injected electrons were trapped in the SiO_2, causing a shift in flat-band voltage, determined from 1 MHz differential capacitance-voltage characteristics.

After reaching a given charge level, the avalanche injection was stopped and the sample mounted in a set-up for photoelectric measurements, consisting of a 900 W xenon arc lamp in combination with a 500 mm grating monochromator (Bausch and Lomb). The incident photon flux at the sample position was measured over the spectrum using a thermopile in combination with an electronic chopper. An electric shutter was used to control the illumination time which was usually 5 min. The change in flat-band voltage induced by this illumination at room

temperature was monitored to within 1 mV with an automatic tracking system. The spectrum was scanned step-by-step in the direction of increasing photon energies.

The detrapping experiments are performed with zero gate bias in order to avoid injection from the contacts at photon energies greater than the Si-SiO_2 or Al-SiO_2 energy barrier, by using the internal fields in the SiO_2 layer due to the trapped negative charges as a potential barrier against this electron injection. This situation is preserved throughout the entire detrapping experiment, since only small portions of the total charge are removed at each step.

PHOTODETRAPPING ANALYSIS

If first order kinetics (neglecting charge retrapping) is assumed, the local depopulation of occupied traps under illumination is governed by the following equation:

$$\delta n_t\,(x,E,t)/\delta t = -F_p(x,\hbar\omega)\;\sigma_p(x,E,\hbar\omega)\;n_t(x,E,t), \qquad (1)$$

where $n_t(x,E,t)$ is the trapped electron concentration per unit energy, $F_p(x,\hbar\omega)$ is the local photon flux in the SiO_2 layer and $\sigma_p(x,E,\hbar\omega)$ is the trap photoionization cross section. The photon flux F_p is a function of both the photon energy $\hbar\omega$ and the position x in the SiO_2 layer due to the optical interference phenomenon [6]. This interference gives rise to a standing wave pattern in the SiO_2 layer, which depends upon photon energy.

The photoionization cross section σ_p is a function of the trap energy level E in the SiO_2 band gap (E=0 and E_g at the top of the SiO_2 valence band and the bottom of the conduction band, respectively) and of the photon energy $\hbar\omega$ since it includes the transition probability to a final state $E+\hbar\omega$, and may be position dependent through variation of the electric field due to the presence of charge in the SiO_2 layer. The field dependence of σ_p was experimentally found to be weak and is, therefore, neglected here.

It was concluded from discharging experiments [4], that the charge centroid $\bar{x}$ (measured

from the Al-SiO_2 interface) is constant in time and that, if an energy spectrum of trapping centers is present, they all have the same spatial charge distribution centroid. These two observations allow us to separate the variables determining n_t, i.e.

$$n_t(x,E,t) = n_t^{o}(t)\, n_t^{1}(E)\, n_t^{2}(x), \tag{2}$$

where n_t^1 and n_t^2 are normalized distributions. For the spatial distribution $n_t^2(x)$ a Gaussian is used with the charge centroid as median value and the same standard deviation as for the ion distribution.

Equation 1 is integrated over the oxide thickness L and over the SiO_2 energy gap, using the expression for the flat-band voltage shift:

$$\Delta V_{FB}(t) = q(\bar{x}/\varepsilon)\int_o^L\int_o^{E_g} n_t(x,E,t)dEdx, \tag{3}$$

where ε is the static permittivity of SiO_2 and q is the electron charge. At a particular photon energy ($\hbar\omega$), only centers between $E=E_g-\hbar\omega$ and $E=E_g$ can be depopulated, if thermal broadening of the trapping levels and two-photon processes are disregarded. We thus get:

$$d[\Delta V_{FB}(t)]/dt = -\Delta V_{FB}(t)\int_o^L F_p(x,\hbar\omega)n_t^2(x)dx\int_{E_g-\hbar\omega}^{E_g}\sigma_p(E,\hbar\omega)n_t^1(E)dE. \tag{4}$$

Let
$$\chi(\hbar\omega) = \int_o^L F_p(x,\hbar\omega)\, n_t^2(x)\, dx \tag{5a}$$

$$\text{and } \Sigma(\hbar\omega) = \int_{E_g-\hbar\omega}^{E_g}\sigma_p(E,\hbar\omega)\, n_t^1(E)\, dE, \tag{5b}$$

where $\chi(\hbar\omega)$ is the convolution of the photon flux with the spatial distribution of the trapping centers and $\Sigma(\hbar\omega)$ is the convolution of the photoionization cross section with the optically accessible trap distribution over energy. The latter quantity will be viewed as an effective photoionization cross section. If a single monoenergetic trap is involved, then $\Sigma(\hbar\omega)$ reduces to $\sigma_p(\hbar\omega)$.

The solution to eq. 4 can be approximated as:

$$[\Delta V_{FB}(0)-\Delta V_{FB}(t)]/\Delta V_{FB}(0) = \chi(\hbar\omega)\Sigma(\hbar\omega)t \quad (6)$$

if

$$t << [\chi(\hbar\omega)\Sigma(\hbar\omega)]^{-1}. \quad (7)$$

If long discharging times were used, the charge centroid would ultimately be determined by the minimum in the standing wave pattern of the light. However, since the illumination interval t was kept small compared to the discharging time constant, we may disregard the effect of light interference upon the charge centroid.

Since the variation in flat-band voltage shift due to illumination for a period t can be measured and the quantity $\chi(\hbar\omega)$ can be calculated knowing the sample geometry, the optical constants of the various materials of the multilayer structure, the incident photon flux and the light energy used, the effective photoionization cross section $\Sigma(\hbar\omega)$ can be determined from Eq. 6.

RESULTS

The photo I-V technique which is a sensitive method of determining both the density and the centroid of oxide charges [7], was initially used to ascertain that the negative oxide charge is removed by exposure to light, and not compensated by positive charge [4]. It was also experimentally verified that the discharging phenomenon obeys first order kinetics, and that the discharging time constant is long compared to the illumination time [4]. Figures 1 and 2 display the effective photoionization cross section spectra, respectively for P and As implanted samples, for which the experimental parameters are summarized in Table 1. All the samples were implanted with a fluence of 1×10^{13} cm^{-2}, except for wafer P8C, which was implanted with 3×10^{13} P^+/cm^2. In the latter case, partial penetration of the P ions into the Si substrate

was taken into account. In view of the low doping level of the SiO_2 introduced by the ion implantation, we used the optical constants for unimplanted SiO_2 in the calculation of the standing wave pattern. Incorporating the finite band-pass of the monochromator (50 Å full width at half maximum) into the analysis reduces the magnitude of $\Sigma(\hbar\omega)$ in Figs. 1 and 2 by 25-40 %, the larger correction being for higher photon energies, without changing the observed structure in the spectra.

DISCUSSION

The nature of the traps that exist in the ion-implanted samples cannot be determined in a direct way. Because of the high annealing temperature used after implantation, it is very likely that all major structural damage in the SiO_2 is healed. Therefore, we consider trapping levels related to the implanted ions themselves rather than due to the damage.

At first, one might expect that P would occupy Si sites and form phosphate-type clusters, as is the case when P is diffused-in instead of implanted. That is possible, but P and As at Si sites would act as donors and not as electron traps and would, therefore, go undetected in our experiments. On the other hand, a simple tight-binding model for substitutional impurities in SiO_2, based on the bond-orbital description of the bulk material [8], reveals that P and As are very likely to be substitutional at O sites. An energy level diagram describing P at an O site is shown in Fig. 3. The energy separation between the O 2p and P 3p levels is about 5.8 eV [9]. The P 3p orbitals bond with the neighboring Si hybrid orbitals and, as a result, two levels are expected at midgap. The lower level contains two electrons, whereas the upper level contains only one, and would, therefore, act as an electron trap. Photoionization of this electron would have a threshold at approximately 3.7 eV, which is close to that observed. Above threshold, a resonance corresponding to the atomic P 3p $\rightarrow$ 4s transition is expected, in analogy with the optical spectrum of the pure material [20]. Such a resonance may be present in the data of Fig. 1. According to the same model, As at an O site would behave just like P with the only exception that the level in the gap will be approximately 0.4 eV lower in energy. The data of

Fig. 2 show that the As threshold is 0.2-0.3 eV higher than that of P, in agreement with the theoretical prediction. We feel that these results suggest that the observed traps are P and As at O sites, but we cannot at present exclude other possibilities.

If our model is correct, we expect the photoionization cross section above threshold to be insensitive to implantation energy and oxide thickness. As observed in Figs. 1 and 2, the analysis indeed compensates for implantation energy, but not completely for oxide thickness. Our experimental oxide thickness range allowed us to perform accurate flat-band voltage measurements on MOS devices, but on the other hand was shown to introduce a strong sensitivity due to minute thickness variations in the interference calculation. In view of this, the structure in the spectra has to be considered preliminary. Experiments are in progress with thinner oxide layers (200-300 Å), in which case the influence of oxide thickness variations upon the photoionization cross section spectrum should be minimized.

ACKNOWLEDGEMENTS

The authors wish to express their gratitude to D. R. Young for stimulating discussions; D. R. Young and M. I. Nathan for a critical reading of the manuscript; B. Yun for the design of the flat-band voltage tracking system; the Silicon Process Studies Group for the sample preparation; E. D. Alley for the metallizations; and J. A. Calise and F. L. Pesavento for the experimental assistance.

REFERENCES

1. F. J. Feigl, S. R. Butler, D. J. DiMaria, and V. J. Kapoor, in (1976) Thermal and Photostimulated Currents in Insulators, ed. D. J. Smyth, The Electrochemical Society, Princeton, p. 118.
2. S. R. Butler, F. J. Feigl, Y. Ota, and D. J. DiMaria, in (1976) Thermal and Photostimulated Currents in Insulators, ed. D. J. Smyth, The Electrochemical Society, Princeton, p. 149.
3. D. J. DiMaria, D. R. Young, R. F. DeKeersmaecker, W. R. Hunter, and C. M. Serrano, The Electrochemical Society Fall Meeting, Atlanta, 1977, Abstract No. 212 (unpublished).
4. R. F. DeKeersmaecker and D. J. DiMaria (unpublished).
5. E. H. Nicollian and C. N. Berglund, J. Appl. Phys. 41, 3052 (1970).
6. D. J. DiMaria and P. C. Arnett, IBM J. Res. Develop. 21, 227 (1977).
7. D. J. DiMaria, J. Appl. Phys. 47, 4073 (1976).
8. S. T. Pantelides and W. A. Harrison, Phys. Rev. B 13, 2667 (1976); S. T. Pantelides, J. Vac. Sci. Technol. 14, 965 (1977).
9. F. Herman and S. Skillman, (1963) Atomic Structure Calculations, Prentice-Hall, Englewood Cliffs.
10. S. T. Pantelides, "The Optical Absorption Spectrum of SiO_2," Proceedings of the Int. Topical Conference on the Physics of SiO_2 and its Interfaces, Yorktown Heights, March 22-24, 1978 (unpublished).

Table 1. Experimental Parameters for the Samples.

Sample	Ion	Oxide thickness (Å)	Aluminum thickness (Å)	Ion energy (keV)	Charge centroid (Å)	Ion standard deviation (Å)
PE	P	1283	135	30	420	142
PG	P	1277	140	40	545	181
P8C	P	583	106	25	290	121
AS7D	As	1433	120	60	470	118
AS7G	As	1415	120	80	570	149
AS4X	As	1272	150	60	465	118
AS8D	As	559	134	20	185	51

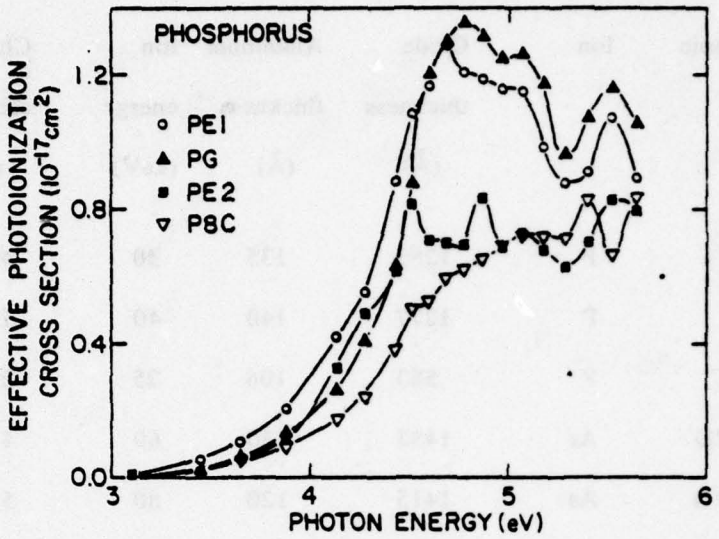

Fig. 1. Effective photoionization cross section spectra for P implanted SiO_2.

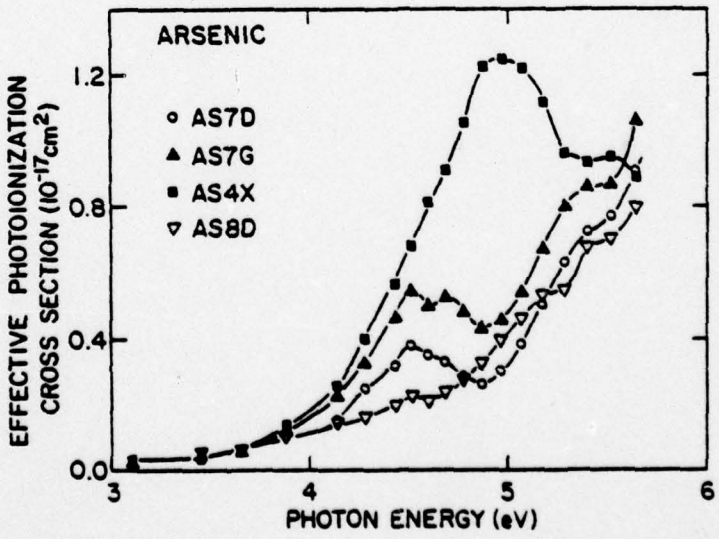

Fig. 2. Effective photoionization cross section spectra for As implanted SiO_2.

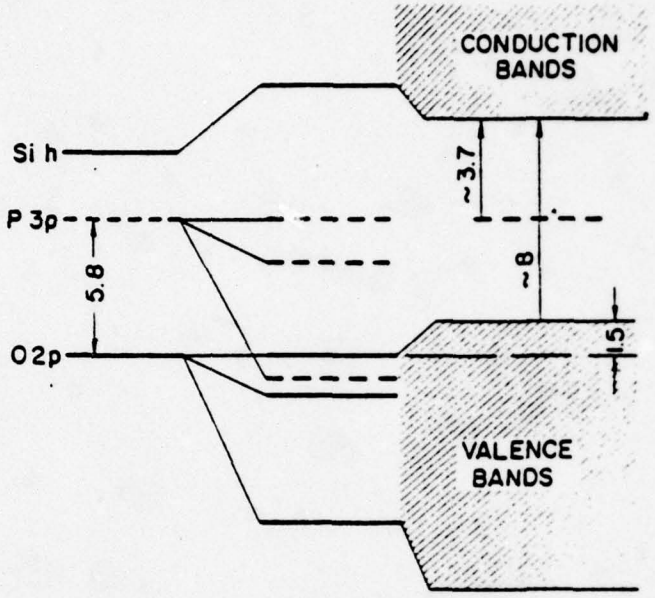

Fig. 3. Bond-orbital energy-level structure for SiO_2:P. The gap marked ~8 eV corresponds to the onset of absorption (not the band gap), so that 3.7 eV is the predicted onset of absorption of the impurity.

RC 7161 (#30410) 4/27/78 (Rec'd 6/7/78)
Solid State Physics 5 pages

Research Report

CONTINUOUS-RANDOM-NETWORK MODELS FOR THE Si-SiO_2 INTERFACE*

Sokrates T. Pantelides

IBM T. J. Watson Research Center, Yorktown Heights, NY 10598

and

Marshall Long‡

Dept. of Physics, Yale University, New Haven, CT 06520

IBM Research Division
San Jose · Yorktown · Zurich

RC 7161 (#30410) 4/27/78 (Rec'd 6/7/78)
Solid State Physics 5 pages

CONTINUOUS-RANDOM-NETWORK MODELS FOR THE Si-SiO_2 INTERFACE*

Sokrates T. Pantelides

IBM T. J. Watson Research Center, Yorktown Heights, NY 10598

and

Marshall Long‡

Dept. of Physics, Yale University, New Haven, CT 06520

ABSTRACT: Continuous-Random-Network (CRN) models have been constructed in order to simulate the atomic arrangement of the Si-SiO_2 interface. It was found that models could be constructed with or without an SiO_x layer between the crystalline Si and the amorphous stoichiometric SiO_2. The atomic coordinates were relaxed using a computer program and a simple force model. In order to probe the width w of the SiO_x layer, additional O atoms were gradually inserted, thus reducing w, and a normalized elastic energy was monitored. Using a wide range of choices for the force constants, it was found that the elastic energy was always lowered as $w \to 0$.

*Work supported in part by the Office of Naval Research under Contract No. N00014-76-C-0934.

‡Participant, IBM Summer Student Program.

The stoichiometry of the Si-SiO_2 interface is a subject that has attracted considerable attention. The interface has been probed experimentally by a wide variety of techniques, many of which are discussed in a series of papers in these Proceedings. The main objective of such experiments is to determine the width of the SiO_x ($x \neq 2$) layer that may exist at the interface. A variety of results has been reported, ranging from less than 4 Å (Refs. 1 and 2) to 8 Å (Ref. 3), 12-15 Å (Ref. 4), 15-20 Å (Ref. 5), and so on. Much of this variation is due to the differences in experimental techniques and interpretation of results. For example, some of the techniques may alter the composition of the sample during measurement. Also, some techniques probe the scattering properties of *atoms*, whereas others probe the behavior of *electrons*, which may see a different effective width. This observation brings up the subject of *how to define* an appropriate width. One possibility is to

define the width strictly on the basis of stoichiometry. Even then a number of alternatives exist. Take, for example, an abrupt (100) interface. One would normally assume that such an interface has no SiO_x layer. However, as Stern[6] has pointed out, the Si atoms in the last crystallographic plane of atoms on the Si side are bonded to two Si atoms and to two O atoms, corresponding to SiO stoichiometry. [For a (111) interface this plane of atoms corresponds to $SiO_{0.5}$ stoichiometry.] Since it is only one plane of atoms, one might define the width to be the distance between atoms on either side of that plane, which is about 3 Å.

Another possibility is to define the width having in mind the behavior of electrons. Clearly, even if one had an abrupt interface, electrons in the vicinity of the first few layers, including core electrons, would not behave as bulk electrons do. One measure of the width could be taken to be the range over which the self-consistent potential is different from bulk values. Calculations by Baraff, Appelbaum, and Hamann have found this width to be very small for the Ge-GaAs interface. No calculations are available for the Si-SiO_2 interface. Other properties, such as the dielectric constant, which depend on excited states, may in fact exhibit differences from bulk values over an even wider range.

In this paper, we attempt to shed some light on the question of the interface stoichiometry by constructing continuous-random-network (CRN) models. This technique has been widely used in modeling the atomic structure of amorphous solids. In fact, pioneering work using CRN models was done for amorphous SiO_2 by Evans and King[8] and by Bell and Dean.[9] Later, the technique was used to study amorphous Si, Ge and other materials.[10-12]

In carrying out the present study we first built several models of amorphous SiO_2. We used the "Framework Molecular Models" manufactured by Prentice-Hall, Inc., of Englewood Cliffs, New Jersey. They consist of sturdy plastic tubing which can easily be cut to size and which fits snugly over the prongs of small metal units, representing atoms. The units used to represent Si atoms have four metal prongs pointing in tetrahedral directions. Oxygen atoms, which ought to have two prongs, were represented by small pieces of bare copper wire bent at an angle of 144°, which corresponds to the observed average angle for amorphous SiO_2.[13] Since, however, the plastic tubing was slightly bendable, the resulting Si-O-Si angles actually have a distribution about 144°. The Si-O bonds were represented by blue tubing cut to 1.6 inches, so that one inch corresponds to 1 Å. Every Si atom was always connected to four O atoms in the tetrahedral directions, and every O atom was always connected to two Si atoms in order to maintain proper stoichiometry. No excessive bending of the plastic tubing connecting atoms was allowed. O atoms were not allowed to approach each other by less than about 2 inches (O nearest-neighbor atoms in crystalline SiO_2 are separated by about 2.5 Å). While in crystalline SiO_2 one finds only six-fold rings (counting an Si-O-Si unit as a "fold"), we allowed from four-fold to eight-fold rings.[9]

For the purpose of modeling the interface, we first had to choose an orientation for the crystalline Si substrate. We chose the (100) orientation because it is the one used most often in devices. We therefore constructed a substrate of several (100)

planes of crystalline Si. Red tubing cut to 2.35 inches was used for the Si-Si bonds (1 inch = 1 Å). The dimensions of the exposed surface were approximately 2 ft × 3 ft. The objective of the study was to continue this structure and build several layers of amorphous SiO_2.

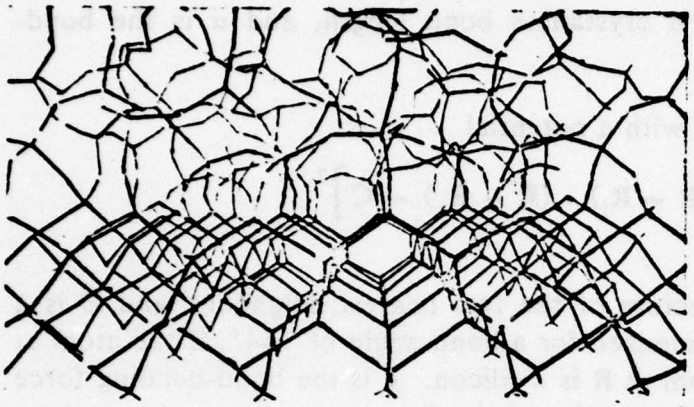

Fig. 1 A photograph of the Si-SiO_2 CRN model showing a stoichiometrically abrupt interface.

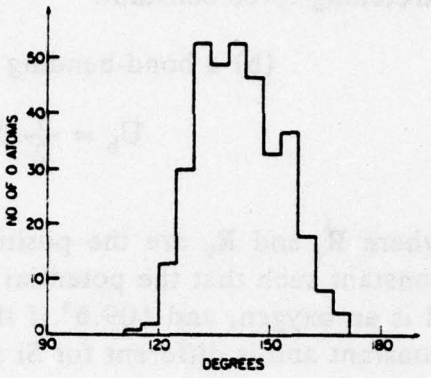

Fig. 2 A histogram of the Si-O-Si angle distribution.

At the first stage of our interface studies we relied totally on visual tests. Clearly, we could use both Si-Si bonds (red) and Si-O bonds (blue) and construct an SiO_x layer of arbitrary thickness. We could also allow an arbitrary amount of roughness.[3,14] Our objective was therefore to attempt to construct a model with an interface region which is as smooth as possible and as thin as possible, without excessive distortions of the bonds and without dangling bonds. Such an exercise would thus not answer the question of how thick the interface region actually is in real systems (it probably varies from sample to sample), but it would provide an indication as to how thin it *can* be and perhaps set a lower limit. Our initial work indicated that an SiO_x region of about 4-6 Å was necessary to avoid excessive distortions. We finally succeeded, however, in constructing a model with a completely abrupt interface, i.e., without an intermediate layer containing both red and blue bonds. The distortions of the bonds were similar to those of the other models. A photograph of this model is shown in Fig. 1. The conclusion that one reaches is that an abrupt interface in real samples is not ruled out by geometrical considerations and should be achievable, unless *energetic* considerations favor an interface with an SiO_x layer several Ångstroms thick.

In the second stage of our work we attempted to calculate which configuration would actually be favored by energetic considerations. For this purpose we used one of the CRN models which had an SiO_x interface region of about 6 Å. The coordinates of all the atoms were measured with a ruler to an accuracy of better than 0.1 inches. These coordinates were then used as a starting point in a computer relaxation program similar to the one used in Ref. 12. The total force on each atom was calculated as the sum of three types of forces:

(a) a bond-stretching force with a potential

$$U_s = \frac{1}{2}\alpha \sum_i \left[(R - R_i)^2 - R_0^2\right]^2$$

where **R** is the position vector of the atom of interest, R_i is the position vector of a nearest neighbor. R_o is the measured crystalline bond length, and α is the bond-stretching force constant.

(b) a bond-bending force with a potential

$$U_b = \frac{1}{2}\beta \left[(R - R_j) \cdot (R - R_k) - C\right]^2$$

where R_j and R_k are the position vectors of the two nearest neighbors, and C is a constant such that the potential is minimized for a bond angle of 144°, if the atom at **R** is an oxygen, and 109.6° if the atom at **R** is a silicon. β is the bond-bending force constant and is different for Si and O atoms (see below).

(c) a van der Waal's force with a Lennard-Jones potential with a cutoff:

$$U_{LJ} = -\frac{A}{|R-R_i|^6} + \frac{B}{|R-R_i|^{12}} \qquad |R - R_i| \le R_c$$

$$= 0 \qquad |R - R_i| > R_c$$

The main role of this force is to keep the O atoms from going too close to one another. The above forces are certainly not the totality of forces on atoms in solids. They are, however, a minimal set needed for a stable solid and have been found to work well within the context of CRN models.[12] The choice of force constants will be discussed later.

In the relaxation procedure, each atom was displaced in turn toward its equilibrium position determined by the total potential $U = U_s + U_b + U_{LJ}$. This was done by computing the local gradient vector and moving the atom in the direction of the force by small steps. The cycle was repeated until the atoms approached a good approximation to equilibrium in both energy and position.

Once the coordinates of the original model were relaxed, a search was made by the computer to locate all the Si-Si bonds lying between 6 and 5 Å from the top layer of the crystalline Si substrate. Oxygen atoms were then inserted at the midpoints of all such bonds and the relaxation program was run again. Fig. 2 shows a typical histogram for the Si-O-Si angle after relaxation. Once equilibrium was reached, the final elastic energy was recorded. Si-Si bonds lying between 5 and 4 Å were then eliminated by inserting oxygen atoms and relaxing. The procedure was repeated for each successive inch until all Si-Si bonds above the top layer of the substrate were eliminated. The result for our initial choice of force constants indicated that the

elastic strain energy decreased as the width of the SiO_x region was decreased. The same result was obtained for the elastic distortion energy of the entire system and also for a bond-normalized elastic distortion energy.[15] We therefore repeated the entire procedure for a wide range of force constants within physically acceptable limits. In all cases an abrupt interface was preferred.

The final conclusion of this work is that an abrupt interface is not ruled out by either geometric or energetic considerations at T = 0° K. The model we used is not reliable enough to allow us to conclude that the abrupt interface would in fact be formed under realistic growing conditions at finite temperatures. The effect of impurities, defects, such as dangling bonds, finite temperature, and other factors would have to be included before a more definite conclusion can be reached.

REFERENCES

1. J. Maserjian, **J. Vac. Sci. Technol. 11**, 996 (1974).
2. T. H. DiStefano, **J. Vac. Sci. Technol. 13**, 856 (1976).
3. C. R. Helms and W. E. Spicer, **Solid State Commun.**, in press.
4. S. I. Raider and R. Flitsch, **J. Vac. Sci. Technol. 13**, 58 (1976).
5. W. L. Harrington, R. E. Honig, A. M. Goodman, and R. Williams, **Appl. Phys. Lett. 27**, 644 (1975).
6. F. Stern, **Phys. Rev. B 17** (May 15, 1978).
7. G. A. Baraff, J. A. Appelbaum, and D. R. Hamann, **Phys. Rev. Lett. 38**, 37 (1977).
8. D. L. Evans and S. R. King, **Nature 212**, 1353 (1966).
9. R. J. Bell and P. Dean, **Nature 212**, 1354 (1966); **Phil. Mag. 25**, 138 (1972).
10. D. E. Polk, **J. Non-Cryst. Solids 5**, 365 (1971).
11. P. Steinhardt, R. Alben, M. G. Duffy, and D. E. Polk, **Phys. Rev. B 8**, 6021 (1973).
12. M. Long, P. Galison, R. Alben, and G. A. N. Connell, **Phys. Rev. B 13**, 1821 (1976).
13. R. L. Mozzi and B. E. Warren, **J. Appl. Crystallogr. 2**, 164 (1969).
14. J. S. Johanessen, W. E. Spicer, and Y. E. Strausser, **J. Appl. Phys. 47**, 3028 (1976).
15. The procedure of monitoring only the changes in the strain energy is equivalent to assuming that the extra oxygen atoms at the interface were taken from the outside of the cluster, where they were bonded with no strain at all.

RC 7163 (#30690) 6/7/78
Solid State Physics 42 Pages

Research Report

SCATTERING-THEORETIC APPROACH TO THE ELECTRONIC STRUCTURE OF SEMICONDUCTOR SURFACES - THE (100) SURFACE OF TETRAHEDRAL SEMICONDUCTORS AND SiO_2

J. Pollmann†

and

Sokrates T. Pantelides

IBM Thomas J. Watson Research Center
Yorktown Heights, New York 10598, USA

Typed by Marilyn Salvatore on CMC (SP.2108)

IBM Research Division
San Jose · Yorktown · Zurich

RC 7163 (#30690) 6/7/78
Solid State Physics 42 Pages

SCATTERING-THEORETIC APPROACH TO THE ELECTRONIC STRUCTURE OF SEMICONDUCTOR SURFACES – THE (100) SURFACE OF TETRAHEDRAL SEMICONDUCTORS AND SiO_2*

J. Pollmann†

and

Sokrates T. Pantelides

IBM Thomas J. Watson Research Center
Yorktown Heights, New York 10598, USA

Typed by Marilyn Salvatore on CMC (SP.2108)

ABSTRACT

We report the development of a method for calculating the electronic structure of semiconductor surfaces. It is based on the Koster-Slater idea for treating localized perturbations, which was later extended to describe surfaces. The present method makes use of semi-empirical tight-binding Hamiltonians and of a novel way to create free surfaces. A Green's function scattering-theoretic formulation is employed. The properties of the bulk crystal are built in and preserved. Bound-surface-state energies are determined unambiguously and accurately even for states whose wavefunctions are very extended. The total and local changes occurring in the density of states due to the surface can be calculated directly and therefore very accurately, without having to subtract two large quantities. Some of the structure in the state-density changes is in the form of narrow peaks, which can be identified as resonances or antiresonances. In order to point out advantages of the method and to compare our results with the results of slab calculations, we present applications to the Si and Ge (100) free surfaces. The present method is shown to be very efficient, accurate and fast. Despite the fact, that a tight-binding Hamiltonian of a truly semi-infinite system is treated exactly, the method employs matrices which are much smaller than those arising in slab calculations. Finally, the method is applied to a study of the (100) surfaces of the isoelectronic series Ge-GaAs-ZnSe and to the (100) surface of cubic SiO_2.

* Work supported in part by the Office of Naval Research under contract No. N00014-76-C 0934

† permanent address: Institut für Physik der Universität Dortmund, D-4600 DORTMUND-50, Pf 500 500, W. Germany

LIMITED DISTRIBUTION NOTICE

This report has been submitted for publication elsewhere and has been issued as a Research Report for early dissemination of its contents. As a courtesy to the intended publisher, it should not be widely distributed until after the date of outside publication.

Copies may be requested from:
IBM Thomas J. Watson Research Center
Post Office Box 218
Yorktown Heights, New York 10598

I. INTRODUCTION

The problem of the electronic structure of solid surfaces has attracted considerable attention during the last several years.[1-6] A variety of methods have been developed and used to study surfaces of metals and semiconductors. These methods belong to one of four general categories: (a) methods that simulate the semi-infinite solid with a finite number of atoms[7-10] (cluster methods); (b) methods that simulate the semi-inifinte solid with a finite number of atomic layers having two-dimensional periodicity[11-24] (slab methods); (c) methods that solve the Hamiltonian of the semi-infinite crystal directly (wavefunction-matching method[25-28]; Green's function matching method[29-35]; transfer-matrix or continued fraction method[36-42]); and (d) methods that treat the creation of a surface as a perturbation of an otherwise perfect infinite solid.[43-53] All the above methods may be used with a variety of one-electron Hamiltonians (semi-empirical, Hartree-Fock, self-consistent pseudopotential, etc.) together with one of many possible basis sets in terms of which the wavefunctions are expanded (plane waves, atomic orbitals, muffin-tin orbitals, etc.)

All four classes of methods have been used widely in studies of ideal model systems as well as studies of real materials. For semiconductors, calculations have thus far been done in terms of only the first three classes of methods. Methods belonging to the fourth class, i.e. those treating the creation of a surface as a perturbation of the otherwise infinte perfect crystal, have been formulated by several authors, in all cases making use of Green's functions. Applications have been mainly on ideal systems that simulate no real material and on the so-called jellium model used to simulate simple metals.[54,55] More recently, limited applications of such methods have been reported for surface states of some transition metals.[50,52]

In this paper we develop a method which treats the creation of a surface as a perturbation and is particularly suited for semiconductors and insulators. Its foundations are the same as those of the methods used or discussed in Refs. (43)-(53), in that it is based on a Green's function formulation of scattering theory. It therefore has a number of distinct advantages. It

deals with a truly semi-infinite solid, instead of a finite cluster of atoms or finite number of layers. As a consequence, the band continua are described in terms of continuous functions, instead of being simulated by a set of discrete states. Furthermore, the changes produced in the electronic structure of the infinite solid by the creation of the free surface are obtained directly, thereby avoiding the subtraction of two large quantities. From the computational point of view, it deals with matrices whose size is determined by the range of the potential change due to the surface. In contrast, cluster and slab methods deal with matrices whose size is determined by the range of surface-state wavefunctions, which is almost always considerably larger.

In our particular formulation, a semi-empirical linear-combination-of-atomic-orbitals (LCAO) representation is used as in Refs. (43-45, 47-53) but a novel way of creating the surface is introduced, which allows the surface perturbation to be represented by very small matrices. More specifically, the matrices encountered in our method are usually an order of magnitude smaller than corresponding slab matrices.

The plan of this paper is as follows. In Sec. II we give the general results of scattering theory in solids, as it has been developed by Callaway,[56] Garcia-Moliner[57] and others, and give the general form of the equations in an LCAO representation. The equations are then specialized for perturbations which, like surfaces, have two-dimensional periodicity. Finally, the form of the perturbation which corresponds to the creation of a surface is described and the method of calculation is discussed. In Sec. III we present applications of the method to the Si and Ge (100) surfaces using the same Hamiltonian employed by Pandey and Phillips[13,58] in slab calculations in order to make a direct comparison and demonstrate the power of the present method to describe real materials. In Sec. IV we apply the method to a study of the (100) surfaces of the isoelectronic series Ge-GaAs-ZnSe and of SiO_2. We end with the conclusions in Sec. V. Details of the calculations are given in a series of Appendices.

II. SCATTERING-THEORETIC FORMALISM

A. General Results

Let H° be a one-electron Hamiltonian describing an infinite periodic solid. The corresponding eigenvalue problem,

$$H^\circ \psi^\circ_{n\underline{k}} = E^\circ_{n\underline{k}} \psi^\circ_{n\underline{k}} \quad . \tag{1}$$

yields the energy bands $E^\circ_{n\underline{k}}$ and the corresponding Bloch functions $\psi^\circ_{n\underline{k}}$. The one-particle Green's function G° of this system is defined for outgoing waves by

$$G^\circ(E) = \lim_{\epsilon \to 0^+} \frac{1}{E+i\epsilon-H^\circ} = \frac{1}{E^+-H^\circ} \tag{2}$$

where the superscript + on E in the second form is a short-hand notation for the full expression involving the limit as $\epsilon \to 0$ from above. The operator G° can also be conveniently expressed in terms of the complete set of Bloch eigensolutions of H° as

$$G^\circ(E) = \sum_{n\underline{k}} \frac{|\psi^\circ_{n\underline{k}}><\psi^\circ_{n\underline{k}}|}{E^+-E^\circ_{n\underline{k}}} \tag{3}$$

As usual, the density of states of H° is given by

$$N^\circ(E) = -\frac{1}{\pi} \operatorname{Im} \operatorname{Tr} G^\circ(E) \, . \tag{4}$$

Now let U be any perturbation, and let

$$H = H^\circ + U \tag{5}$$

be the new one-electron Hamiltonian for the perturbed system. The new eigenvalue problem is

$$(H^\circ+U)\,\psi = E\,\psi \, , \tag{6}$$

and the solutions fall into two categories: States with energies within the forbidden gaps of

the spectrum of H°, and states within the band continua. One therefore usually seeks to determine the positions of the discrete states in the band gaps and the changes produced in the density of states within the band continua.

For states in the band gaps one can immediately rewrite (6) in the form

$$(1-G^\circ U)\,\psi = 0\,. \tag{7}$$

If ψ is expanded in terms of an orthonormal basis set ϕ_α, i.e.

$$\psi = \sum_\alpha c_\alpha\,\phi_\alpha\,, \tag{8}$$

eq. (7) can be transformed to a set of linear algebraic equations for c_α

$$\sum_\beta \left[\delta_{\alpha\beta} - \sum_\gamma G^\circ_{\alpha\gamma}(E)\,U_{\gamma\beta}\right] c_\beta = 0\,, \tag{9}$$

where the Green's function in the $\{\phi_\alpha\}$ representation is directly obtained from eq. (3):

$$G^\circ_{\alpha\beta}(E) = \sum_{n\underline{k}} \frac{\langle\phi_\alpha|\psi^\circ_{n\underline{k}}\rangle\langle\psi^\circ_{n\underline{k}}|\phi_\beta\rangle}{E-E^\circ_{n\underline{k}}} \tag{10}$$

From eq. (9), bound states correspond to zeros of the determinant

$$D(E) = \det \parallel \delta_{\alpha\beta} - \sum_\gamma G^\circ_{\alpha\gamma}(E)\,U_{\gamma\beta} \parallel\,. \tag{11}$$

An important feature of this result is that the effective order of the determinant in eq. (11) is equal to the order of the matrix U, so that the method is particularly suitable for short-range perturbations. The scattering-theoretic aspect of this approach is quite obvious in that, in more formal terms, equation (11) actually determines the discrete poles of the scattering matrix. The process under consideration here is, of course, the scattering of Bloch waves by the perturbation potential creating the surface.

Once the bound-state energy is determined from equation (11), the corresponding wave function is calculated from equation (9).

The change in the density of states $\Delta N(E) = N(E) - N^{\circ}(E)$ within the bands, is obtained by first defining the Green's function G(E) for the perturbed system by

$$G(E) = \frac{1}{E^{+}-H} \tag{12}$$

and relating it to $G^{\circ}(E)$ by Dyson's equation, i.e.

$$G = G^{\circ} + G^{\circ}UG\,. \tag{13}$$

The new density of states is given by

$$N(E) = -\frac{1}{\pi}\,\mathrm{Im\ Tr}\ G(E)\,. \tag{14}$$

The change in the density of states $\Delta N(E)$ can now be conveniently written as

$$\Delta N(E) = \frac{1}{\pi}\,\frac{d\delta(E)}{dE}\,, \tag{15}$$

where the quantity $\delta(E)$ is the phase shift, given by

$$\delta(E) = -\tan^{-1}\,[\mathrm{Im}\ D(E)/\mathrm{Re}\ D(E)] \tag{16}$$

where D(E) is as defined by eq. (11). It should be noted, that $\Delta N(E)$ depends only on G° and U, so that its evaluation does not require the solution of Dyson's equation (13). Equation (16) shows that $\delta(E)$ goes through an odd multiple of $\pi/2$ every time Re D(E) = 0. If such an energy is labeled E_o, one may then expand D(E) in the vicinity of E_o to obtain the corresponding contribution to the change in the density of states in a Lorentzian form centered at E_o

$$\Delta N(E) = \frac{\Gamma}{2\pi}\quad\frac{1}{(E-E_o)^2+\Gamma^2/4}\,, \tag{17}$$

with the half-width Γ given by

$$\Gamma = \frac{2\ \mathrm{Im}\ D(E_o)}{\mathrm{Re}\ D'(E_o)}\,. \tag{18}$$

In (18), the prime denotes differentiation with respect to energy. When $\Gamma>0$, $\Delta N(E)$ corresponds to a resonance of half-width Γ, whereas when $\Gamma<0$, $\Delta N(E)$ corresponds to an antiresonance with half-width $|\Gamma|$. Notice that the same expressions apply within the gaps where Im $D(E) = 0$ so that $\Gamma=0$ and eq. (17) reduces to a δ-function indicating a discrete state.

$\Delta N(E)$ satisfies the important sum rule

$$\int_{-\infty}^{\infty} \Delta N(E) = 0 , \tag{19}$$

known as Levinson's theorem. When the discrete states in the gaps are counted separately, (19) becomes

$$\int_{\text{bands}} \Delta N(E) = - N_b \tag{20}$$

where N_b is the number of discrete states in the gaps.

The relation for the discrete states, eq. (9), as it applies to point defects in semiconductors was first derived by Koster and Slater.[59] A more general treatment has been given by Callaway[56] and by Garcia-Moliner.[57] Callaway employed Wannier functions for the set ϕ_α, which are convenient for general analytical results but very cumbersome for actual calculations. More recently, the problem was formulated in terms of LCAO basis sets in the above fashion by Bernholc and Pantelides,[60] who used the method to calculate the electronic structure of the vacancy in several semiconductors. Here, we turn to surface-related problems and study an arbitrary perturbation that retains two-dimensional periodicity. Before we proceed further, however, we must introduce some necessary LCAO terminology.

B. LCAO Representation – Planar Perturbations

In order to describe a perfect infinte crystal in an LCAO representation, we introduce atomic-like orbitals on each atom in the primitive unit cell and denote them by $\varphi_\alpha(\underline{r}-\underline{\tau}_\nu)$, where $\underline{\tau}_\nu$ are the positions of the atoms in the unit cell and α labels the s, p ... etc. character of the

orbitals. For the purpose of solving for the eigensolutions of H° we first define the Bloch sums

$$\chi_{\underline{k}}^{\alpha\nu}(\underline{r}) = \frac{1}{\sqrt{N_3}} \sum_j e^{i\underline{k}\cdot(\underline{R}_j+\underline{\tau}_\nu)} \varphi_\alpha (\underline{r}-\underline{R}_j-\underline{\tau}_\nu) \tag{21}$$

where $\underline{R}_j$ are the Bravais lattice vectors and N_3 is the number of Bravais lattice points in the 3-dim. bulk lattice. The Bloch functions are then expanded as follows:

$$\psi^\circ_{n\underline{k}}(\underline{r}) = \sum_{\alpha\nu} C^n_{\alpha\nu}(\underline{k})\, \chi_{\underline{k}}^{\alpha\nu}(\underline{r}) \,. \tag{22}$$

Upon diagonalization of the secular matrix $\langle \chi_{\underline{k}}^{\alpha\nu} | H^\circ | \chi_{\underline{k}}^{\alpha'\nu'} \rangle$ at each $\underline{k}$, one obtains the eigenvalues $E^\circ_{n\underline{k}}$ and the corresponding eigenvectors $C^{\alpha\nu}_{n\underline{k}}$, which define the Bloch functions. In the applications to be presented in this paper, the matrix elements $\langle \varphi_{\alpha j\nu} | H^\circ | \varphi_{\alpha' j'\nu'} \rangle$ which are needed to construct $\langle \chi_{\underline{k}}^{\alpha\nu} | H^\circ | \chi_{\underline{k}}^{\alpha'\nu'} \rangle$ are treated as parameters. The method has often been referred to as the Empirical Tight Binding Method (ETBM).

For an arbitrary perturbation U, one must first choose a basis set in terms of which to expand the new wavefunctions ψ, express the Green's function G°, evaluate the matrix of U, and proceed with the formalism described in the previous subsections. In early formulations of the problem, the Wannier functions were thought to be the natural set for localized perturbations. When an LCAO representation is used for the bulk band structure, however, the set of atomic orbitals $\{\varphi_\alpha\}$ has been shown to be a more natural and useful choice for point defects.[61] Along the same lines, for planar perturbations, it is natural to use the set $\{\varphi_\alpha\}$ and define <u>layer orbitals</u> in order to take advantage of the fact that the system retains two-dimensional periodicity. Because of this periodicity, a two-dimensional $\underline{q}$ vector is a good quantum number and layer orbitals are simply Bloch sums in two dimensions. They are defined by

$$\Phi_{\underline{q}}^{\alpha m\nu}(\underline{r}) = \frac{1}{\sqrt{N_2}} \sum_j e^{i\underline{q}\cdot(\underline{\rho}_j+\underline{\lambda}^m_\nu)} \varphi_\alpha(\underline{r}-\underline{\rho}_j-\underline{\lambda}^m_\nu) \tag{23}$$

where $\underline{\rho}_j$ are the lattice vectors of the two-dimensional Bravais lattice and $\underline{\lambda}^m_\nu$ are the position

vectors of the atoms in the two-dimensional unit cell. The number of Bravais lattice points in the 2-dim. lattice is denoted as N_2. The index m labels different planes of atoms and the index ν labels different atoms in the same plane. The above definition of layer orbitals is the same as that used for slab calculations in an LCAO representation. For convenience, we will occasionally use a composite index $\ell=(\alpha m\nu)$ for the layer orbitals.

States of the perturbed system are then expanded in terms of the layer orbitals

$$\psi_{s\underline{q}}(\underline{r}) = \sum_{\ell} A^{\ell}_{sq}\, \Phi^{\ell}_{\underline{q}}(\underline{r}) \qquad . \qquad (24)$$

where s numbers the various states at each $\underline{q}$. The Green's function G° and the perturbation matrix U can then be evaluated in the $\{\Phi^{\ell}_{q}\}$ representation at each $\underline{q}$, from which the determinant D(E), the bound states, the change in the state density $\Delta N(E)$, etc. can be determined.

C. Free Surfaces

The next task is to identify the perturbation U describing the creation of a free surface. There are essentially two ways to accomplish this task. One possibility is to "switch off" the interactions between orbitals on the atoms on a number of adjacent planes (Fig. 1a) so that two non-interacting semi-infinite solids are formed. Clearly, the number of planes involved in this procedure is determined by the number of nearest-neighbour interactions that are included in the tight-binding Hamiltonian H° of the bulk. For example, if only first-nearest-neighbour interactions are included in the bulk Hamiltonian, switching off the interactions between only two adjacent planes will accomplish the decoupling between the twin surfaces. The interaction between orbital α and orbitals β on two different atoms is formally switched off by simply setting $U_{\alpha\beta} = - H^{\circ}_{\alpha\beta}$. In this procedure both atoms become involved in the process of creating a surface.

An alternative way to create a free surface is to remove one or more layers of atoms so that again two non-interacting semi-infinite solids are formed (Fig. 1b). As it is clear from

Fig. 1, the number of atoms involved in creating the surface is now smaller (in most cases smaller by a factor of two). The "removal" of atoms is accomplished by simply setting their diagonal matrix elements to a constant u and then letting that constant go to infinity. This procedure was first introduced by Bernholc and Pantelides[60] in the case of the vacancy in a bulk semiconductor. In fact, the creation of a surface is equivalent to the introduction of a "planar vacancy" (in the case of nearest-neighbour coupling) or "planar divacancy" (in the case of next-nearest-neighbour coupling) etc. For example in a one-dimensional crystal with only nearest-neighbour interactions, a vacancy creates two non-interacting semi-infinite solids. Algebraically, the matrix elements of the perturbation U between atomic orbitals α and β are of the form

$$U_{\alpha\beta} = u\delta_{\alpha\beta} \tag{25}$$

for α and β on the atoms to be removed. With this form of perturbation and in the limit $u \to \infty$, the condition for bound states, eq. (11), becomes

$$\tilde{D}(E) = \det \| G^{\circ}_{\ell\ell'}(E) \| = 0 \tag{26}$$

where ℓ and ℓ' are layer orbitals on the planes of atoms to be removed. The change in the density of states $\Delta N(E)$ is given by the same expression (15) and (16) with D(E) replaced by $\tilde{D}(E)$ defined by eq. (26).

The new procedure of creating free surfaces, which we will refer to as the "removal method", has a number of distinct advantages over the previously used method, which we will refer to as the "switch-off method". (a) In the "switch-off" method one must set up the Green's function matrix and the nondiagonal perturbation matrix $U_{\ell,\ell'}$, whereas in the "removal method" it is sufficient to calculate the Greens' function matrix, as can be seen in equation (26). This result illustrates that the bulk Green's function contains complete information about the electronic structure of an ideal surface (i.e. no change of the bulk matrix elements up to the surface). (b) Computationally, the dimension of the resultant matrix in the

"removal method" is usually smaller by a factor two. (c) The Green's function matrix G° is Hermitian for the bound states, whereas $1-G^{\circ}U$, encountered in the "switch off" method is generally not. As a result, the labor may be reduced at various stages by at least a factor of four or eight.

In the above discussion we compared the relative merits of two different ways of constructing the perturbation that creates a free surface in the scattering-theoretic formalism. In either way, the relevant matrices are substantially smaller than the secular matrices encountered in slab calculations. In particular, as will be seen in the next section, the secular matrices of typical slab calculations are an order of magnitude larger than our Green's function matrices.

III. THE (100) SURFACE OF Si and Ge – COMPARISON WITH OTHER CALCULATIONS

In this section we present calculations of the electronic structure of the ideal (100) surface of Si and Ge in order to illustrate that calculations using the scattering-theoretic method described above are in fact rather straightforward for real materials and can easily provide a wealth of information.

The geometrical arrangement of the atoms for the 100 surface of Si is shown in Fig. 2. The axes shown are the crystallographic y and z axis. The two-dimensional unit cell is marked out by the dashed line; it contains one atom in each layer. The corresponding two-dimensional Brillouin zone is shown in Fig. 3. We will use the same ETBM Hamiltonian used by Pandey and Phillips[13,58] to study the (100) surface of Si and Ge so that a direct comparison will be possible. This Hamiltonian uses only s and p orbitals on every atom and retains only first- and some second-nearest neighbour interactions. The values of the parameters in standard notation are given in Table I. An ideal surface is then defined as an abrupt termination of the bulk crystal, keeping all the intra- and inter-atomic interactions unaltered. In this approxima-

tion, no new parameters are necessary for the calculation of the electronic structure of the free surface. The creation of the surface can be accomplished by removing two layers, as shown in Fig. 4.

A. Energy Levels of Bound Surface States

In the scattering-theoretic method, the first task is the evaluation of the projected band structure (PBS), i.e. the projection of the bulk bands $E_{n\underline{k}}$ with $\underline{k} = (\underline{q}, k_\perp)$ for each $\underline{q}$ in the surface Brillouin zone. The PBS is needed for the calculation of the G°-matrix (Appendix A), but it is also extremely useful in its own right. It allows one to identify all the gaps and "pockets" where a search must be made in order to determine the positions of states that are truly bound at the surface. We have calculated the PBS for Si (100) and Ge (100) and display them in Figs. 5 and 6. Instead of the usual practice of cross hatching the continuum regions uniformly, we display the actual projected eigenvalues at each $\underline{q}$ for a fixed set of $k_\perp$ values. These are precisely the subset of bulk states which would have to be used if the surface-state wavefunctions were to be expanded in terms of bulk Bloch functions. The distribution of points at each $\underline{q}$ in Figs. 5 and 6, therefore, provides visual information about which bands contribute more heavily to the formation of surface states. In particular it gives a visual impression of the density of bulk states at each $\underline{q}$.

Bound states in the gaps and pockets of the PBS are determined in an unambiguous way by searching for the zeros of $\tilde{D}_{\underline{q}}(E)$ given by

$$\tilde{D}_q(E) = \det \| \langle \Phi_{\underline{q}}^{\alpha m \mu} | G^\circ | \Phi_{\underline{q}}^{\alpha' m' \mu'} \rangle \| \qquad (27)$$

where, for the examples under consideration, the indices m and m′ run over only the <u>two</u> layers that are removed for the creation of the twin non-interacting semi-infinite solids (Fig. 4). The size of the relevant Green's function matrix is therefore 8×8 and can be evaluated with modest effort (Appendix A). The search for bound states can then be made by using an

efficient algorithm described in Appendix B. The results are shown as solid lines in Figs. 5 and 6. We will collectively refer to the surface bands as the surface band structure (SBS).

We turn now to a comparison of the above results with those obtained by Pandey[58] using the slab method in which the semi-infinite solid is simulated by a slab of finite thickness. For the (100) surfaces of Si and Ge Pandey[58] used 20 layers of atoms. The electronic states of the slab were then expanded in terms of layer orbitals and the corresponding secular matrix $\langle \Phi_{\underline{q}}^{\alpha m \mu} | H^{\circ} | \Phi_{\underline{q}}^{\alpha' m' \mu'} \rangle$ was set up and diagonalized at each $\underline{q}$. The size of the slab matrix is thus 80×80, which is an order of magnitude larger than the corresponding scattering-theoretic matrix of eq. (27). The slab matrix needs of course be diagonalized only once at each $\underline{q}$, instead of at a mesh of energies and furthermore the Hamiltonian matrix elements encountered in the slab method are easier to evaluate than the Green's function matrix elements. Nevertheless, the scattering theoretic method is less time-consuming if our way of creating the surface is used together with the efficient root-finding algorithm employed in our calculations. As for the actual results in Figs. 5 and 6, a comparison with the slab calculation shows excellent agreement. For highly localized states the surface state energies in the case of Si agree within better than 0.01 eV so that there was no reason to plot the slab results separately. In the case of Ge the same agreement is found for most of the states except for a rigid shift[62] of 0.06 eV. (States in the small pockets and the empty states in the conduction band were not reported in Ref. 58.) As one might expect, for extended states there are appreciable differences in the energy positions of surface states. One example is the surface state at Γ in Ge. We find that the state extends over more than 20 layers. Thus, it is not surprising, that the slab-calculation result deviates from our surface state-energy by 0.32 eV. Theoretically, these differences are significant in that we try to solve a given model problem as accurately as possible. Experimentally, extended states are difficult to detect, so that the slab method describes the experimentally interesting states satisfactorily. We will now turn to a discussion of surface state wavefunctions.

B. Surface-State Wavefunctions

The calculation of the wavefunction in our method is rather straightforward, and is described in detail in Appendix C.

In Figs. 7 and 8 we plot orbital sums of the wavefunction amplitude on each layer defined by

$$f^{m}_{sq}(E) = \sum_{\alpha} \| A^{m,\alpha}_{s,q}(E_s) \|^2 , \tag{28}$$

for several surface states of Si and Ge. In Fig. 7 we plot for comparison a number of wavefunctions with distinct behavior. Example 7a shows the wavefunction amplitude of a gap state which is completely localized in the surface plane. An orbital decomposition of $f^{m}_{s,q}(E)$ shows, that this state is 50% p_y- and 50% p_z- like. This type of bond acts like a link between surface atoms and is therefore referred to as the bridge bond. The second type of gap states usually encountered on a 100-surface in group IV semiconductors is the so called dangling bond. The wavefunction corresponding to the dangling-bond state at J is shown in Fig. 7b. The orbital decomposition of $f^{m}_{s,q}(E)$ for this state shows that it has predominantly s- and p_x-character, resulting in charge density that "dangles" perpendicular to the surface. A typical example for a backbond is given in Fig. 7c. This state is again very localized, but its amplitude is shared mainly by the first two layers indicating a charge buildup in the "back bond". Example 7d shows the wavefunction of an empty state in one of the tiny pockets in the conduction band part of the PBS. Such states lie very near the bulk energy continua and are therefore very extended. Similar states in the valence band pockets are more localized, but interestingly enough they are localized in the third to fifth layer.

When a surface state band approaches the bulk band projection, the states might, depending on the symmetry of their wavefunctions, become more and more extended. This is shown for the dangling-bond band in Ge between Γ and K in Fig. 8. At K (Fig. 8d) the wavefunction decays within 2 layers. As the surface band approaches the bulk band projection

(Figs. 8b and c) the wavefunction becomes more extended and eventually at Γ (Fig. 8a) it extends over more than 20 layers.

We have included in Figs. 7 and 8 a comparison between the surface state energies calculated by our method and by the slab method (energy values in parenthesis) for the states, whose wave functions we show. For highly localized states (see e.g. 7a, 7c, 8c, 8d) the energies are exactly the same in the two calculations. For extended states (7b, 8a, 8b) more or less pronounced deviations occur. For such states the slab method would have to employ thicker and thicker slabs. The accuracy of the scattering-theoretic method, remains unaffected by the extent of the wavefunctions, because it deals with a truly semi-infinite solid. Where the results of the two methods disagree, the scattering-theoretic method is to be viewed as more accurate.

C. Changes in State Densities – Surface Resonances

In addition to the bound surface states lying within the gaps and pockets of the PBS, the presence of a surface also induces changes in the density of states within the band continua. These changes can be calculated directly by using eq. (15). For the particular problem at hand we have

$$\Delta\tilde{N}_{\underline{q}}(E) = \frac{1}{\pi}\frac{d}{dE}\tilde{\delta}(E) \tag{28}$$

where

$$\tilde{\delta}_{\underline{q}}(E) = -\tan^{-1}\left[\mathrm{Im}\,\tilde{D}_{\underline{q}}(E)/\mathrm{Re}\,\tilde{D}_{\underline{q}}(E)\right] \tag{29}$$

The changes given by eq. (28), however, apply to the complete "algebraic" system, consisting of two semi-infinite solids and the "removed" layers with states at infinity. In particular, if we define $n_{\underline{q}}^{m}$ to be the new partial density of states for the m^{th} layer and $n_{\underline{q}}^{\circ}$ to be the partial density of states for any layer in the infinite bulk crystal, we have

$$\Delta\tilde{N}_{\underline{q}}(E) = \sum_{m}\left[n_{\underline{q}}^{m}(E)-n_{\underline{q}}^{\circ}(E)\right], \tag{30}$$

where the sum is over all the layers, including those "removed" by the perturbation. For the actual physical system of interest, i.e. a semi-infinite solid, the relevant quantity should not include the "removed" layers and their states at infinity. Leaving those terms out, we obtain

$$\Delta N_q(E) = [\Delta \tilde{N}_q(E) + 2n_q^\circ(E)]/2 \qquad (31)$$

where the factor 2 inside the square brackets corresponds to the number of removed layers and the division by 2 gives the final value for one semi-infinite solid.

Both quantities, i.e. $\Delta \tilde{N}_q(E)$ and $\Delta N_q(E)$ were calculated and found to satisfy Levinson's theorem: $\Delta \tilde{N}_q(E)$ integrates over the energy range of the bulk bands to -8 corresponding to the 8 states at infinity introduced by the "removal" perturbation and $\Delta N_q(E)$ integrates to zero. The number of states is thus conserved.

A typical $\Delta N_q(E)$ for Si at $q=(0.5, 0.5)\ 2\pi/a$ (the J point of the surface Brillouin zone see Figs. 3 and 5), broadened by 0.1 eV is given in Fig. 9. If comparison is made with Fig. 5, one observes that the spikes at 1.5 eV and -1 eV correspond to true surface states in the gap; the remaining structure corresponds to changes in the continuum density of states. Some of the structure can be identified as resonances and antiresonances, as discussed in Sec. II. For example, the negative spikes at -10 eV, -1.2 eV, and 4.3 eV are clearly antiresonances. The structure that appears in the range -8.5 eV to -5 eV looks rather peculiar. At first glance, one might view it as two neighbouring resonances giving rise to a twin-peak feature. Such an explanation is not adequate, however, because the integral of $\Delta N_q(E)$ over this range corresponds only to one extra state. More careful examination reveals that the structure corresponds to two resonances of about the same width plus a wider antiresonance between the two. The two negative dips are thus the remnants of the antiresonance tails. Therefore, the net change in the number of states in this energy region should be one, as it was indeed found to be. This structure, therefore, helps demonstrate the fact that the change in the continuum

density of states may be considerably more complicated than a mere succession of Lorentzian-type resonances and antiresonances.

If we integrate $\Delta N_{\underline{q}}(E)$ of Fig. 9 over the valence bands, i.e. up to about -1 eV (the top of the projected valence bands at J; see Fig. 5), we find that a total of one state has been removed. Similarly, if we integrate over the energy range of the projected conduction bands alone, we also find that a total of one state has been removed. The two missing states are of course balanced by the two states in the gap, and Levinson's theorem is satisfied. However, the finding also reveals that the two bound states are derived from both the valence and the conduction bands. This realization raises some questions about the validity of a semi-empirical Hamiltonian which is chosen to fit the valence bands very well while doing rather poorly for the conduction bands. It is plausible that the lower of the two gap states is determined predominantly by the valence bands and is thus quite reliable, while the upper state is determined by the conduction bands (this point is explored further in Sec. III D below). The most crucial test of a semi-empirical surface Hamiltonian is of course a comparison with the surface states obtained by self-consistent calculations, as pursued by Pandey,[58] who concluded that the results were quantitatively accurate.

In Fig. 10 we give the total change in the density of states $\Delta N(E)$, which was obtained by summing over $\underline{q}$ in the surface Brillouin zone. The main features can be understood by referring to Fig. 5. The states in the gap correspond primarily to what we described as the bridge-bond band. The peak at about -0.8 eV corresponds to the dangling-bond band, also shown in Fig. 5. Finally, the extra states at about -6 eV correspond to the surface band that runs from a point near K toward J' in Fig. 5.

We turn now to compare with the slab method once more. By its nature, the slab method is less suitable for the description of changes in the band continua because, unlike the scattering theoretic method, it simulates the continuum with a set of discrete states. In the case of the (100) surface of Si and Ge discussed here, the 80×80 slab secular matrix yields 80 energy

levels at each $\underline{q}$. A few of these correspond to the bound states in the gaps and pockets discussed earlier. Some of the remaining states which lie within the band continua may be identified as resonances if their wavefunctions exhibit localization. For example in Ref. 58 a resonance was found at the J point of Si (100) at −7 eV which is in the middle of the broad structure we discussed earlier (Fig. 9). We found that there are actually two resonances and an antiresonance within that region. It is clear that the procedure of examining slab wavefunctions is likely to miss both antiresonances and broad resonances. The latter correspond to charge localization building up from small contributions by states over a rather wide energy range.

One procedure that has been used in conjunction with slab calculations is to construct a histogram out of the discrete states. Such histograms for each $\underline{q}$ tend to be rather crude because of the small number of states. They become more meaningful for the total density of states when a sum over $\underline{q}$ is carried out. Note, however, that this procedure yields the total density of states for the perturbed system. One must subtract large similar total state densities for the perturbed and unperturbed systems in order to obtain the small changes due to the perturbation – a clearly error-prone procedure.

D. Local Densities of States

In the previous subsection we discussed the total changes in the density of states within the band continua. Those curves contain resonances, antiresonances and other structure, but convey no information about how localized these features are. What is needed is something analogous to the wavefunctions of bound states discussed in subsection B above. Such information at each $\underline{q}$ vector is contained in local densities of states which are defined for each layer by

$$N_\ell(q, E) = -\frac{1}{\pi} \operatorname{Im} \operatorname{Tr} G_{\ell\ell}(q, E) .$$

The calculation of these quantities needs the explicit determination of the new Green's function G in a layer-orbital representation. For this purpose, Dyson's equation [eq. (13)] must be solved. The procedure is given in detail in Appendix D. Typical results of such calculations are shown in Fig. 11, where $\underline{q}$ was chosen to be (0.5, 0.5), as was the case in Fig. 9. In Fig. 11a we display $N_\ell(q, E)$ beginning with the surface layer $\ell=1$ and continuing into the bulk to $\ell=7$, for which $N_\ell(q, E)$ becomes almost identical with the layer density of states in the bulk infinite crystal. The curves are broadened by 0.3 eV and contain the bound states in the gaps as well. In Fig. 11b we display the changes in the local density of states for each layer which illustrate more clearly the decay characteristics of the bound states, the resonances and antiresonances. In particular note that the bound state at 1.54 eV, whose wavefunction was shown in Fig. 7a, is once more seen in Fig. 11 to be localized in the first layer. In contrast, the bound state at −0.9 eV (Fig. 7b), is seen in Fig. 11b to extend over several layers. We also see in Fig. 11b that the prominent antiresonances at about −10 eV is localized within about three layers, whereas the broad feature between −6 and −8 eV, which we discussed in connection with Fig. 9, extends over more than seven layers. Note that for the first two layers, this feature appears to be a single broad resonance at about −7 eV, and was so identified in the slab calculation of Ref. 58. Fig. 11 confirms the interpretation of the broad feature as a sum of two resonances and one antiresonance, as discussed in subsection C above.

In conclusion, we find that the scattering-theoretic method provides a much more direct and accurate description of the changes in the continuum density of states than the procedures used in slab methods.

The Koster-Slater-type scattering-theoretic approach also has advantages over the transfer-matrix method.[42] Both these methods describe truly semi-infinite solids and the labour involved may be comparable. However in the transfer-matrix method one calculates the new Green's function directly, without making use of the unperturbed-crystal solutions, so that

changes in the electronic structure must be calculated by subtracting two large quantities as in slab techniques. Furthermore the calculation of the surface energy bandstructure in the transfer-matrix method is significantly more laborious as compared to the scattering theoretic approach.

E. An Alternate Calculation for Ge (100)

In addition to our calculation based on the Pandey, Phillips Hamiltonian for Ge, we have also performed surface state calculations for Ge (100) using the tight binding parameters of Chadi[63]. Chadi obtained a good fit to the Ge valence bands with only first-nearest-neighbour interactions (Table 1). By comparing our results of the two calculations we are able to arrive at several conclusions about the origins and the nature of the surface states.

The complete PBS and the surface states obtained with Chadi's parameters are given in Fig. 12, which should be compared with Fig. 6. It is clear that the valence-band projections are very similar in the two cases whereas the conduction-band projections are quite different. The first-nearest-neighbour parameters yield a conduction band with a width of 7 eV and its minimum at Γ. The second-nearest-neighbour Hamiltonian yields a conduction band with a width of 3.5 eV and its minimum at the L-point (which maps onto J and J'). It is also clear from Figs. 6 and 12 that the surface states obtained in the two cases are qualitatively similar. In the valence bands there is even quantitative agreement in both the energy position and dispersion. The dangling-bond band calculated with the Chadi Hamiltonian is shifted upward by only 0.3 eV, whereas the bridge-bond band is shifted upward by about 1.3 eV with respect to Fig. 6. The width of the bridge-bond band calculated with the first-nearest-neighbour Hamiltonian is smaller (.3 eV) than the width resulting from the second-nearest neighbour Hamiltonian (1.45 eV). These results suggest that the dangling-bond band is indeed derived mainly from the valence bands, whereas the bridge-bond band is derived mainly from the conduction bands. It should be noted, that in the first-nearest-neighbour approximation the bridge bond band lies at the atomic p-level energy. This is a direct consequence of the high

localization of the bridge bond and the fact, that neighbouring atoms in the (100) plane are second nearest neighbours.

IV. APPLICATIONS TO OTHER MATERIALS

A. The (100) Surfaces of Ge, GaAs, and ZnSe

In this section we apply the scattering-theoretic method to the (100) surfaces of the isoelectronic series Ge, GaAs, and ZnSe. This study will allow us to address a number of issues that arise in the application of the method to compound semiconductors. The materials were chosen in order to carry out a study of the variation of the surface electronic structure with increasing ionicity. Similar studies of the (110) and the (111) surfaces of this isoelectronic series have been done by others.[64-66]

We again use ETBM Hamiltonians as in Sec. III. For this study of qualitative trends, we use the first-nearest neighbour Hamiltonians given by Chadi[63] (Table 1).

The geometry for the zincblende semiconductors is the same as for Si or Ge (Figs. 1-4) except that we have alternate layers of anions and cations. For example, to create a Ga- or an As- terminated surface in GaAs, it is sufficient to remove one As or one Ga layer, respectively. This removal yields a 4×4 Green's function matrix and creates two inequivalent surfaces.[67] The left-hand semi-infinite solid is rotated about the x-axis by 90° compared to the right-hand semi-infinite solid with respect to their common y-z coordinate-system. As a result, the zeros of det $\| G^{\circ} \|$ yield singly degenerate states (except at Γ and K) corresponding to the two surfaces. The states on the two opposite surfaces are related by a simple 90° rotation, so that, e.g., the J point of the one surface corresponds to the J' point of the other, and vice versa. This complication may be avoided by removing two layers, namely a Ga and an As layer. The size of the Green's function matrix is increased to 8×8, but the energies of the surface states of both Ga- and As- terminated (100) surfaces are obtained from the zeros of one determi-

nant. The states of the two surfaces can then be distinguised by either examining the wave-functions or, even more simply, by performing a complementary calculation with 4×4 matrices (only one layer removed).

The surface band structure (SBS) for Ge (100), calculated in the first-nearest-neighbour approximation has already been given in Fig. 12 and was discussed in Section III D. Our results for the GaAs and the ZnSe (100) surfaces are shown in Figs. 13 and 14, where separate plots for the anion- and the cation-terminated surfaces are given.

The first result that is evident from Figs. 13 and 14 is that surface states of an anion-terminated surface tend to be within the valence band region. Conversely, surface states of a cation-terminated surface tend to be within the conduction bands. This result correlates nicely with the well known fact that bulk valence bands are dominated by anion-like states while conduction bands are dominated by cation-like states (see also Fig. 15). It also demonstrates that the character and energetic position of most surface states depend primarily on the nature of atoms in the first layer.

If we recall that our ETBM Hamiltonians describe bulk valence bands quite accurately and bulk conduction bands rather poorly, it follows immediately that our calculations of the SBS of the ideal anion-terminated surfaces are quite reliable, whereas the corresponding calculations of the SBS of the ideal cation-terminated surfaces are qualitative at best. We will therefore first discuss anion-terminated surfaces in detail and then make a few remarks about cation-terminated surfaces.

Both GaAs and ZnSe anion-terminated surfaces have a backbond-type band that lies entirely within the heteropolar gap. These states are highly localized and are predominantly anion s-like, very much like the bulk band immediately below them. These characteristics become more prominent as one goes from GaAs to ZnSe. Similarly, the dispersion of the

backbond-type surface band gets smaller with increasing polarity, as does the dispersion of the bulk band immediately below it.

Both GaAs and ZnSe have another backbond-type surface state that appears in the pocket around −4 to −6 eV. These states turn out to be more spread out and their dispersion decreases much more slowly along the isoelectronic series.

We turn now to the two surface bands in the fundamental gap. As in the case of Ge, the lower band has a dangling-bond character formed by s and p_x orbitals, whereas the upper band has a bridge-bond p_y-p_z character. In fact, the separation between the bridge bond and the dangling bond may be largely due to the presence of the s admixture in the latter. This is consistent with the fact that the average separation between the two types of states is smaller in ZnSe where the Se atomic s states is lower in energy than in As and thus does not admix as much. As for the dispersion of the two types of states, we note that the bridge-bond band is almost dispersionless and lies at the atomic p level, whereas the dangling-bond band has more dispersion through interactions mediated by the second layer.

Turning to the cation-terminated surfaces, Figs. 13 and 14 reveal that, qualitatively, a similar set of surface bands is obtained. As noted earlier, the bulk conduction bands are given rather poorly by the ETBM Hamiltonian used in our calculations. The two surface bands within the range of the projected conduction bands are therefore only qualitatively meaningful. The dangling-bond band of GaAs, however, which lies in the fundamental gap appears to agree rather well with the self-consistent results of Appelbaum, Baraff, and Hamann.[28] We investigated the origins of this state at sample $\underline{q}$ points by calculating $\Delta N_{\underline{q}}(E)$ and integrating it over the projected valence bands. The resulting integral was −1 indicating that the state is mainly derived from the valence bands, very much like the dangling-bond band of the (100) surfaces of Si and Ge and the anion-terminated (100) surfaces of GaAs and ZnSe. This finding suggests that the dangling-bond bands even of cation-terminated surfaces can be calculated fairly reliable in a first-nearest-neighbour approximation. Finally, the back-bond states

appearing in the valence band pocket of cation-terminated surfaces (Figs. 13 and 14) are probably derived totally from valence states and are therefore even more reliable.

B. The (100) Surface of SiO_2

In this section we study the Si- and the O- terminated (100) surfaces of the ideal cubic form of SiO_2, i.e. β-cristobalite. SiO_2 is an important technological material and is widely used as a substrate for depositing other substances. Knowledge of the surface electronic structure of this material might help understand the way it bonds with other substances. The study we present here is somewhat crude, since we calculate only surface states with the β-cristobalite geometry. On the other hand, studies based on β-cristobalite-like geometries have helped understand most electronic properties of bulk crystalline and amorphous SiO_2. We therefore expect that the present study of SiO_2 surfaces, which is the first to be attempted, will serve as a guide for more detailed understanding in the future.

The first-nearest-neighbour parameters (Table 1) used in the bulk ETBM Hamiltonian, were found by fitting to the SiO_2 bulk valence bands given in Ref. (68) and to a band gap of 9 eV.[69] The valence bands and the band gap are reproduced accurately by retaining only the Si-O and the O-O first-nearest-neighbour matrix elements. The Si-Si interactions are left out. The geometrical arrangement of the atoms for a Si-terminated (100) surface of SiO_2 is shown in Fig. 16, where we have depicted the first 8 layers, including the surface layer. The two-dimensional unit cell is again marked by a dashed line. It should be noted, that the unit cell contains one atom in each Si layer but two atoms in each O-layer. The point-group symmetry (C_{2v}) and the SBZ are the same as in the zincblende materials (Fig. 3).

The creation of two adjacent Si-terminated surfaces is accomplished by removing one O layer, yielding an 8×8 Green's function matrix (2 atoms per unit cell). The creation of two adjacent O-terminated surfaces cannot, however, be accomplished by removing only one Si layer, because the resulting two semi-infinite solids are still coupled via the first-nearest-

neighbour O-O interactions. In order to accomplish the desired decoupling, at least two layers (one Si and one O layer) must be removed. The result is a 12×12 Green's function matrix describing one Si-terminated surface and one O-terminated surface. The calculated states can then be sorted by comparing with the previously obtained states for the Si-terminated surface.

The projected valence bands of SiO_2 are shown in Fig. 17. The upper part of the projection, with a width of about 3 eV, results mainly from the nonbonding or "lone pair" O 2p-orbitals which lie perpendicular to the Si-O-Si chain. The lower part, with a width of about 7 eV, results mainly from the bonding O 2p-orbitals, which lie along the Si-O-Si chain. The bonding bands have the same overall structure as the valence bands of Si. The similarity in the corresponding parts of the projected band structures may be seen by compairing Figs. 17 and 5.

The surface states for the Si- and O-terminated (100) surfaces of cubic SiO_2 are shown in Figs. 17a and b. No bound surface states were found in the optical gap for either surface. The nonbonding bands are affected very little by the creation of the surface. No dangling-bond bands are split off, as expected, because there are no bonds to begin with. Instead, the states in the non-bonding bands are very much atomic in character, so that the creation of the surface is only a weak perturbation, as far as the lone pair orbitals are concerned. The bonding bands, on the other hand, show pronounced surface states, as one might expect, since bonds are broken by the creation of the surface.

For the Si-terminated surface (Fig. 17a) we find a number of surface states which are predominantly localized on the O 2p-orbitals in the O layer immediately below the surface Si layer. They are therefore best described as backbond states. The Si dangling-bond states are high in the conduction bands. Most of the backbond states lie very close to the bulk band projections and show similar dispersion. This behaviour may be explained by the fact that the O atoms in the strengthened backbonds retain all their Si neighbours and four out of their six O neighbours.

In the case of the O-terminated (100) surface (Fig. 17b), the perturbation has an even stronger effect. Two of the six O neighbours and one of the two Si neighbours of each surface-layer O atom are removed. The 2p-orbitals on the surface-layer oxygen atom are, therefore, left dangling, giving rise to two dangling-bond like bands at around -4 eV in the gap of the PBS between the projection of the non-bonding and the bonding bands. These two dangling-bond bands (resulting from the two atoms in an O layer) are almost degenerate at Γ, but split slightly at other $\underline{q}$-points, because the two 2p orbitals point in different directions. Finally, the lower lying bands have again back-bond character.

The most significant of the above results is the finding that oxygen atoms at the free surface give rise to occupied dangling-bond states which lie in the gap between the bonding and non-bonding valence bands. This finding is independent of our Hamiltonian parametrization and special crystal structure, since the dangling bond states must lie in the gap[70] above the bonding bands and below the non-bonding bands (the energy of a Si-O bond is lower than the energy of an O 2p-orbital, and the energy of a Si-O-Si bond is even lower). These states should be observable and can probably be detected by high resolution experiments.

V. Conclusions

We have demonstrated that the Koster-Slater method for dealing with localized perturbations can be formulated in a way that allows the study of the electronic structure of surfaces of real materials. We have pointed out the various advantages of the method, when used in conjunction with tight-binding Hamiltonians. We illustrated applications of the method to the free (100) surfaces of Si, Ge, GaAs, ZnSe and cubic SiO_2. The method would be particularly suited for the study of reconstructed surfaces, where large unit cells are involved. Such studies have not been persued yet. Instead, we have modified the method to treat interfaces between two semi-infinite crystalline solids. This work will be reported in a separate paper. Finally the method has the potential of being a very efficient way of carrying out self-consistent calculations of the electronic structure of surfaces and interfaces.

Acknowledgements

We are indebted to J. F. Janak for a general program to calculate tight-binding bulk energy bands of arbitrary crystalline materials and to J. Bernholc, J. F. Janak, S. G. Louie and A. R. Williams for valuable discussions.

Appendix A

Evaluation of the Green's Function Matrix Elements

The matrix elements of the Green's function $G^{\circ}(E)$ (equation (3)) in the layer-orbital representation (equation (23)) are given by

$$G^{\circ}_{\ell,\ell'}(E, q) = \sum_{n\underline{k}} \frac{\langle \ell \underline{q} \mid n\underline{k} \rangle \langle n\underline{k} \mid \ell' \underline{q} \rangle}{E^{+} - E_n(\underline{k})}, \tag{A.1}$$

where $|n\underline{k}\rangle$ are the Bloch functions [eq. (22)] and $|\ell\underline{q}\rangle$ are the layer-orbitals defined by eq. (23).

In order to evaluate the matrix elements in (A.1), we must introduce further notation. We first rewrite the bulk atomic position vectors in terms of two-dimensional Bravais lattice vectors $\underline{\rho}_j$ plus appropriate basis vectors in the form

$$\underline{R}_j + \underline{\tau}_\mu = \underline{\rho}_j + \underline{\lambda}^m_\mu . \tag{A.2}$$

Furthermore we need to decompose the basis vector $\underline{\lambda}^m_\mu$ into a surface-parallel component $\underline{\sigma}^m_\mu$ and a perpendicular component $\underline{\kappa}^m$:

$$\underline{\lambda}^m_\mu = \underline{\sigma}^m_\mu + \underline{\kappa}^m \tag{A.3}$$

Note that for any bulk-atom, $\underline{\rho}_j$ locates a two-dimensional Bravais lattice point, $\underline{\kappa}^m$ locates a particular plane, and finally $\underline{\sigma}^m_\mu$ defines the atomic position in the two-dimensional unit cell in that plane.

Along the same lines, the bulk $\underline{k}$ vector must be decomposed into surface-parallel and perpendicular components:

$$\underline{k} = (\underline{q}+\underline{g}) + \underline{k}_\perp \tag{A.4}$$

Note that the surface-parallel component has been written as the sum of a $\underline{q}$ vector in the surface Brillouin zone (SBZ) and a two-dimensional reciprocal lattice vector $\underline{g}$, because the projection of $\underline{k}$ onto the surface does not necessarily lie within the two-dimensional Brillouin zone.

With the above decompositions, the matrix elements appearing in (A.1) can be evaluated. The result is

$$G^{\circ}_{\ell\ell'}(E, \underline{q}) = \frac{N_2}{N_3} \sum_{n} \sum_{\underline{k}_\perp} \sum_{\underline{g}}' \frac{1}{E^{+}-E_n(\underline{k}_\perp,\underline{q}+\underline{g})} P^{n}_{\ell\ell'}(\underline{k}_\perp,\underline{q}+\underline{g}). \qquad (A.5)$$

The auxiliary function P is given by

$$P^{n}_{\ell\ell'}(\underline{k}_\perp, \underline{q}+\underline{g}) = C^{n}_{\alpha' m' \mu'}(\underline{k}_\perp,\underline{q}+\underline{g})\ C_{\alpha m \mu}(\underline{k}_\perp, \underline{q}+\underline{g}) \times$$

$$\times \exp\left[i\underline{g}\cdot(\underline{\sigma}^{m}_{\mu}-\underline{\sigma}^{m'}_{\mu'})\right] \exp\left[i\underline{k}_\perp\cdot(\underline{\kappa}^{m}-\underline{\kappa}^{m'})\right]. \qquad (A.6)$$

Note that the Bloch-function coefficients C now have the double index m, μ in place of the single index ν appearing in eq. (22) because of the decomposition given in (A2). Finally, the prime on the $\underline{g}$-sum in eq. (A5) means that the sum is carried out only over those $\underline{g}$ vectors neccessary to cover the projection of the bulk Brillouin zone onto the surface as required by the decomposition (A4).

For the (100) surface of a diamond- or zince-blende-type material, the projection of the bulk Brillouin zone is shown in Fig. A1 together with the SBZ. Also shown is the irreducible segment of the SBZ, marked by the four high-symmetry points Γ, J, J′, and K. For $\underline{q}$ vectors inside the cross-hatched region of the SBZ, no $\underline{g}$ vectors contribute to the sum in eq. (A5). For $\underline{q}$ vectors in the remainder of the irreducible square there exist non-trivial contributions to the $\underline{g}$-sum in eq. (A5). This means that one must sum over $k_\perp = k_x$ both at the $\underline{q}$ point itself and at the corresponding $\underline{q}+\underline{g}$, as shown by the hatched regions in Fig. A1.

For $\underline{q}$ points inside the cross-hatched region of the SBZ, the sum over $k_\perp = k_x$ extends from $-2\pi/a$ to $+2\pi/a$, where a is the lattice constant, as illustrated for $\underline{q}$ points along the ΓJ line in Fig. A2. The figure is simply the cut of the bulk Brillouin zone by the plane which is perpendicular to the surface and contains the line ΓJ. For $\underline{q}$-points outside the cross-hatched region of the irreducible square, the limits at $\underline{q}$ and $\underline{q}+\underline{g}$ are different and $\underline{q}$-dependent, as illustrated in Fig. A2 for one such point q. By making use of symmetry considerations, it can be shown that instead of summing over the appropriate ranges of k_x at both $\underline{q}_o$ and $\underline{q}_o+\underline{g}$, the same result may be obtained by simply summing only at $\underline{q}_o$ over the range $-2\pi/a$ to $2\pi/a$ (Fig. A2). This alternative way of evaluating the sums in eq. (A5) is a substantial simplification especially for $\underline{q}$ points away from high-symmetry lines in the SBZ.

For the (100) surfaces of diamond- and zinc-blende-type materials, $\kappa^m = am/4$ and eqs. (A5) – (A6) simplify to

$$G^\circ_{\ell\ell'}(\underline{q},E) = \frac{1}{2} \sum_n \int_{-1}^{1} dx \exp[i\pi x(m-m')/2] \frac{C^{\eta}_{\ell'}(x\underline{q}) C^{\eta}_{\ell}(x\underline{q})}{E^+ - E_n(x,\underline{q})}, \qquad (A.7)$$

where $x = k_x a/2\pi$. Before this expression can be evaluated, one must deal with the fact that E^+ stands for $E+i\epsilon$, and the limit $\epsilon \to 0$ is to be taken. In the gaps and pockets of the PBS one can simply set $\epsilon = 0$ and evaluate $G^\circ_{\ell\ell'}(q, E)$ without any complication, because the denominator in (A7) is never zero. In addition, $G^\circ_{\ell\ell'}$ is Hermitian, which reduces the computational effort even further. Within the PBS continua, however, ϵ cannot be set to zero. There are two ways to proceed: The most direct way is to set ϵ to a small but finite energy and evaluate eq. (A7) as it stands. The result will be a Green's function which is broadened by the amount ϵ. Alternatively, one introduces the spectral function

$$S_{\ell\ell'}(\underline{q}, E) = \sum_{n\underline{k}} \langle \ell\underline{q} | n\underline{k} \rangle \langle n\underline{k} | \ell'\underline{q} \rangle \delta(E - E_{n\underline{k}}), \qquad (A.8)$$

and takes the limit $\epsilon \to 0$ analytically resulting in

$$G^\circ_{\ell\ell'}(\underline{q},E) = \mathcal{P} \int \frac{S_{\ell\ell'}(\underline{q},E)}{E-E'} dE' - i\pi S_{\ell\ell'}(\underline{q},E) \qquad (A.9)$$

where the bar on the integral sign denotes principal value. $S_{\ell\ell'}$ can be evaluated directly. The result is

$$S_{\ell\ell'}(q, E) = \frac{N_2}{N_3} \sum_n \sum_i \sum_{\underline{g}}' P^{\eta}_{\ell\ell'}(k_{\perp}^{i}, \underline{g}+\underline{g}) \left[\frac{\partial E_n(k_{\perp}, q+g)}{\partial k_{\perp}} \Big|_{k_{\perp}=k_{\perp}^{i}} \right]^{-1} \quad \text{(A.10)}$$

where $k_{\perp}^{i}$ are defined by

$$E = E_n(k_{\perp}^{i}, \underline{g}+\underline{g}) . \quad \text{(A.11)}$$

For our particular case, the final result for $S_{\ell\ell'}$ is ($x_j = k_{\perp}^{j} \quad 2\pi/a$)

$$S_{\ell\ell'}(q, E) = \frac{1}{2} \sum_j \exp[i\pi x_j(m-m')/2] \sum_n C^{\eta *}_{\ell'}(x_j, \underline{g}) C^{\eta}_{\ell}(x_j, \underline{g}) \left[\frac{\partial E_n(x, \underline{g}+\underline{g})}{\partial_x} \Big|_{x=x_j} \right]^{-1} \quad \text{(A.12)}$$

where x_j is defined by

$$E = E_n(x_j, \underline{g}) \quad \text{(A.13)}$$

and $-1 < x_j < 1$.

Appendix B

Search for the Bound State Energies

The energies of bound surface states are determined by the zeros of

$$\tilde{D}(E) = \det \| G^{\circ}_{\ell,\ell'}(E, \underline{q}) \| = 0 , \qquad (B.1)$$

where ℓ and ℓ' run over the layers which have to be removed for the creation of the surface. (See Appendix A for the evaluation of the matrix $G^{\circ}_{\ell,\ell'}$). The determinant in (B.1) may be evaluated numerically in a variety of ways but the search for the zeros could be a time-consuming task. Instead, the zeros can be located much more efficiently by first converting the matrix $G^{\circ}_{\ell\ell'}$, to triangular form and counting the number of negative diagonal elements. If this number is different at the two ends of a given energy range, the difference corresponds to the number of zeros of $\tilde{D}(E)$ in that range. The chosen range is then systematically bisected until the positions of zeros are determined to the desired degree of accuracy. In our calculations the surface states of the chosen Hamiltonians were determined with an accuracy of 1 meV.

Appendix C

Calculation of the Wavefunctions

The eigenvectors of the Hamiltonian H are given by the Lippmann-Schwinger equation

$$\psi = \varphi + G^{\circ} U \psi = \varphi + G U \varphi , \tag{C.1}$$

where φ is the solution of H°, i.e. φ stands in our problem for a bulk Bloch function. In the pockets and gaps of the PBS, where the true surface states are encountered, there exists no nontrivial solution of H°. Therefore, the wavefunction for the surface states is given as

$$\psi = G^{\circ} U \psi \tag{C.2}$$

In the surface problems discussed in this paper, the perturbation operator acts only on a very limited part of the Hilbert space of H°, as was extensively discussed in Section II. We, therefore, partition the perturbation operator, the Green's operator and the wavefunction in the two subspaces of H°, which we label A and B:

$$U = \begin{pmatrix} u 1_A & 0 \\ 0 & 0 \end{pmatrix}; G^{\circ} = \begin{pmatrix} G^{\circ}_{AA} & G^{\circ}_{AB} \\ G^{\circ}_{BA} & G^{\circ}_{BB} \end{pmatrix}; \psi = \begin{pmatrix} \psi_A \\ \psi_B \end{pmatrix} , \tag{C.3}$$

where 1_A is the unit operator in the subspace A. With (C.3) inserted in (C.2) we find

$$\psi_A = G^{\circ}_{AA} u \psi_A \tag{C.4a}$$

$$\psi_B = G^{\circ}_{BA} u \psi_A . \tag{C.4b}$$

Eq. (C4a) may also be written as

$$\left(\frac{1}{u} 1_A - G^{\circ}_{AA} \right) (u\psi_A) = 0 . \tag{C5a}$$

This is a homogeneous set of linear equations and can be solved for $(u\psi_A)$ for any arbitrary value of u. In the limit $u \to \infty$ one simply diagonalizes G°_{AA} and the resulting eigenvectors $u\psi_A$

are finite so that $\psi_A=0$, as expected. The quantities $u\psi_A$ are then inserted in (C4b) and ψ_B can be directly calculated by simply multiplying the matrix G°_{BA} by the column vector $(u\psi_A)$.

Appendix D

The Solution of The Dyson Equation

The formal solution of the Dyson equation (13)

$$G = G^\circ + G^\circ U G \tag{D.1}$$

can conveniently be written in terms of the scattering matrix

$$T = U (1-G^\circ U)^{-1} \tag{D.2}$$

so that

$$G = G^\circ + G^\circ T G^\circ . \tag{D.3}$$

Equation (D.3) shows, that the complete information about the new features of the perturbed system $H = H^\circ+U$ is contained in the scattering matrix T. Due to the limited range of U, the scattering matrix can be calculated exactly. To calculate T, we have to evaluate $(1-G^\circ U)^{-1}$. We introduce the notation

$$Q = 1 - G^\circ U \tag{D.4}$$

and employ the same partitioning convention as in (C.3). The matrix Q is of the form

$$Q = \begin{pmatrix} Q_{AA} & 0 \\ Q_{BA} & 1_B \end{pmatrix} \tag{D.5}$$

and can be inverted analytically, even though Q_{BA} and 1_B are infinite submatrices. The result is

$$Q^{-1} = \begin{pmatrix} [Q_{AA}]^{-1} & 0 \\ -1_B\, Q_{BA}\, [Q_{AA}]^{-1} & 1_B \end{pmatrix} . \tag{D.6}$$

Using this result we obtain:

$$G_{AA} = G^{\circ}_{AA} + G^{\circ}_{AA}\, U_{AA}\, [Q_{AA}]^{-1}\, G^{\circ}_{AA}$$

$$G_{AB} = G^{\circ}_{AB} + G^{\circ}_{AA}\, U_{AA}\, [Q_{AA}]^{-1}\, G^{\circ}_{AB} \qquad \text{(D.7)}$$

$$G_{BA} = G^{\circ}_{BA} + G^{\circ}_{BA}\, U_{AA}\, [Q_{AA}]^{-1}\, G^{\circ}_{AA}$$

$$G_{BB} = G^{\circ}_{BB} + G^{\circ}_{BA}\, U_{AA}\, [Q_{AA}]^{-1}\, G^{\circ}_{AB} .$$

This result holds for any perturbation confined to subspace A. Note that Q_{AA} is precisely the matrix one has to evaluate in order to search for bound states. The complete evaluation of the Green's function matrix for the perturbed system can then be done directly by inverting the small matrix Q_{AA} and multiplying matrices as required by (D.7).

The above results simplify further in the case of the perturbation that creates surfaces used in this paper. The perturbation is of the form

$$U_{AA} = u\, 1_A \qquad \text{(D.8)}$$

where u is a constant that is eventually let go to infinity. Eq. (D7) then becomes

$$G_{AA} = 0$$

$$G_{AB} = 0 \qquad \text{(D.9)}$$

$$G_{BA} = 0$$

$$G_{BB} = G^{\circ}_{BB} - G^{\circ}_{BA}\, [G^{\circ}_{AA}]^{-1}\, G^{\circ}_{AB} .$$

These equations are valid for all finite energies[74]. Note that $G_{AA}=0$ corresponds to the fact that there are no states at finite energies in the space occupied by the "removed" layers. $G_{AB}=0$ and $G_{BA}=0$ correspond to the fact that the "removed" layers are completely decoupled from the two semi-infinite solids described by G_{BB}. It is of particular interest that G_{BB} is

given entirely in terms of G°, which describes the infinite bulk solid. This result is of course true because no electronic or lattice relaxation is included at the surface.

G_{BB} contains a wealth of information. In particular, one can evaluate the local density of states at the ℓ^{th} layer (with ℓ in subspace B) as follows:

$$N_{\ell}(\underline{q}, E) = -\frac{1}{\pi} \text{Im Tr} \left\{ G^{\circ}_{\ell\ell}(\underline{q}, E) - \sum_{ij} G^{\circ}_{\ell i} [G^{\circ}_{AA}]^{-1}_{ij} G^{\circ}_{j\ell} \right\} \qquad (D.10)$$

where i and j run over the layer orbitals in the "removed" layers in the subspace A. The second term in the curly brackets clearly yields directly the change in the local density of states for the ℓ^{th} layer (The sum of these quantities over all layers is equal to $\Delta N(q, E)$ discussed in Sec. III).

Table 1

Tight binding matrix elements in eV defining the bulk Hamiltonians of the various materials in standard notation. The superscripts (c) and (a) in the headings of the first four columns denote cation and anion, respectively, and the superscripts 1 and 2 refer to first- and second-nearest-neighbours.

	$E_s^{(c)}$	$E_p^{(c)}$	$E_s^{(a)}$	$E_p^{(a)}$	V_{ss}^1	V_{sp}^1	V_{ps}^1	$V_{pp\sigma}^1$	$V_{pp\pi}^1$	$V_{pp\sigma}^2$	$V_{pp\pi}^2$
Si[a]	−4.203	0.187	/	/	−2.08	2.12	2.12	2.32	−0.52	0.58	−0.10
Ge[a]	−5.830	0.610	/	/	−1.69	2.03	2.03	2.55	−0.67	0.41	−0.08
Ge[b]	−5.63	1.72	/	/	−1.69	2.76	2.76	3.13	−0.92	/	/
GaAs[b]	−3.07	3.47	−8.09	1.28	−1.69	2.37	2.06	3.51	−0.96	/	/
ZnSe[b]	+0.01	6.20	−12.03	1.10	−1.69	2.59	1.07	3.46	−0.75	/	/
SiO_2	13.86	18.36	16.36	−1.77	−1.5	3.76	3.5	5.71	−0.64	/	/
O-O Interactions	/	/	/		−0.6	0.8	0.8	1.29	−0.16	/	/

a. Ref. 58

b. Ref. 63

References

1. V. Heine, Surf. Science 2, 1 (1964); Proc. Roy. Soc. London A331, 307 (1972); the compilation of literature is not intended to be complete, but most of the references to theoretical papers in this field can be found in Refs. 1 to 55.
2. See e.g. Proceedings of the 2-nd International Conference on Solid Surfaces, Kyoto, Japan (1974).
3. J. C. Phillips, Surf. Science 53, 474 (1975).
4. J. R. Schtieffer and P. Soven, Physics Today, 28, 24 (1974).
5. J. A. Appelbaum and D. R. Hamann, Reviews of Modern Physics 48, 479, (1976).
6. F. Forstmann, in Photoemission and the Electronic Properties of Surfaces, ed. by B. Feuerbacher, B. Fitton, and R. F. Willis (Wiley, New York, 1978).
7. L. P. Batra and O. Roubaux, Surf. Science 49, 653 (1975).
8. G. S. Painter, P. J. Jennings and R. O. Jones, J. Phys. C8, L199 (1975).
9. J. Harris and G. S. Painter, Phys. Rev. Let. 36, 151 (1976).
10. I. P. Batra and S. Citaci, Phys. Rev. Let. 36, 170 (1976).
11. K. Hirabayashi, J. Phys. Soc. Japan 27, 1475, (1969).
12. Ed Caruthers, L. Kleinmann, G. P. Alldredge, Phys. Rev. B8, 4570 (1973).
13. K. C. Pandey and J. C. Phillips, Phys. Rev. Let. 32, 1433 (1974); Phys. Rev. Let. 34, 1450 (1975); Phys. Rev. B13, 750 (1976).
14. R. V. Kasowski, Phys. Rev. Let. 33, 83 (1974); Sol. St. Com. 17, 179 (1975).
15. M. Schlüter, J. R. Chelikowsky, Steven G. Louie and M. L. Cohen Phys. Rev. B12, 4200 (1975).
16. D. G. Dempsey, L. Kleinmann, Ed Caruthers, Phys. Rev. B12, 2932 (1975).
17. K. S. Sohn, D. G. Dempsey, L. Kleinmann, Ed Caruthers, Phys. Rev. B14, 3185 (1976).
18. S. Ciraci and I. P. Batra, 18, 1149 (1976).
19. C. Calandra and G. Santoro, J. Vac. Sci. and Technol., 13, 773 (1976).
20. C. M. Bertoni, O. Bisi, C. Calandra, F. Manghi, Il Nuovo Cimento, 38B, 96 (1977).
21. O. Bisi and C. Calandra Il Nuovo Cimento 38B, 81 (1977).
22. S. Ciraci and I. P. Batra, 15, 3524 (1977).

23. I. Ihm, S. G. Louie, M. L. Cohen, Phys. Rev. B 17, 769 (1978).

24. G. P. Kerker, S. G. Louie and M. L. Cohen, Phys. Rev. B17, 769 1978.

25. J. A. Appelbaum and D. R. Hamann, Phys. Rev. B6, 2166 (1972).

26. J. A. Appelbaum and D. R. Hamann, Phys. Rev. Let. 31, 106 (1973).

27. J. A. Appelbaum, G. A. Baraff, D. R. Hamann, Phys. Rev. B11, 3822 (1975).

28. J. A. Appelbaum, G. A. Baraff and D. R. Hamann, Phys. Rev. B14, 1623 (1976).

29. F. Garcia-Moliner and J. Rubio, J. Phys. C. (Sol. St. Phys.) 2, 1789 (1969).

30. F. Garcia-Moliner, V. Heine, J. Rubio, J. Phys. C. (Sol. St. Phys.) 2, 1797 (1969).

31. F. Garcia-Moliner and J. Rubio, Proc. Roy. Soc. London A324, 257 (1971).

32. F. Flores, Il Nuovo Cimento 14B, 1, 1973.

33. M. Elices, F. Flores, E. Louis, J. Rubio, J. Phys. C. (Sol. St. Phys.) 7, 3020 (1974).

34. J. A. Vergeás and E. Louis, Sol. St. Com 22, 663 (1977).

35. C. Noguera, D. Spanjaard, D. W. Jepsen, Phys. Rev. B17, 607 (1978).

36. R. Haydock, V. Heine, M. J. Kelly, J. Phys. C. (Sol. St. Phys.) 5, 137 (1972).

37. R. Haydock and M. J. Kelly, Surf. Science 38, 139 (1973).

38. M. C. Desjonquieres and F. Cyrot-Lackmann, J. Phys. F5, 1368 (1975).

39. V. Anishchick, L. M. Falicov, F. Yndurain, Surf. Science 57, 375 (1976).

40. I. B. Ortenburger, S. Ciraci, I. P. Batra, J. Phys. C. (Sol. St. Phys.) 9, 4185 (1976).

41. E-Ni Foo, M. F. Thorpe, D. Weaire, Surf. Science 57, 323 (1976).

42. E. J. Mele and J. D. Joannopoulos, Phys. Rev. B17, 1816 (1978).

43. J. Koutecky, Phys. Rev. 108, 13 (1957).

44. J. Koutecky in Advances in Chemical Physics Vol. IX, 85 (1965), (Interscience) London.

45. D. Kalkstein and P. Soven, Surface Science 26, 85, (1971).

46. A. A. Maradudin, E. Q. Montroll, G. H. Weiss and I. P. Ipatova, Sol. State Physics, Suppl. 3, edited by F. Ehenreich et al. (Academic Press, New York, 1971).

47. A. van der Avoird, S. P. Liebmann and D. J. M. Fassaert, Phys. Rev. B10, 1230, (1974).

48. S. P. Liebmann, A. van der Avoird, D. J. M. Fassaert, Phys. Rev. B11, 1503 (1975).

49. J. W. Davenport, T. L. Einstein, J. R. Schrieffer, Proceedings of the 2nd International Conference on Solid Surfaces, Kyoto, Japan (1974).

50. R. Feder and K. Sturm, Sol. St. Com. 14, 1317 (1974); Phys. Rev. B12, 537, (1975).

51. V. M. Tapilin, S. L. Cunningham and W. H. Weinberg, Phys. Rev. B. July 1977.

52. S. L. Weng, Phys. Rev. Let. 38, 434 (1977).

53. J. Ladik, Phys. Rev. B 17, 1663 (1978).

54. N. Lang and W. Kohn, Phys. Rev. B1, 4555 (1970); B3, 1215 (1971).

55. N. D. Lang and A. R. Williams, Phys. Rev. Let. 34, 531 (1975).

56. J. Callaway, J. Math. Phys. 5, 783, (1964); Phys. Rev. 154, 515, (1967).

57. F. Garcia-Moliner, in "Theory of Imperfect Crystaline Solids: Trieste Lectures 1970", International Atomic Energy Agency Vienna.

58. K. C. Pandey, Thesis (unpublished) Columbia University, New York (1974).

59. G. F. Koster and J. C. Slater, Phys. Rev. 95, 1167 (1954).

60. J. Bernholc and S. T. Pantelides, Phys. Rev. B, to be published.

61. It should be noted, that LCAO orbitals are in general not orthogonal and, therefore, present an additional complication over the use of Wannier functions. In the applications discussed in this paper the empirical tight binding Hamiltonians we use are defined in terms of orthogonal LCAO orbitals (Refs. 13 and 58) so that no complications arise. Use of non-orthogonal orbitals in such schemes results in equations which are modified by the overlap matrix without adding serious complications.

62. The rigid shift may be due to the definition of the zero of energy in a slab calculation.

63. D. J. Chadi, Phys. Rev. B16, 790 (1977).

64. J. D. Joannopoulos and Marvin L. Cohen, Phys. Rev. B10, 5075 (1974).

65. J. R. Chelikowsky and Marvin L. Cohen, Phys. Rev. B13, 826 (1976).

66. D. J. Chadi and Marvin L. Cohen, Phys. Rev. B 11, 732 (1976).

67. The (100) surfaces in zincblende materials are charged surfaces and are therefore very unlikely to exist in the ideal unrelaxed unconstructed form.

68. S. T. Pantelides and W. A. Harrison, Phys. Rev. B13, 2667 (1976).

AD-A058 426 IBM THOMAS J WATSON RESEARCH CENTER YORKTOWN HEIGHTS N Y F/G 20/12
ELECTRONIC STRUCTURE AND PROPERTIES OF THE OXIDES OF THE TETRAH--ETC(U)
JUL 78 S T PANTELIDES N00014-76-C-0934
UNCLASSIFIED NL

2 OF 2
ADA
058426

END
DATE
FILMED
11-78
DDC

69. T. H. Di Stefano and D. E. Eastman, Sol. St. Com. 9, 2259 (1971).

70. Theoretical calculations (Ref. 68, 71-73) find a gap of about 2-3 eV for cubic SiO_2, α quartz and amorpous SiO_2. Broadened densities of states show only a dip and agree very well with photoemission data. The presence of the gap is therefore well supported.

71. J. R. Chelikowsky and M. Schlüter, Phys. Rev. B15, 4020 (1977).

72. S. Ciraci and I. P. Batra, Phys. Rev. B15, 4923 (1977).

73. P. M. Schneider and W. B. Fowler, Phys. Rev. Lett. 36, 425 (1976).

74. G_{AA} has poles at infinity corresponding to the states on the removed layers.

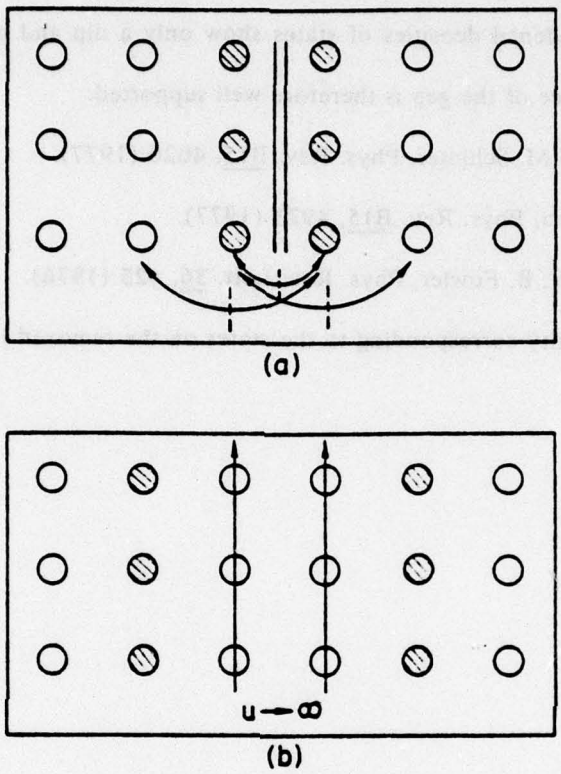

Fig. 1 **Schematic graphs showing the creation of the twin surfaces in the two different methods: (a) "switching off" interactions, (b) "removal" of layers. In both cases the resulting surface layer atoms are shaded.**

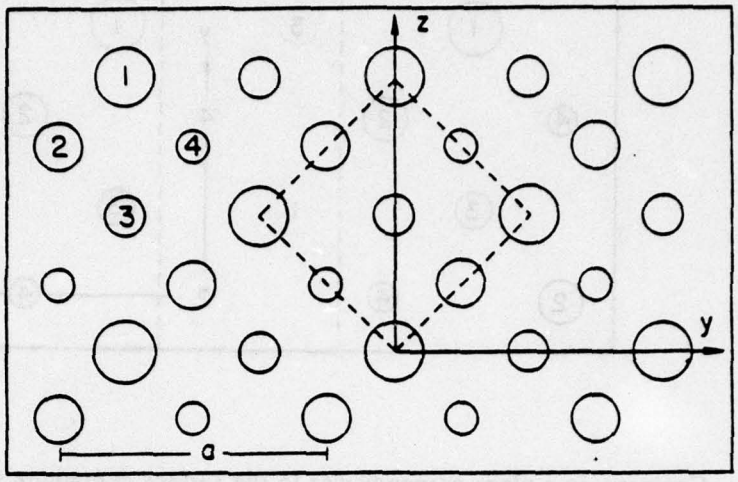

Fig. 2 The topmost (100) surface layer and the following three layers for diamond or zincblende lattices. In the case of a zincblende material even and odd layers contain either anions or cations, respectively. We retain the crystal y- and z-axis. The bulk lattice constant, denoted by a.

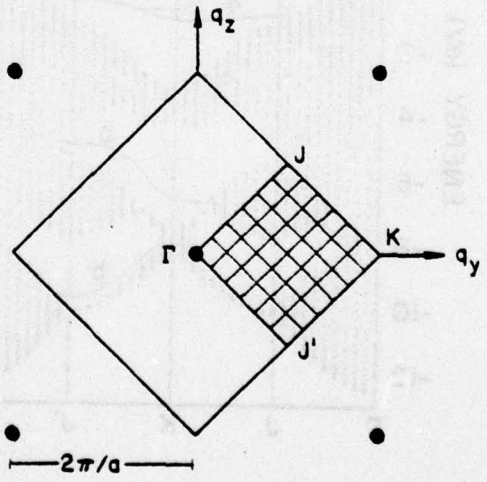

Fig. 3 Reciprocal lattice (dots) for a diamond or zincblende (100) surface together with the surface Brillouin zone. The irreducible square (C_{2v} symmetry) is cross-hatched.

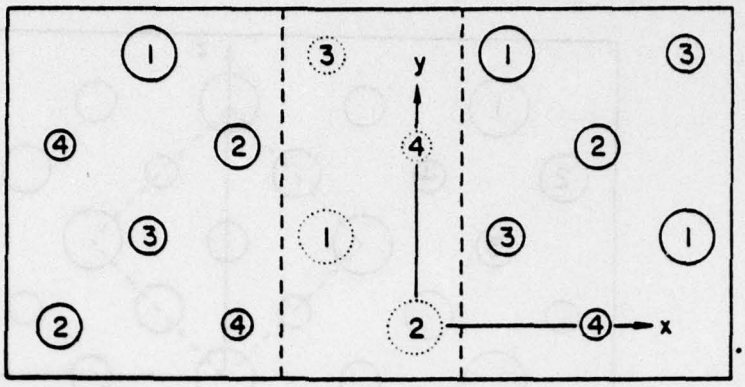

Fig. 4 Geometry in a plane prependicular to the surface containing the y-axis. The two dotted layers are "removed" to create the adjacent surfaces.

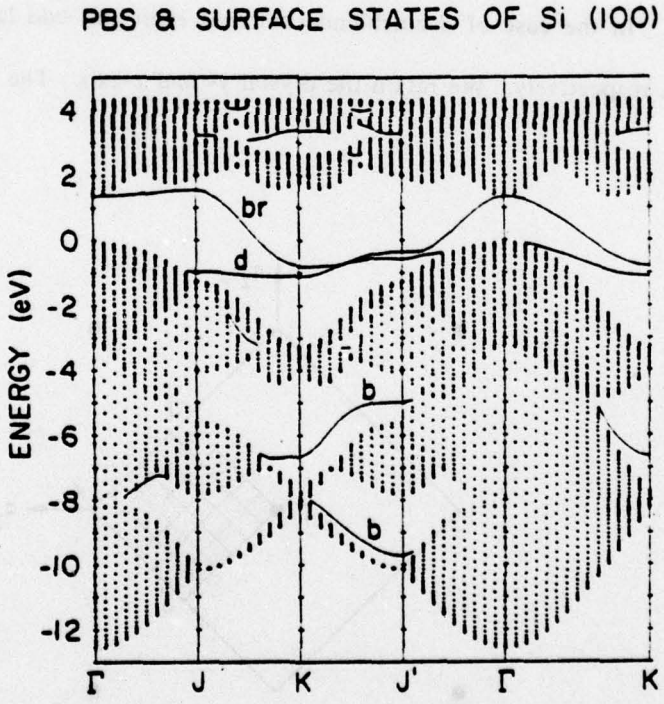

Fig. 5 Projected bulk band structure and surface band structure of Si (100) calculated with the second-nearest-neighbour tight-binding Hamiltonian given in Ref. 58. The letters b, d, and br denote the back bond, dangling bond and bridge bond bands, respectively. See text.

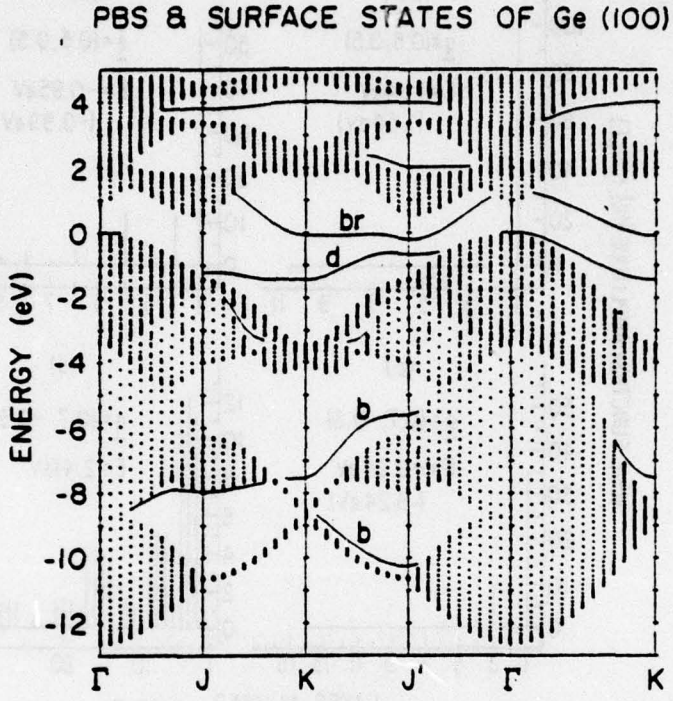

Fig. 6 **Surface band structure of Ge (100); for details see caption of Fig. 5.**

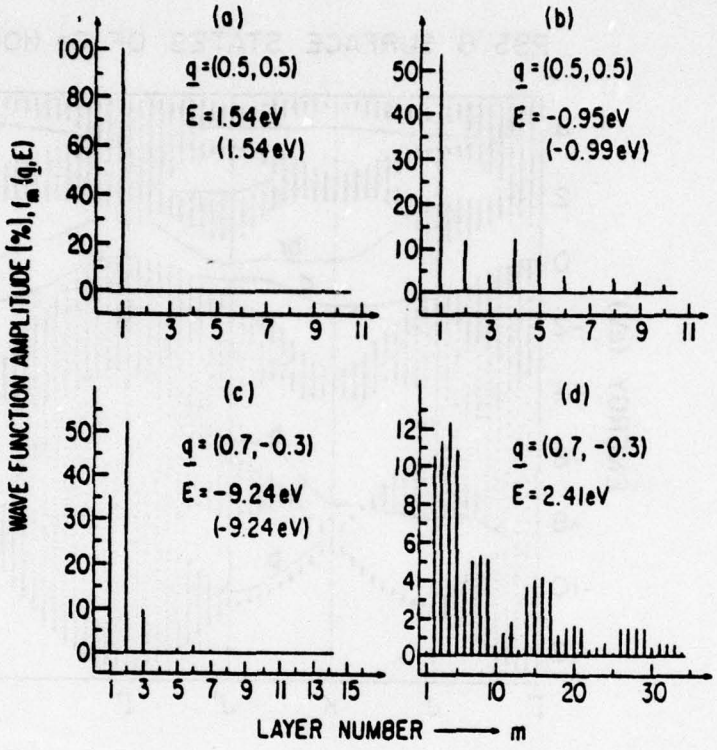

Fig. 7 **Wavefunction amplitudes as a function of the layer number for some surface states in Si (100) (summed over the s and p orbitals). The corresponding $\underline{q}$ and E values are explicitly given. The energy values resulting from a 20-layer slab calculation (Ref. 58) are also given in parenthesis for comparison.**

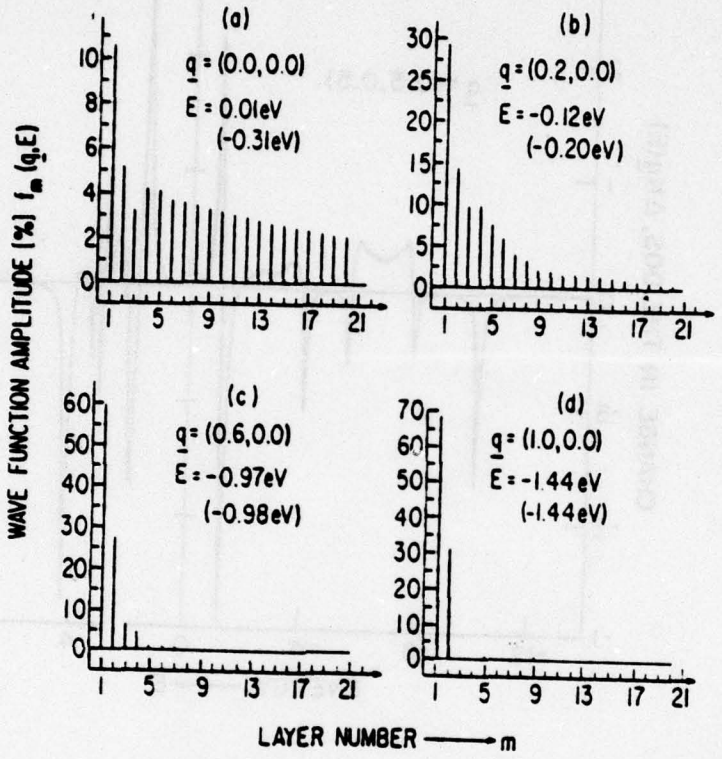

Fig. 8 Wavefunction amplitudes for the dangling bond state of Ge (100); for details see Fig. caption 7.

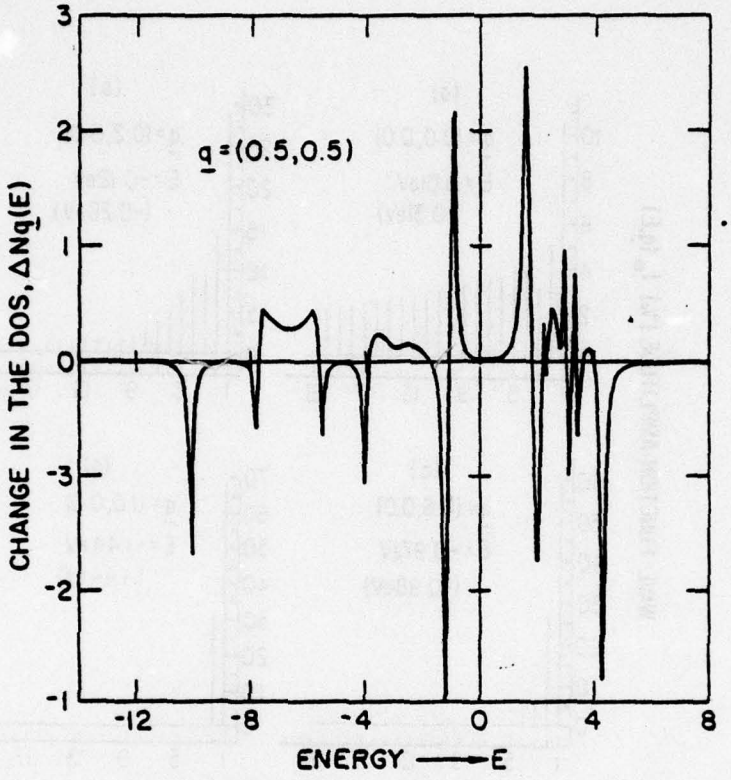

Fig. 9 Total change in the density of states at the symmetry point J for Si (100), broadened by 0.1 eV.

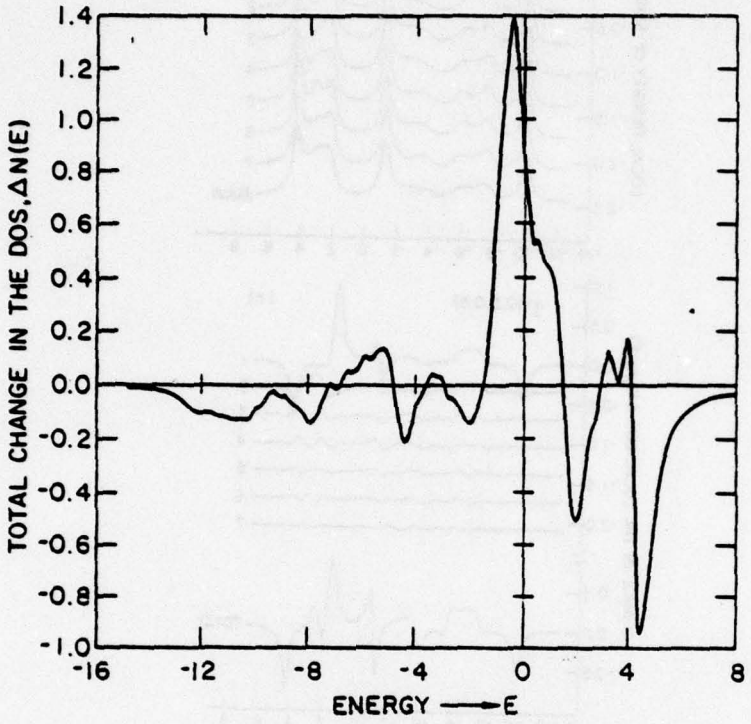

Fig. 10 **Total change in the density of states (in units of states/eV/unit cell) summed over the surface Brillouin zone for Si (100), broadened by 0.3 eV.**

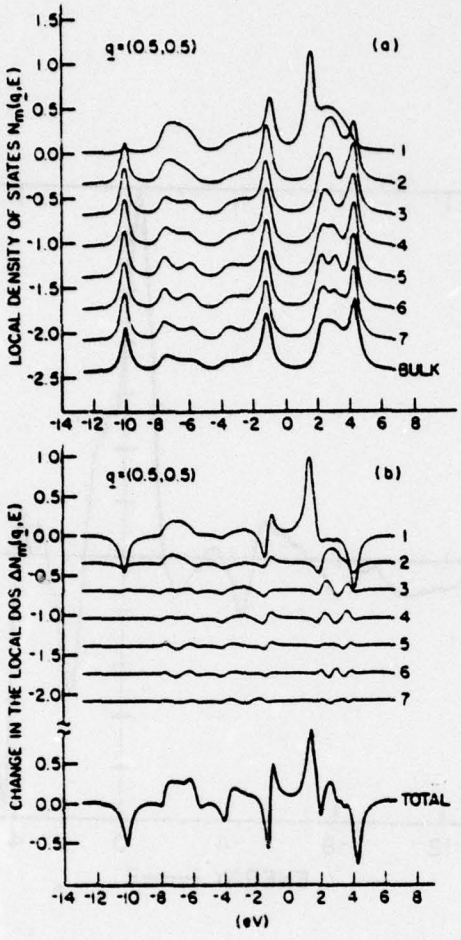

Fig. 11 (a) Local densities of states (in units of states/eV/unit cell) at each one of the first seven layers of the Si (100) surface at the symmetry point J of the surface Brillouin zone. The local density of states at any bulk layer of the infinite crystal is shown by the heavy line. (b) The changes in the local density of states at each of the first seven layers. The total change is given by the heavy line and is the same as that shown in Fig. 9, except for different broadening. All the curves in this figure are broadened by 0.3 eV. The vertical scale applies in (a) and (b) for the first layer only. The other curves are all shifted down by .4, .8 etc.

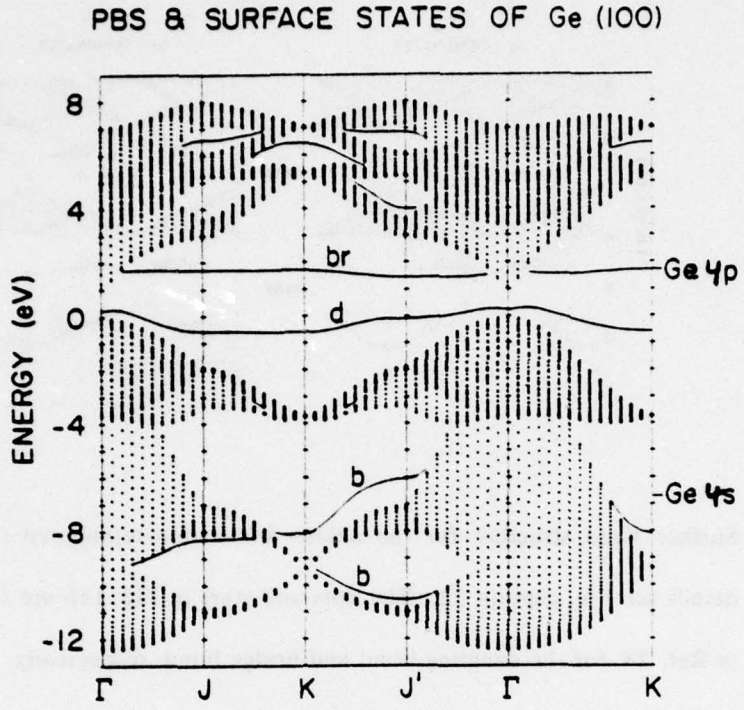

Fig. 12 Projected bulk band structure and surface band structure of Ge (100) calculated with the first-nearest-neighbour tight-binding Hamiltonian as given in Ref. 63. The letters b, d and br again denote the back bond, dangling bond and bridgebond bands, respectively. The "atomic" energy levels are shown for convenience. Note that the bridge-bond band is at the 3p atomic level in a first-nearest-neighbour approximation.

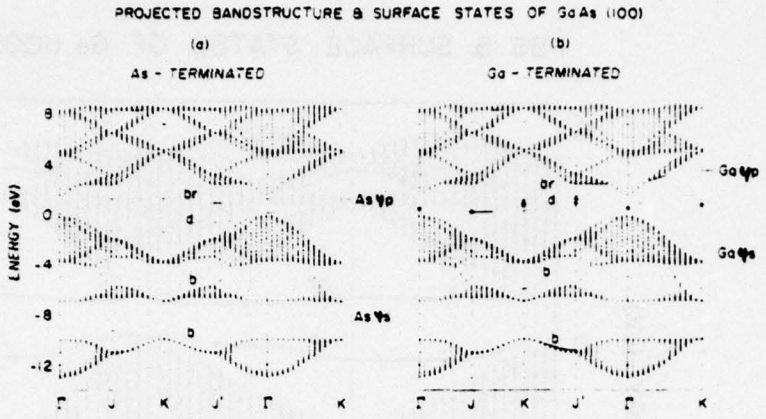

Fig. 13 Surface band structure for the anion- and cation-terminated (100) surfaces of GaAs. For details see Fig. caption 12. The dots and stars in Fig. 13b are the selfconsistent results, given in Ref. 28, for the dangling bond and bridge bond, respectively.

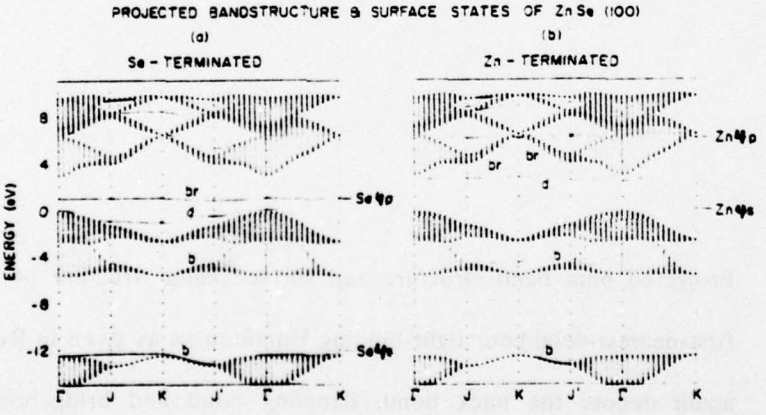

Fig. 14 Surface band structure for the anion- and cation-terminated (100) surfaces of ZnSe. For details see Fig. caption 12.

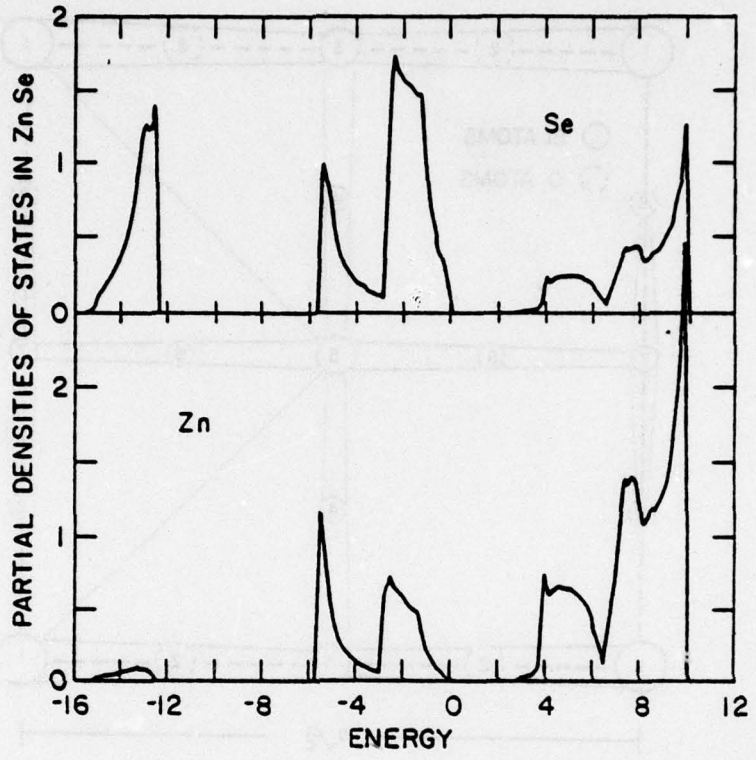

Fig. 15 Partial bulk densities of states at a Se atom (top) and a Zn atom (bottom) for ZnSe calculated with the tight binding Hamiltonian given in Ref. 63.

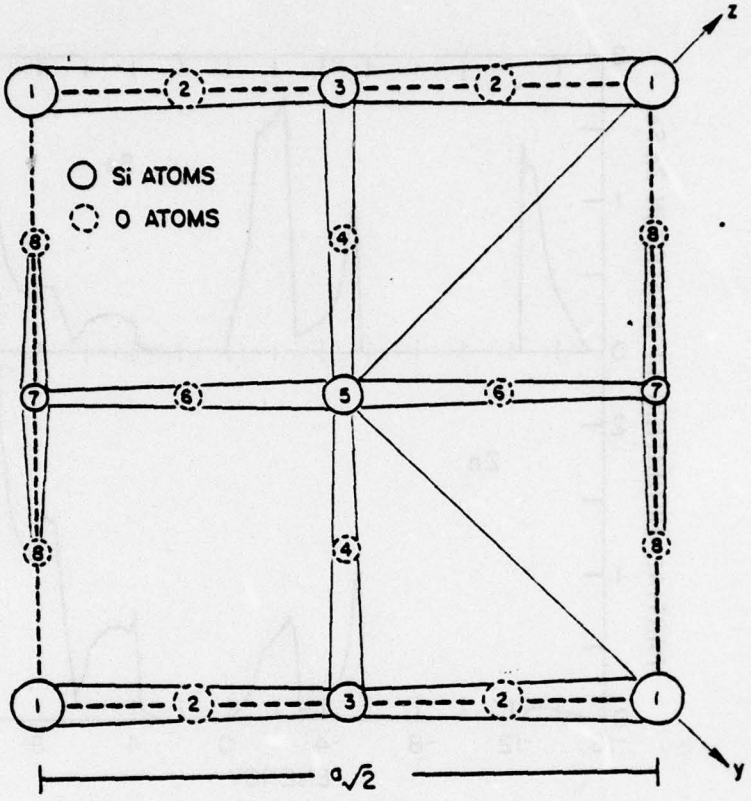

Fig. 16 The topmost (100) surface layer and the following 7 layers for the cubic SiO_2 (ideal β-cristobalite) lattice. We again retain the bulk crystal cartesian coordinate system. The bulk lattice constant is denoted by a. Si atoms are shown as full and O atoms as dashed circles.

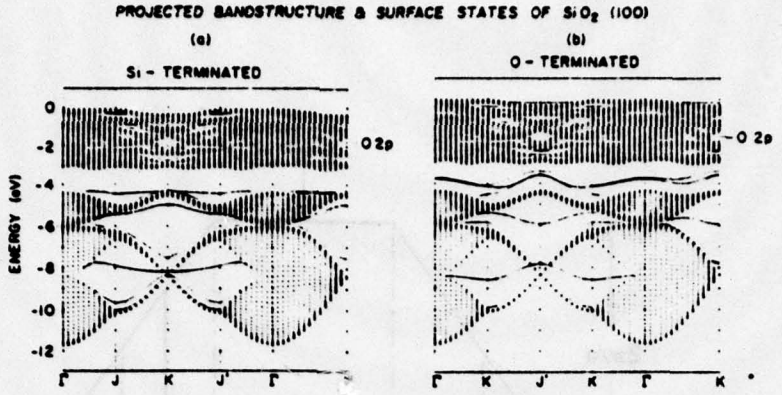

Fig. 17 Projected valence bands and surface band structure for the Si- and O- terminated (100) surfaces of cubic SiO_2. The energetic position of the "atomic" O_{2p} orbitals is indicated.

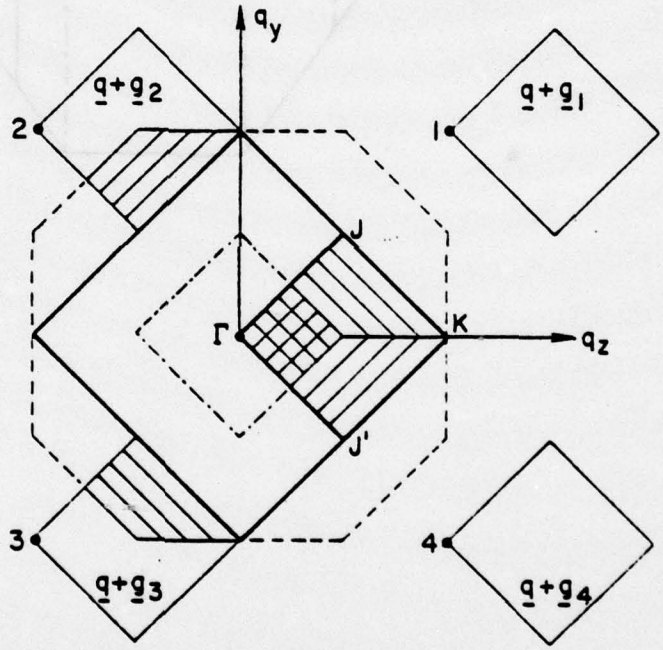

Fig. A1 The dots at Γ and at 1, 2, 3 and 4 are reciprocal lattice points for the Si (100) surface. The heavy line shows the Surface Brillouin zone. The square denoted by Γ, J, K, J' is the irreducible part of the surface Brillouin zone. When $\underline{q}$ runs over this irreducible part, the vectors $\underline{q} + \underline{g}_i$ for i=1, 2, 3, 4 ($\underline{g}_i$ being surface reciprocal-lattice vectors) run over the four squares marked by the corresponding $\underline{q}+\underline{g}_i$. The dashed octagon is the projection of the bulk Brillouin zone onto the (100) surface and the dashed-dotted square is the projection of that part of the bulk Brillouin zone, for which $-2\pi/a \leq k_x \leq 2\pi/a$ holds. The details concerning the cross-hatched and the shaded areas are discussed in Appendix A.

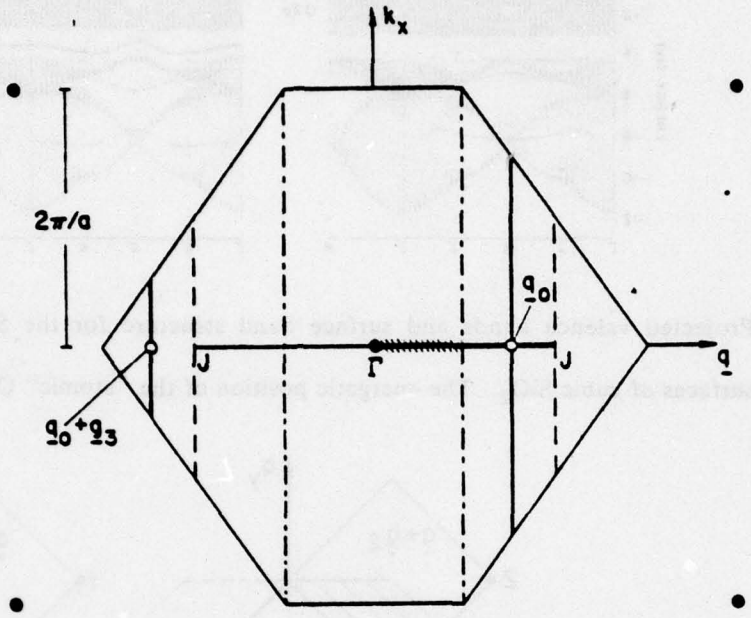

Fig. A2 **Cut of the bulk Brillouin zone perpendicular to the (100) surface containing the line J, Γ, J of the surface Brillouin zone. For details see discussion in Appendix A.**

RC 7200 (#30973) 6/26/78
Solid State Physics 7 pages

Research Report

NEW METHOD FOR THE ELECTRONIC STRUCTURE OF HETEROJUNCTIONS – APPLICATION TO THE (100) Ge-GaAs INTERFACES*

Sokrates T. Pantelides and J. Pollmann†

IBM Thomas J. Watson Research Center
Yorktown Heights, New York 10598

Typed by Linda P. Rubin (SP.2162)

IBM Research Division
San Jose · Yorktown · Zurich

RC 7200 (#30973) 6/26/78
Solid State Physics 7 pages

NEW METHOD FOR THE ELECTRONIC STRUCTURE OF HETEROJUNCTIONS – APPLICATION TO THE (100) Ge-GaAs INTERFACES*

Sokrates T. Pantelides and J. Pollmann†

IBM Thomas J. Watson Research Center
Yorktown Heights, New York 10598

Typed by Linda P. Rubin (SP.2162)

ABSTRACT: A new method which for the first time can treat two truly semi-infinite semiconductors in contact is introduced and used to study the electronic structure of the (100) Ge-GaAs interfaces. Both the Ge-Ga and the Ge-As interfaces exhibit essentially three interface bands. The nature and origin of these bands are discussed in detail in terms of local densities of states. The results are used to obtain a new interpretation of the experimental data.

* Work supported in part by the office of Naval Research under contract No. N00014-76-C-0934.

† Permanent address: Institut für Physik der Universität Dortmund, Dortmund, W. Germany.

Interfaces between two different semiconductors, often referred to as heterojunctions, have been investigated extensively in connection with device fabrication.[1] Theoretical studies of the electronic structure of realistic models of heterojunctions, however, have been carried out only during the last year. Methods used thus far simulate the solids in contact with either a finite-thickness slab on a semi-infinite substrate,[2] or with two finite-thickness slabs in contact[3], or with a superlattice of such finite-thickness slabs.[4]

In this paper, we report the development and first applications of a new method which for the first time describes the electronic structure of the interface between two truly semi-infinite semiconductors. We use the method to give a detailed description of the electronic structure of the (100) Ge-GaAs interfaces. We compare our results for the Ge-Ga interface with previous theoretical work (no other calculations have been reported for the Ge-As interface). Finally we use our results to obtain a new interpretation of available experimental data.

The present method is based on the old Koster-Slater[5] idea for the description of localized perturbations of otherwise infinite periodic solids. That idea, originally proposed for point defects has since been extended to describe free surfaces,[6-8] which may be viewed as arising from a perturbation that has two-dimensional periodicity and is localized in the third direction. We will demonstrate that the creation of an interface between two crystalline semiconductors can also be described by a localized perturbation if the unperturbed system is taken to be two infinite non-interacting solids.

In order to describe the local perturbation that creates the interface, we use the Ge-GaAs (100) interface as an example and describe the two unperturbed bulk materials by nearest-neighbor tight-binding Hamiltonians.[9-11] Each (100) layer of atoms in GaAs has either Ga or As atoms, so that we can schematically denote an entire layer of atoms with the proper geometry by a single circle. Fig. 1 shows the local perturbation that creates the interface: One As and one Ge layer is removed[12] (as discussed extensively in Ref. 8 for the case of free

surfaces), while at the same time one of the two resulting "free-surface" Ge layers is "connected" with the appropriate "free-surface" Ga layer, as shown. The net result of this perturbation is a system which consists of three decoupled subsystems[14]: a Ge-GaAs interface between two semi-infinite solids, a semi-infinite Ga-terminated GaAs crystal and a semi-infinite Ge crystal.

Once the interface is described by a localized planar perturbation, the full machinery of the Koster-Slater Green's function formulation can be used[8]. The main advantages of this approach are: (a) it deals with semi-infinite solids; (b) it exploits the fact that there exists an unperturbed system which has full three-dimensional translation periodicity whose solutions are easily obtainable and whose Green's functions can be calculated accurately using standard band-theoretic techniques. Thus, all properties of the bulk solids are built in from the start and preserved, and *changes* in the electronic structure are calculated directly, rather than by subtracting two large quantities, as in the case of slab approaches. The method yields the positions, the dispersion and the wavefunctions of the bound states in the gaps and pockets of the joint projected band structure (PBS), the changes in the density of states within the projected band continua and local densities of states (LDOS) at each layer of atoms.

As a first application of the new method for interfaces we have studied the electronic structure of the (100) Ge-GaAs and Ge-ZnSe interfaces. We have used the tight-binding Hamiltonians of Chadi[9] which use only s and p orbitals on every atom and retain only nearest-neighbor Hamiltonian interactions[10]. The interface matrix elements (Ge-Ga hopping integrals) were chosen to be the averages of the corresponding Ge and GaAs bulk matrix elements. In this communication, we discuss only[15] the results for Ge-GaAs for which other calculations are available for immediate comparison.[2,4]

In Fig. 2 we show the joint[17] PBS of Ge and GaAs together with the bound states for the Ge-Ga and Ge-As interfaces. It is seen that very few bound states appear in the gaps and pockets of the joint PBS and that the bound states are in fact very near band edges. Such a

situation is consistent with the fact that the two solids are connected without lattice mismatch and have very similar electronic structures, so that the junction is a weak perturbation. Figure 2 by itself, however, does not provide a complete description of all the changes in the electronic structure produced by the formation of the heterojunction. Changes also occur within the band continua, the dominant features of which are usually referred to as resonances or antiresonances. In Fig. 3 we show the q-integrated (i.e., summed over the two-dimensional Brillouin zone) LDOS on the two layers next to each interface and compare them with q-integrated LDOS on the corresponding bulk layers. (The q-integrated LDOS on other layers is virtually identical with the corresponding bulk LDOS indicating strong localization of the interface effects). Fig. 3 reveals that both heterojunctions give rise to essentially three interface bands. (see also Fig. 2)

In the case of the Ge-Ga interface (Figs. 2a and 3a), the three bands lie immediately *aboye* bulk bands, and their dispersion follows closely the nearest band edge. In fact, Fig. 3 shows that each interface band is actually derived from bulk states immediately below it. Physically, what happens is that bulk propagating states decay at the interface and have little or no amplitude on the interface layer. (The situation corresponds to localized antiresonances). The missing amplitude is shifted *up* in energy into new states that are localized at the interface layers and are either bound states (if in gaps or pockets) or resonances (if within the band continua). A more detailed illustration of this situation, is given by Fig. 4 where layer densities of states at the J' symmetry point are shown. Note, for example, how the bulk states at -11 eV on the Ge side and at -12 eV at the GaAs side decay at the interface layers and give rise to a bound state at -10 eV. The reason that amplitude at the interface is shifted *up* in energy and interface states appear *above* the bulk bands is the fact that Ge-Ga bonds are weaker than either Ge-Ge or Ga-As bonds, since the strength of the atomic potentials[4] is in the order Ga < Ge < As. This behavior is also consistent with the fact that Ge-Ga bonds are acceptor bonds, in the sense that simple valence counting shows that the two atoms participating in such a bond contribute a total of 1.75 electrons.

In the case of the Ge-As interface (Figs. 2b and 3b), all the effects are of the same nature except that the three interface bands now appear *below* the band edges, because Ge-As bonds are stronger than either Ge-Ge or Ga-As bonds. Furthermore, Ge-As bonds are "donor bonds", in the sense that the two atoms participating in Ge-As bonds contribute a total of 2.25 electrons.

The results described above for the Ge-Ga interface are in agreement with and complement the results obtained by Baraff, Appelbaum, and Hamann (BAH)[2] who carried out a self-consistent pseudopotential calculation. These authors used as a model geometry three Ge overlayers on a semi-infinite GaAs substrate and saturated the dangling bonds at the outermost Ge layer with hydrogen atoms. Calculations were carried out at high symmetry points in the two-dimensional Brillouin zone and interface states were sought only near the top of the projected valence bands. An interface band was identified going through K and J' at the points shown as heavy dots in Fig. 2a (Because of a different choice of coordinate systems, the J point in Ref. 2 corresponds to the J' point in our case). In addition a state at Γ at -0.1 eV was found which is resonant with Ge bulk states. This state is also present in our results, but at -0.2 eV. It behaves like a resonance on the Ge side and decays over four layers on the GaAs side. BAH assumed that in addition to the above-mentioned interface band, which for local neutrality must be 3/4 filled[2], there exists another fully occupied interface band at lower energies as is required by local charge neutrality. Our results show that the situation is actually somewhat more complicated in that the interface charge is built up from more than one interface band as well as from some bulk states (Fig. 3a).

The results for both the Ge-Ga and Ge-As (100) interfaces allow for an interesting qualitative comparison with the results obtained for the (110) Ge-GaAs heterojunction by Picket, Louie and Cohen[4]. It should be noted that the Ge-GaAs (110) interface contains both types of bonds, Ge-Ga and Ge-As bonds. One would therefore expect to find interface bands both *above* and *below* band edges, very similar to a superposition of our Figs. 2a and 2b. This

qualitative conclusion is born out in the results of Pickett et al.[4]

Finally, we turn to a comparison of the theoretical results with available experiments. Esaki et al.[18] concluded from transport measurements that no empty interface states ($<5 \times 10^{10}$ cm^{-2}) are present in the heterojunction. Experimentally, however, it is not possible to decide whether the sample contains a Ge-Ga interface, a Ge-As interface or some other mixed interface. In fact, since according to our calculations both the ideal abrupt interfaces are metallic[19] in disagreement with experiment, we believe that the most likely configuration is a *stoichiometrically mixed interface*, i.e. there exists at least one layer which contains both Ge and Ga or both Ge and As atoms so that there are on the average an equal number of Ge-Ga and Ge-As bonds. In the simplest such case, one can have the last Ge layer followed by a layer in which Ge and Ga atoms occupy alternate sites, followed in turn by an As layer, etc. Such a configuration would have interface states very much like those of the (110) interface[4] and no empty states would be present in the gap in agreement with experiment.

In conclusion, we have presented a novel method to calculate the electronic structure of two semi-infinite semiconductors in contact. We have shown that the method can provide a detailed description of bound states, resonances, antiresonances and local densities of states for semiconductor interfaces. The good agreement with the results of self-consistent calculations provides further support to the notion that empirical tight-binding Hamiltonians can provide a meaningful description of the electronic structure of semiconductors, their surfaces and interfaces in the valence band region.

We would like to thank S. G. Louie, P. Maldague and A. R. Williams for valuable discussions.

References

1. A.G. Milnes and D.G. Feucht, *Heterojunctions and Metal-Semiconductor Junctions*, Academic Press, New York, 1972).
2. G.A. Baraff, J.A. Appelbaum, and D.F. Hamann, Phys. Rev. Lett 38, 237 (1977); J. Vac. Sci. Technol. 14, 999 (1977).
3. J.N. Schulman and T.C. McGill, Phys. Rev. Lett. 39, 1680 (1977).
4. W.E. Pickett, S.G. Louie, and M.C. Cohen, Phys. Rev. B. 17, 815 (1978).
5. G.F. Koster and J.C. Slater, Phys. Rev. 95, 1167 (1954).
6. J. Koutecky, Adv. in Chem. Phys. *9*, 85 (1965).
7. D. Kalkstein and P. Soven, Surf. Sci. 26, 85 (1971).
8. J. Pollmann and S.T. Pantelides, Phys. Rev. B, to be published.
9. D.J. Chadi, Phys. Rev. B. 16, 3572 (1977).
10. Such Hamiltonians provide a realistic description of the valence bands and have been successfully used to describe surfaces of semiconductors (see e.g. Ref. 11 and 8).
11. K.C. Pandey and J.C. Phillips, Phys. Rev. B. 13, 750 (1976).
12. An individual atom is removed by setting the on-site Hamiltonian matrix elements to infinity so that its interactions with all the atoms are effectively cancelled. See Refs. 8 and 13.
13. J. Bernholc and S.T. Pantelides, Phys. Rev. ***B 18*** Aug. 15 1978
14. The total perturbation matrix is 16 × 16 since four layers are involved; there is one atom in each layer unit cell and each atom has four orbitals.
15. The results for the Ge-ZnSe interfaces are qualitatively similar with those of the corresponding Ge-GaAs interfaces, but the effects of the interface are more pronounced. A discussion of all the results and details of the calculations will be given elsewhere (Ref.16)
16. J. Pollmann and S. T. Pantelides, to be published
17. The valence-band discontinuity was taken to be 0.9 eV as calculated in Ref. 2.

18. L. Esaki, W.E. Howard, and J. Heer, Surf. Sci. 2, 127 (1964).

19. For the Ge-As interface, electron counting reveals that all valence states and interface states within the valence band energy region (see Figs. 2b and 3b) are full and an excess of 0.5 electrons per two-dimensional unit cell would have to partially occupy an interface band in the conduction bands.

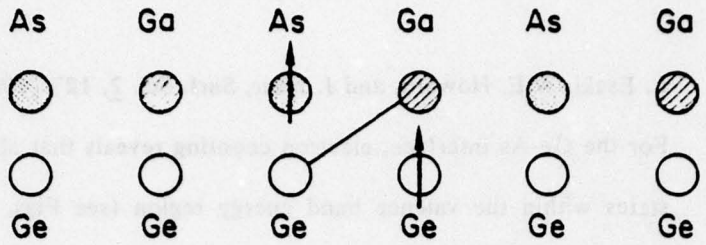

Fig. 1 Interface creation by a local perturbation. Each circle represents a two-dimensional plane of atoms. The perturbation consists of the "removal" of an As and a Ge plane (arrows) and the appropriate link between a Ge and a Ga plane as shown (solid line).

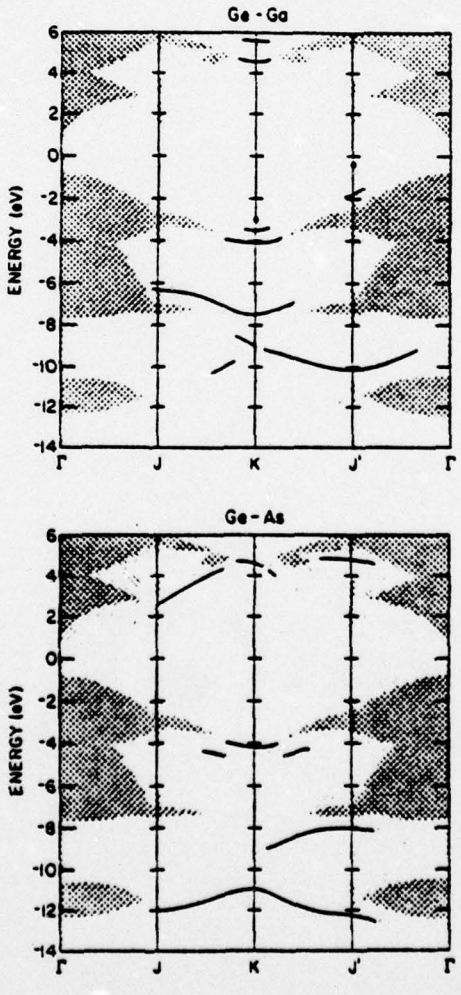

Fig. 2 Joint PBS and bound states for the two Ge-GaAs interfaces.

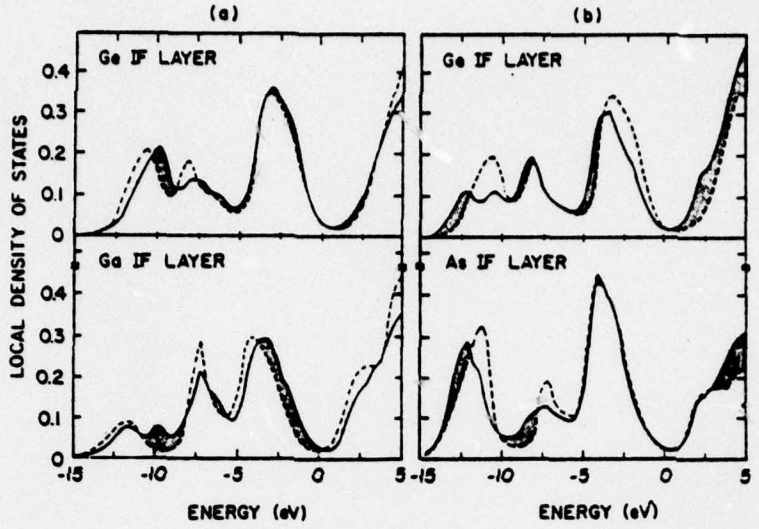

Fig. 3 q-integrated LDOS on the Ge, Ga and Ge, As layers next to the interfaces of Ge-GaAs in comparison with the LDOS on the corresponding bulk layers (dashed lines). The shaded areas show the excess density due to the interface.

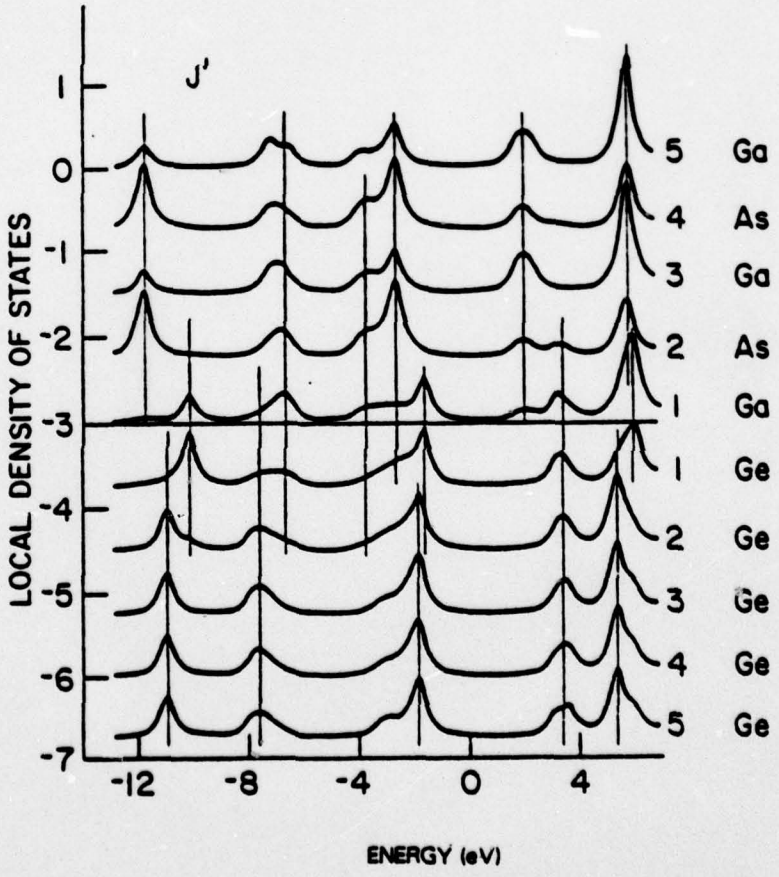

Fig. 4 LDOS on the first five layers on both sides of the interface (J' point).

Temperature and intensity dependence of rate of introduction of neutral traps in SiO_2 by e-beam irradiation*

J. A. Van Vechten, C. M. Serrano, and J. M. Aitken
IBM Thomas J. Watson Research Center
Yorktown Heights, New York 10598

Recent experiments have shown that uncharged electron traps are created in SiO_2 films during the course of irradiation with x-rays[1] and with electron-beams[2] at energies sufficiently low that Frenkel pair formation is excluded. These defects are in addition to the well known positively charged electron traps which are also introduced by irradiation. The neutral defects are not removed by the usual ~ 400 C anneals[2] which remove the positively charged defects. Because any electron traps that remain in the SiO_2 of the final device will aggravate hot-electron related threshold instabilities, and because many devices are exposed to ionizing radiation at some point in their fabrication (during e-beam or x-ray lithography, during reactive ion etching, RIE, etc.), it is important to understand the nature and origin of the trapping centers.

Here we report the dependence of the radiation induced neutral trap density upon e-beam intensity and upon sample temperature during irradiation. A model is proposed to account for these results.

The experiments were performed on 50 nm SiO_2 films grown on 0.2 Ω cm, p-type <100> substrates at 1000 C in dry O_2. 500 nm thick Al dots were rf evaporated through a shadow mask to form capacitor structures which were subsequently annealed at 400 C for 20 min. in forming gas. Individual capacitors were diced from the wafers, placed in the column of a JEOL 200 scanning transmission electron microscope, STEM, on a liquid N_2 cold stage. Samples were irradiated with ~ 6 nA of 50 KV electrons at both room temperature and at the temperature of the cold stage when filled with liquid N_2, which is about 90 K. (The same arrangement was used at both temperatures to insure that the exposure conditions were otherwise the same.) Exposure intensity was controlled by varying the diameter of the beam. The entire area of each sample was scanned and the total time the beam scanned the sample was the same for all intensities. Thus, the total dose given all samples was the same and all but the highest intensity samples were multiply scanned.

After irradiation, the samples were annealed in forming gas at 400 C for 30 min. This removed all the positively charged and some of the neutral centers that were introduced by the radiation. The remaining neutral traps were studied by injecting hot-electrons from the substrate into the oxide[1,2], where a small fraction were trapped at the defects. The resulting shift in flat-band voltage is proportional to the number of electrons trapped in the oxide. Fig. 1 shows total flat-band shift for samples irradiated at $1x10^3$ and at 0.1 W/cm^2 for 5 min. plus an unirradiated control sample plotted against the time that a constant d.c. current of 2×10^{-8} A is passed through the oxide. We see that the flat-band shift in the samples irradiated at the higher intensity is less for low temperature than for room temperature irradiation, that the shift in samples irradiated at room temperature is less for low intensity irradiation although the total dose is the same, and that for low temperature, low intensity irradiation, the shift is essentially the same as that in the unirradiated control. Analysis of the trapping cross sections of the trapping centers showed that the were two types of defect present in the oxide. One defect had a cross section of about 10^{-17} cm^2 and was not present in samples irradiated at 90 K. The other defect had a cross section of about 10^{-15} cm^2 and was not present in samples irradiated at intensities below 10 W/cm^2.

ECS Spring Mtg., Seattle, Wash., Electrochem. Soc. Extended Abstracts, Vol.78-1, p.331 (1978)

We propose the following explanation of these results. From the fact that the neutral defects in question do not anneal out we conclude that they are more stable configurations of the material than that in the as grown oxide. The energy of the incident radiation is much lower than the threshold required for direct lattice displacements. However, point defects (vacancies and impurities) may migrate by means of recombination enhanced diffusion[3], RED, during irradiation to form bound complexes. These processes are normally thermally activated but depend only on dosage and not on intensity. An intensity dependent mechanisim is required to explain the data in Fig. 1. Dislocations are known to exist in amorphous materials[4]. Misfit dislocations have been induced to glide in GaAlAs heterostructures by ionizing radiation[5]. This process has a sharp threshold[6] at about 10^5 W/cm^2. Such motion is reasonable in the present case since migration to the interface would remove the misfit strain due to the difference in thermal expansion coefficients between Si and SiO_2. Both types of process are required to explain the data in Fig. 1. We have no explanation for the apparent discrepancy with the results of EerNisse and Norris[7] who conclude interfacial strain is increased by irradiation.

*This work was supported in part by the Office of Naval Research under contract No. N00014-76-C-0934.

1. J. M. Aitken and D. R. Young, J. Appl. Phys. *47*, 1196 (1976).
2. J. M. Aitken, D. R. Young and K. Pan, J. Appl. Phys., to be published (1978).
3. D. V. Lang and L. C. Kimerling, Phys. Rev. Lett. *33*, 489 (1974).
4. J. J. Gilman, J. Appl. Phys. *44*, 675 (1973).
5. B. Monemar and G. R. Woolhouse, Appl. Phys. Lett. *29*, 605 (1976).
6 B. Monemar, R. M. Potemski, M. B. Small, J. A. Van Vechten, and G. R. Woolhouse, to be published.
7. E. P. EerNisse and C. B. Norris, J. Appl. Phys. *45*, 5196 (1974).

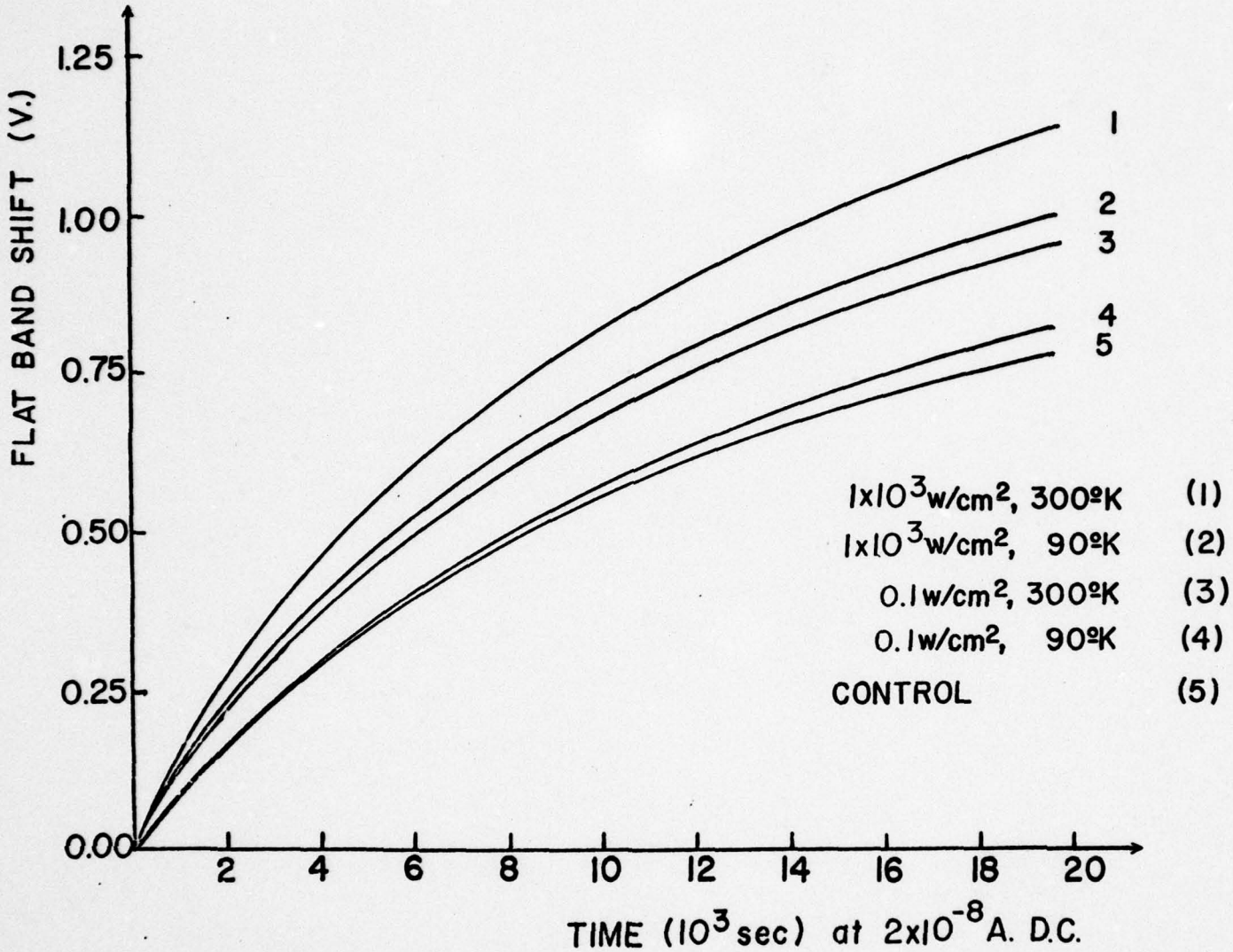
FLAT BAND SHIFT (V.)
1.25
1.00
0.75
0.50
0.25
0.00
2
4
6
8
10
12
14
16
18
20
TIME (10^3 sec) at 2×10^{-8} A. D.C.
1
2
3
4
5
1×10^3 w/cm^2, 300°K (1)
1×10^3 w/cm^2, 90°K (2)
0.1 w/cm^2, 300°K (3)
0.1 w/cm^2, 90°K (4)
CONTROL (5)

FIG. 1

Electronic States of Impurities Located at or near Semiconductor-Insulator Interfaces

Nunzio O. Lipari

IBM T.J. Watson Research Center

P.O. Box 218

Yorktown Heights, New York 10598

ABSTRACT

We solve the effective mass equations describing donor impurities localized at semiconductor-insulator interfaces using a method which involves an expansion of the impurity wavefunction in terms of spherical harmonics. We also investigate the behaviour of the impurity energies as a function of the donor distance from the interface both in the insulator and in the semiconductor. This allows, for the first time, the connection between surface and bulk donor properties. Results for the Si-SiO_2 case are presented.

J. Vac. Sci. Tech., in press
(Aug. 1978).

I. Introduction

A number of properties of MOS devices are strongly influenced by the presence of impurities at the semiconductor-oxide interfaces. Karpushin[1] and Bell et al[2] have investigated the behavior of donor localized at semiconductor surfaces without inversion layers. The effect of inversion layers was studied by Stern and Howard[3], but their numerical results are restricted to the two-dimensional limit. Very recently[4], Martin and Wallis have given a theoretical treatment of wavefunctions and binding energies of donors localized at semiconductor surfaces in inversion layers, using simple variational wavefunctions which are adequate only for extremely high electric fields. They show that the two-dimensional limit is approached only for unrealistically high electric fields.

The purpose of the present paper is twofold. First, to solve more accurately the same hamiltonian as that used by Martin and Wallis for all realistic values of the electric field in the inversion layer. Second, to extend the treatment to include the case of donors situated not just at the semiconductor-oxide interface but also near it, i.e. as a function of the donor distance from the interface both in the insulator and in the semiconductor.

In section II, we present the equation for the case of a donor impurity situated at the interface and define the basic approximations using in deriving it. The method of solution is also presented. In section III the case of donors situated near, and not just at, the interface is discussed and solved. Numerical results are presented in section IV and discussed with particular reference to the recent experimental data of Hartstein and Fowler[5].

II. Theoretical framework and method of solution.

We consider two contiguous, semi-infinite half spaces and assume that the potential energy of an electron undergoes a discontinuous jump as the electron passes from the semiconductor to the insulator. For the Si-SiO_2 case this discontinuity is about 3 eV[3]. Here we shall

assume that this discontinuity is infinite and that the electron wavefunction vanishes at the boundary. The effect of this approximation on the binding energy has been shown to be negligible[6]. In the region of the inversion layer there is an electric field present which is in general a complicated function of the distance from the interface. We shall assume the electric field to be constant, which has been shown to be a good approximation[3]. For simplicity, we assume the <100> orientation for Si (for Ge it would be the <111>) even though the present method could be applied to any other orientation. For this situation, Karpushin[1] has shown that the lowest lying bound states are primarily derived from the energy ellipsoids whose major axis are perpendicular to the interface. Therefore only these ellipsoids will be considered here. We also neglect intervalley interaction between the two ellipsoids perpendicular to the surface. With the above assumptions the Hamiltonian for an impurity of charge e can be written as

$$H = -\left(\frac{\partial^2}{\partial x^2} + \frac{\partial^2}{\partial y^2} \right) - \gamma \frac{\partial^2}{\partial z^2} + \frac{\delta}{z} + aEz + U(\vec{r}) \tag{1}$$

where

$$\gamma = \frac{m_t}{m_\ell} \tag{2a}$$

$$\delta = \frac{\epsilon_2 - \epsilon_1}{4\,\epsilon_1} \tag{2b}$$

$$a = \frac{\epsilon_1 + \epsilon_2}{4 m_t^2 e^5} \tag{2c}$$

where E is the external electric field, m_t and m_ℓ are the transverse and longitudinal effective masses, respectively; ϵ_1 and ϵ_2 are the dielectric constants of the insulator and semiconductor respectively, as illustrated in figure 1a. Equation (1) has been written using as unit of energy and length, respectively, the following quantities

$$R_y = \frac{2m_t e^4}{(\varepsilon_1+\varepsilon_2)^2} \tag{3a}$$

$$a_o = \frac{\varepsilon_1+\varepsilon_2}{2m_t e^2} \tag{3b}$$

Finally, the potential energy $U(\vec{r})$ is approximated by

$$U(\vec{r}) = -\frac{2}{r} \tag{4}$$

i.e. the screening of the impurity ion potential by the electrons in the inversion layer is neglected. Hamiltonian (1) is exactly the same hamiltonian as that considered by Martin and Wallis[4].

To solve equation (1), we note that, in the absence of the electric field, the image potential and the anisotropy (i.e. $\gamma = 1$), Levine[7] has shown that a state cannot exist unless $\ell+m$ is an odd integer, with the ground state being the $2p_o$ level, in the usual hydrogen atom nomenclature. When the anisotropy, the image potential and the electric field are switched on ℓ is no longer a good quantum number but m still is. Therefore, one can write the solution of (1) as

$$\psi_m(\vec{r}) = \sum_i f_i(r)\, Y_{\ell_i m}(\theta,\varphi) \tag{5}$$

where the angles $0 \le \theta \le \pi/2$ and $0 \le \varphi \le 2\pi$. As a result of the angle θ varing only in half space, the spherical harmonics obey different orthogonality rules[8]. In particular, spherical harmonics with different m are still orthogonal, but those with different ℓ are orthogonal only if $\ell-\ell'$ is even. The matrix elements of all operators appearing in (1) in the basic function (5) can be calculated analytically, and they will be given elsewhere[8]. As a result, one is left with a system of radial differential equations, whose order is given by the number of terms in expression (5). This system can be solved by using the following expansion

$$f_i(r) = \sum_j C_{ij} e^{-\alpha_j r} \tag{6}$$

This allows one to transform the problem from that of solving a system of differential equations to that of diagonalizing a secular matrix. The size of the secular determinant is given by the product of the number of terms (N) in expansion (5) times the number of terms (M) in (6). The convergence of the results with respect to the number of these terms and the choice of the parameters α_i is discussed in section IV.

In order to calculate binding energies[4], we must also solve Hamiltonian (1) in the absence of an impurity potential. As shown by Martin and Wallis[4], it is sufficient to solve the Hamiltonian.

$$H_o = -\gamma \frac{\partial^2}{\partial z^2} + \frac{\delta}{z} + aEz \tag{7}$$

This one-dimensional Hamiltonian can be solved very accurately by using an expansion of the type (6), i.e., by assuming

$$\psi(z) = \sum_j C_j e^{-\alpha_j z} \tag{8}$$

and diagonalizing the corresponding secular matrix, as discussed in section IV. The binding energies are therefore given by

$$E_b = E(H_o) - E(H) \tag{9}$$

III. Impurity located near the interface.

In the previous section we have considered the situation in which the impurity is located exactly at the interface. We now consider the situation in which the impurity is located either in the semiconductor or the oxide (fig. 1b). In the first case, the potential experienced by the electron is given by

$$V_1(r) = \frac{\epsilon_1+\epsilon_2}{\epsilon_2}\,\frac{1}{r_1} - \frac{\epsilon_1-\epsilon_2}{\epsilon_2}\,\frac{1}{r_2} \tag{10}$$

where

$$r_1 = \sqrt{x^2+y^2+(d-z)^2} \tag{11a}$$

$$r_2 = \sqrt{x^2+y^2+(d+z)^2} \tag{11b}$$

d being the distance of the donor ion from the interface. In the second case, i.e. when the donor is located in the oxide,

$$V_2(r) = -\frac{2}{r_2} \tag{12}$$

In order to calculate the matrix elements of (10) and (12) in the basis (5) we use the well known expression

$$\frac{1}{|\vec{r}-\vec{d}|} = \sum_{\ell=0}^{\infty} \frac{r_<^{\ell}}{r_>^{\ell+1}}\, P_\ell(\cos\gamma) \tag{13}$$

where $r_<$ ($r_>$) is the smaller (large) of $|\vec{r}|$ and $|\vec{d}|$, and γ is the angle between $\vec{r}$ and $\vec{d}$. Since d is chosen along the z axis, we can write

$$\frac{1}{r_1} = \frac{1}{|\vec{r}-\vec{d}|} = \sum_{\ell=0}^{\infty} \frac{r_<^{\ell}}{r_>^{\ell+1}} P_\ell(\cos\theta) \tag{14}$$

$$\frac{1}{r_2} = \frac{1}{|\vec{r}+\vec{d}|} = \sum_{\ell=0}^{\infty} (-1)^{\ell} \frac{r_<^{\ell}}{r_>^{\ell+1}} P_\ell(\cos\theta) \tag{15}$$

The matrix elements of (14) and (15) in the basis states (5) can be also calculated analytically[8]. In actual calculations the number of terms in (14) and (15) is kept finite and the convergence of the results with respect to the number of terms is discussed in the next section.

IV. Numerical results and discussions

All the calculations reported here are for the case of the Si-SiO_2 interface using the parameters given by Stern and Howard[3]. We first address the problem of convergence of the calculated binding energies as a function of the basis functions in (6). All the results reported here are for the ground state but the analysis can be extended in a straightforward manner to treat other excited states as well. The exponents α_j should in principle be treated as variational parameters. In practice, however, as we have previously seen[9], the α_i can be fixed and not considered as variational parameters if one chooses a sufficiently large number of terms in (6) and if the α_i's are selected in a sensible way. We have seen that it suffices 1) to include 15 terms in (6), and 2) to choose the largest and the smallest α_i to be 50 and 0.05 respectively, with the rest of them in geometrical progression, to insure a convergence in the eigenvalues to better than 1 part in 10^4. The next question regards how many terms should be included in (5). This number obviously should increase with the strength of the electric field. In table I we show the contribution of the various terms in expression (5) for fields up to 10^4 esu, which corresponds to 3×10^6 volt/cm. Since 10^3 esu corresponds to the physically highest achievable fields, we see that usually less than 5 terms provide very accurate solutions. Also Hamiltonian (7) can be solved very accurately using 15 terms in expansion (8). In fig. 2 we compare our

results with the previous results of Martin and Wallis and we see that our analysis is more accurate and that the two methods agrees for very large values of the electric field. In figure 3 we illustrate the individual effect of the anisotropy, and of the image potential on the binding energy. We see that, for small and intermediate fields, all these effects are important, whereas, as shown by Martin and Wallis, the binding energy tends always to 4 in the limit of infinitely large electric fields, which corresponds to the two-dimensional limit. In fig. 4 we plot the mean radius for the ground state as a function of the electric field.

We now discuss the case in which the donor ion is not located at the interface but near it. In fig. 5 we plot the binding energy of the ground state as a function of the distance of the impurity ion from the interface in the absence of the electric field. In the case in which the donor moves in the semiconductor, the binding energy increases and reaches a value which corresponds to the bulk donor binding energy for the ground state. It is important to note that the value of ~.7 is in units of the Rydberg (3a) appropriate for the interface while for the bulk one would define a Rydberg in terms of ϵ_2 only; this means that, in terms of the bulk effective rydberg, one has for the binding energy the value ~1.6 which is in exact correspondence to the value calculated using bulk analysis[10]. From fig. 5a we see also that the bulk value is reached after 2 effective radii (i.e. after about 40 Å), and that for distances from the interface larger than that the binding energy does not change since the radius for the ground state is smaller than the distance of the donor ion from the interface. In fig. 5b we show the dependence of the binding energy of the ground state as a function of the impurity distance from the interface in the oxide. We see that the binding energy decreases as the distance increases, as expected.

We now briefly compare our theoretical results with the experimental findings of Hartstein and Fowler[5], who have measured the conductivity of n-channel silicon MOSFET devices in which Na^+ ions were diffused through the oxide to the semiconductor-oxide interface. The temperature dependence of the peak conductivity can be described by an activation energy which Hartstein and Fowler identify as the binding energy of an impurity band. By varying

the substrate bias Hartstein and Fowler were able to study the activation energy as a function of the electric field. For electric fields of 19.9 esu and 60.4 esu they found activation energies of 18 meV and 25 meV respectively. In fig. 6 we show the calculated binding energy as a function of the electric field for the cases in which the impurity ion is at the interface and at .2 a.u (~4 Å) in the oxide. We see that the observed binding energies agree much better with the case in which the impurity ion is located not exactly at the interface but very close to it. It is, however, important to note that the present model neglects important effects as discussed in the beginning of section II. Therefore one should take the result, presented in fig. 6, as only a qualitative indication rather than quantitative determination of distance of the impurity ion from the interface. Fig. 6 shows that the solution is sensitive to the distance of the donor ion from the interface.

In conclusion, we have presented a method which provides accurate binding energies of donors located at semiconductor-insulator interfaces for any value of the anisotropy and of the electric field. We found that the binding energy depends strongly on the distance of the impurity from the interface. Clearly, one should now improve the theoretical model before an accurate description of the experimental data is attempted. In particular, the screening of the impurity ion potential due to the electrons in the inversion layer has to be included. Furthermore, intervalley coupling has to be considered and a better model for the interface should be used. This aspect is currently under investigation.

Acknowledgments

The author would like to thank Dr. F. Stern for very helpful discussions.

References

1. A.A. Karpushin, Fiz. Tverd. Tela 11, 2163 (1969) (Soviet Physics - Solid State 11, 1748 (1970)).

2. R.J. Bell, W.T. Bousman, Jr., G.M. Goldman, and D.G. Rathbun, Surf. Sci. 1, 293 (1967).

3. F. Stern and W.E. Howard, Phys. Rev. 163, 816 (1967).

4. B.G. Martin and R.F. Wallis, Phys. Rev. to be published.

5. A. Hartstein and A.B. Fowler, in Proceeding of the 13th International Conference on the Physics of Semiconductors, Rome, 1976, p. 741.

6. J. Laur and T.S. Jayadevarah, Solid State Electronics, 16, 644 (1973).

7. J.D. Levine, Phys. Rev. 140, A586 (1965).

8. To be published.

9. N.O. Lipari and M. Altarelli, Phys. Rev. B15, 4883 (1977).

10. J. Pollmann, Solid State Commun. 19, 361 (1976).

Table I

Contribution of various terms in the expansion (5) given in text for different values of the electric field E. Only the ℓ = odd terms contribute tot he ground state. Contributions are given in percent.

E \ ℓ	1	3	5	1	9	11	13	15
0	91.2	8.3	.5					
1	91.1	8.4	.5					
10	90.3	9.1	.6					
10^2	85.2	13.1	1.5	.2				
10^3	70.7	21.9	5.5	1.4	.4	.1		
10^4	50.7	20.5	12.5	5.2	2.1	.8	.3	.1

Figure Captions

Fig. 1. Schematic structure of semiconductor insulator structure. In fig. (1a) the impurity ion is located at the surface z=0. In fig. (1b) the impurity ion is located in the semiconductor (1) or in the oxide (2), at a distance d from the interface. The coordinate axes are also shown.

Fig. 2. Binding energy for the ground state as a function of the electric field for the Si-SiO_2 case. Comparison with the results of Martin and Wallis, ref. 4 in text, is shown.

Fig. 3. Impurity ground state binding energy as a function of the electric field for the Si-SiO_2 case. The effects of the image potential and of the conduction band anisotropy are illustrated.

Fig. 4. Effective radius for the impurity ground state as a function of the electric field. The symbols are the same as in fig. 3.

Fig. 5. Impurity ground state binding energy as a function of the impurity ion from the interface. Fig. (5a) show, the case in which the donor ion is located in the semiconductor, while fig. (5b) represents the case in which the donor ion is located in the insulator. The numerical values correspond to the Si-SiO_2 situation.

Fig. 6. Impurity ground state binding energy as a function of the electric field for two values of the distance of the impurity ion from the interface. The first value (d=0) corresponds to the impurity ion located at the interface; the value d=0.2 eff. units corresponds to the impurity ion located in the oxide.

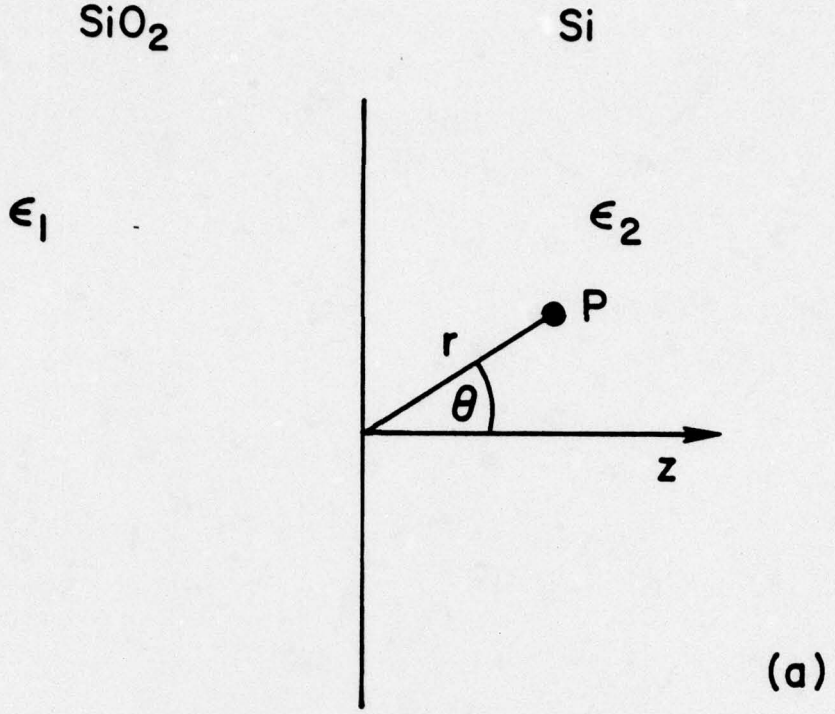
SiO_2
Si
ϵ_1
ϵ_2
P
r
θ
z

(a)

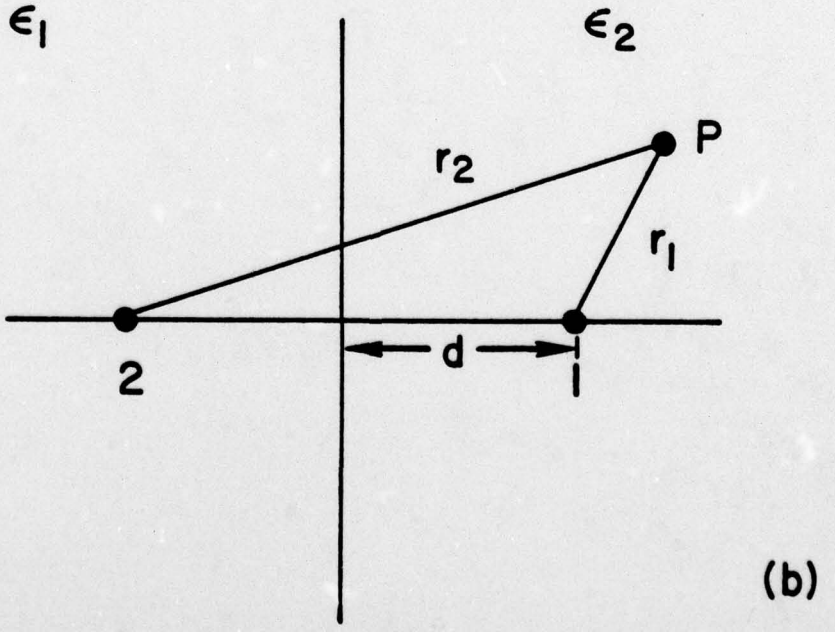
ϵ_1
ϵ_2
P
r_2
r_1
2
d
1

(b)

Fig 1

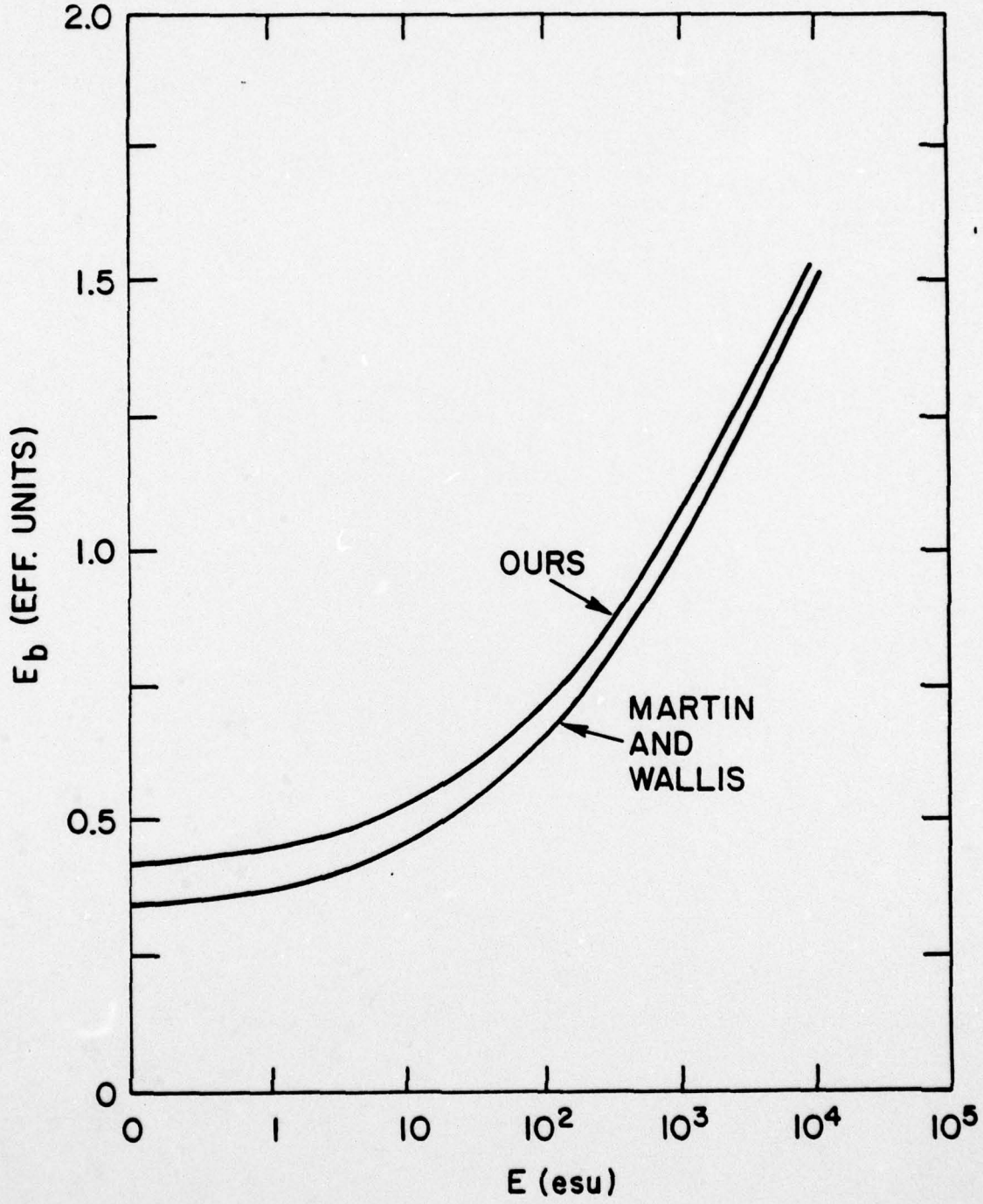
2.0
1.5
1.0
0.5
0
E_b (EFF. UNITS)
OURS
MARTIN
AND
WALLIS
0
1
10
10^2
10^3
10^4
10^5
E (esu)

Fig. 2

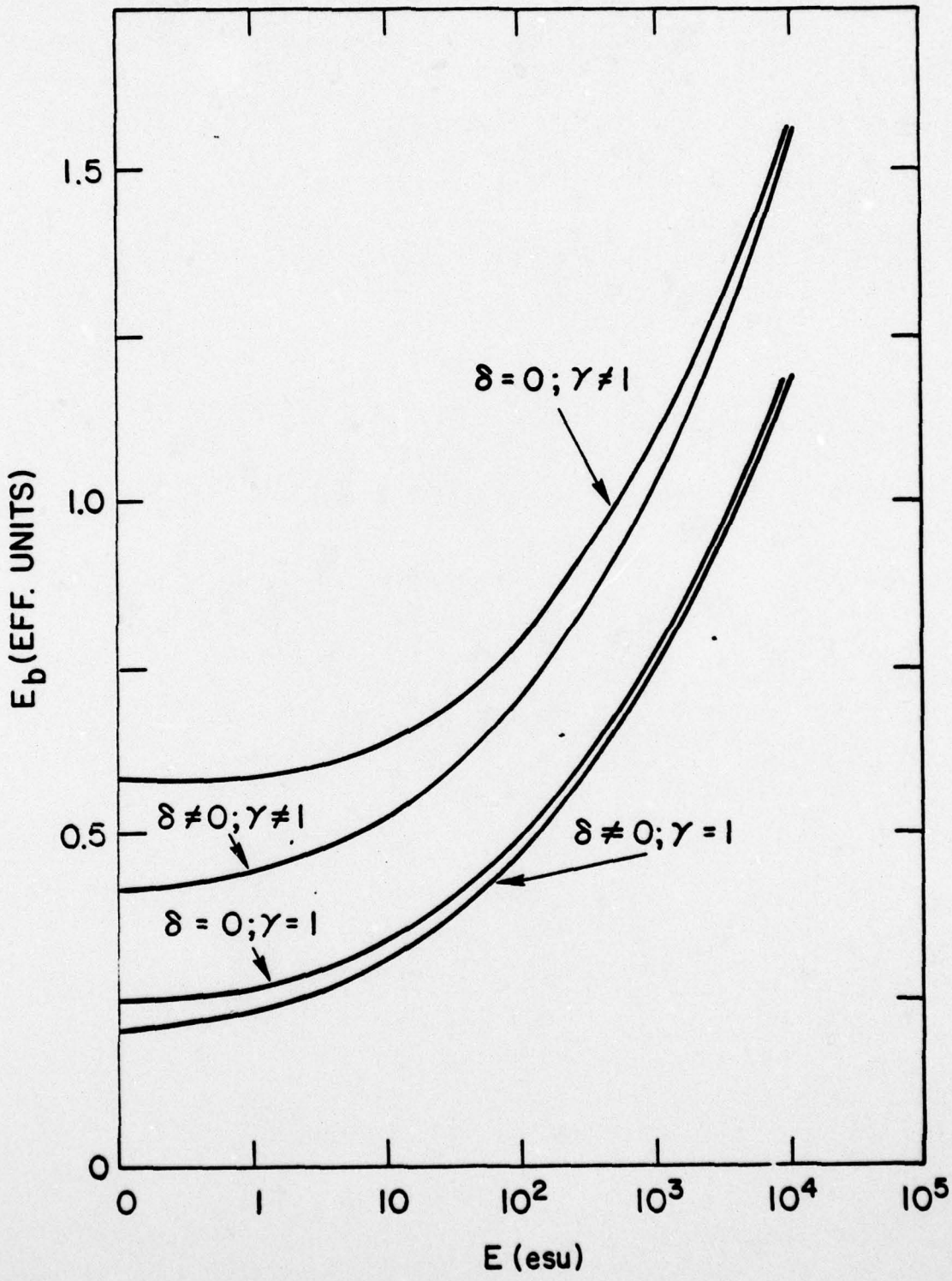
1.5
1.0
0.5
0
E_b(EFF. UNITS)
$\delta = 0; \gamma \neq 1$
$\delta \neq 0; \gamma \neq 1$
$\delta \neq 0; \gamma = 1$
$\delta = 0; \gamma = 1$
0
1
10
10^2
10^3
10^4
10^5
E (esu)

Fig 3

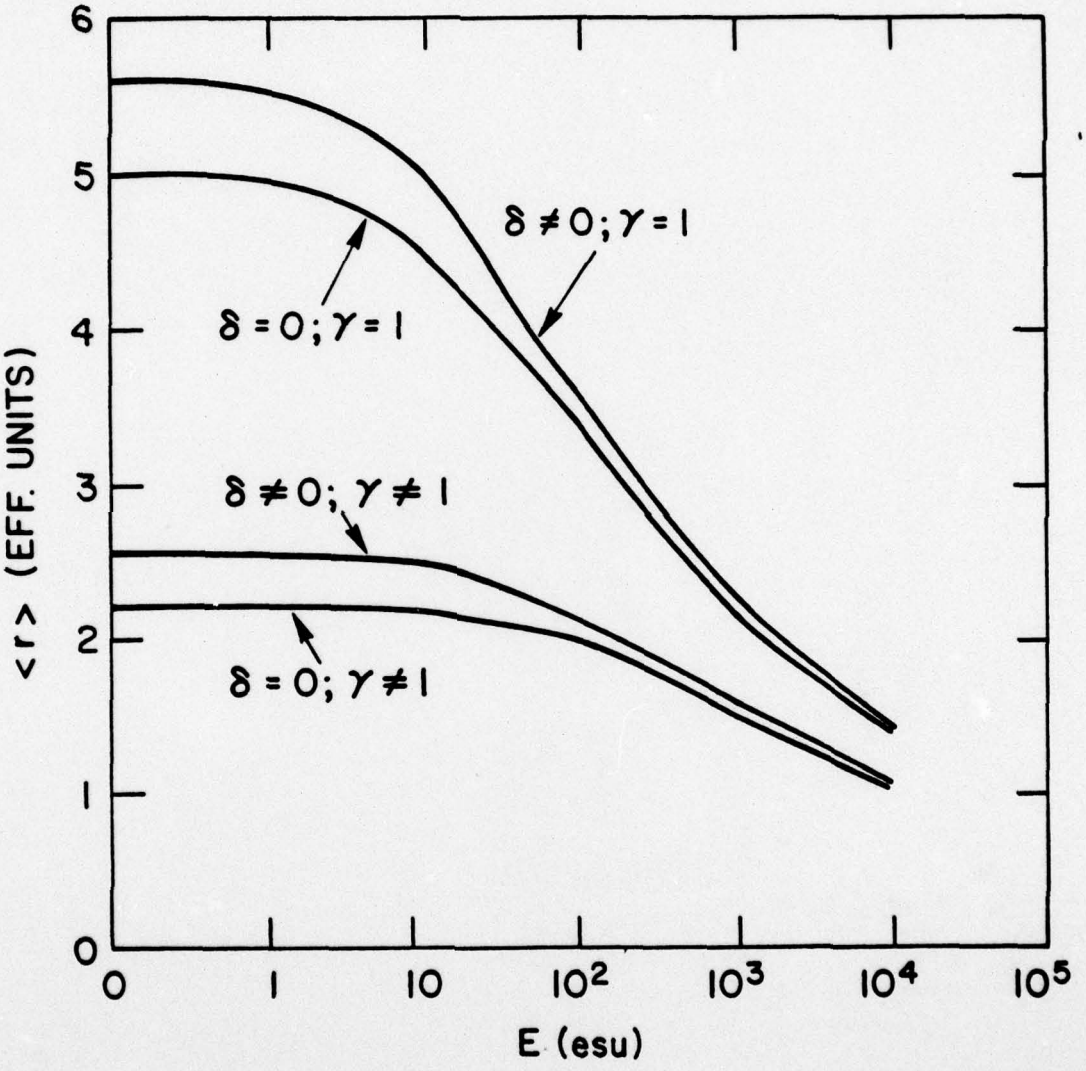
6
5
4
3
2
1
0
<r> (EFF. UNITS)
δ ≠ 0; γ = 1
δ = 0; γ = 1
δ ≠ 0; γ ≠ 1
δ = 0; γ ≠ 1
0
1
10
10²
10³
10⁴
10⁵
E (esu)

Fig 4

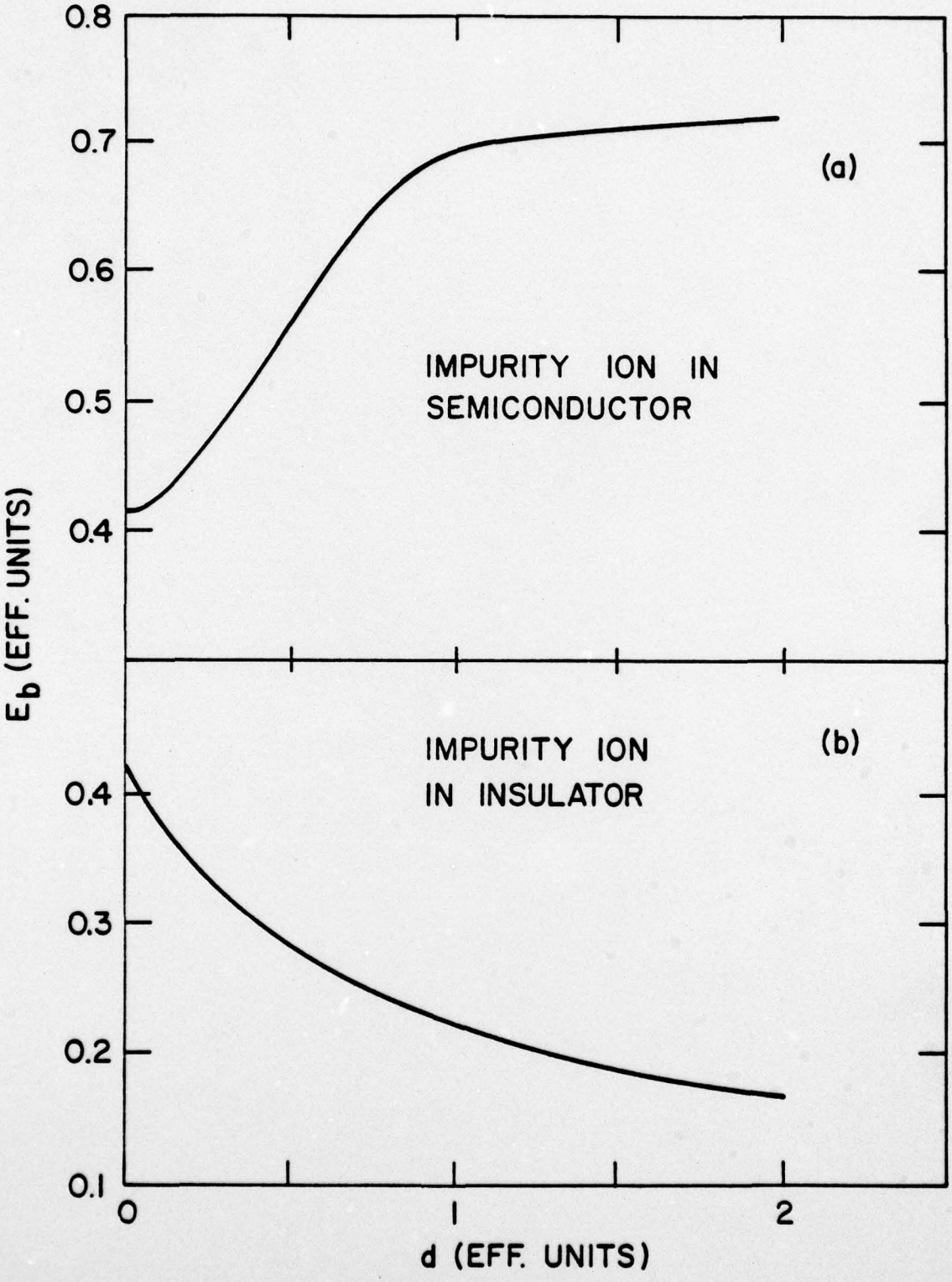
0.8
0.7
0.6
0.5
0.4
(a)
IMPURITY ION IN
SEMICONDUCTOR
E_b (EFF. UNITS)
IMPURITY ION
IN INSULATOR
(b)
0.4
0.3
0.2
0.1
0
1
2
d (EFF. UNITS)

Fig 5

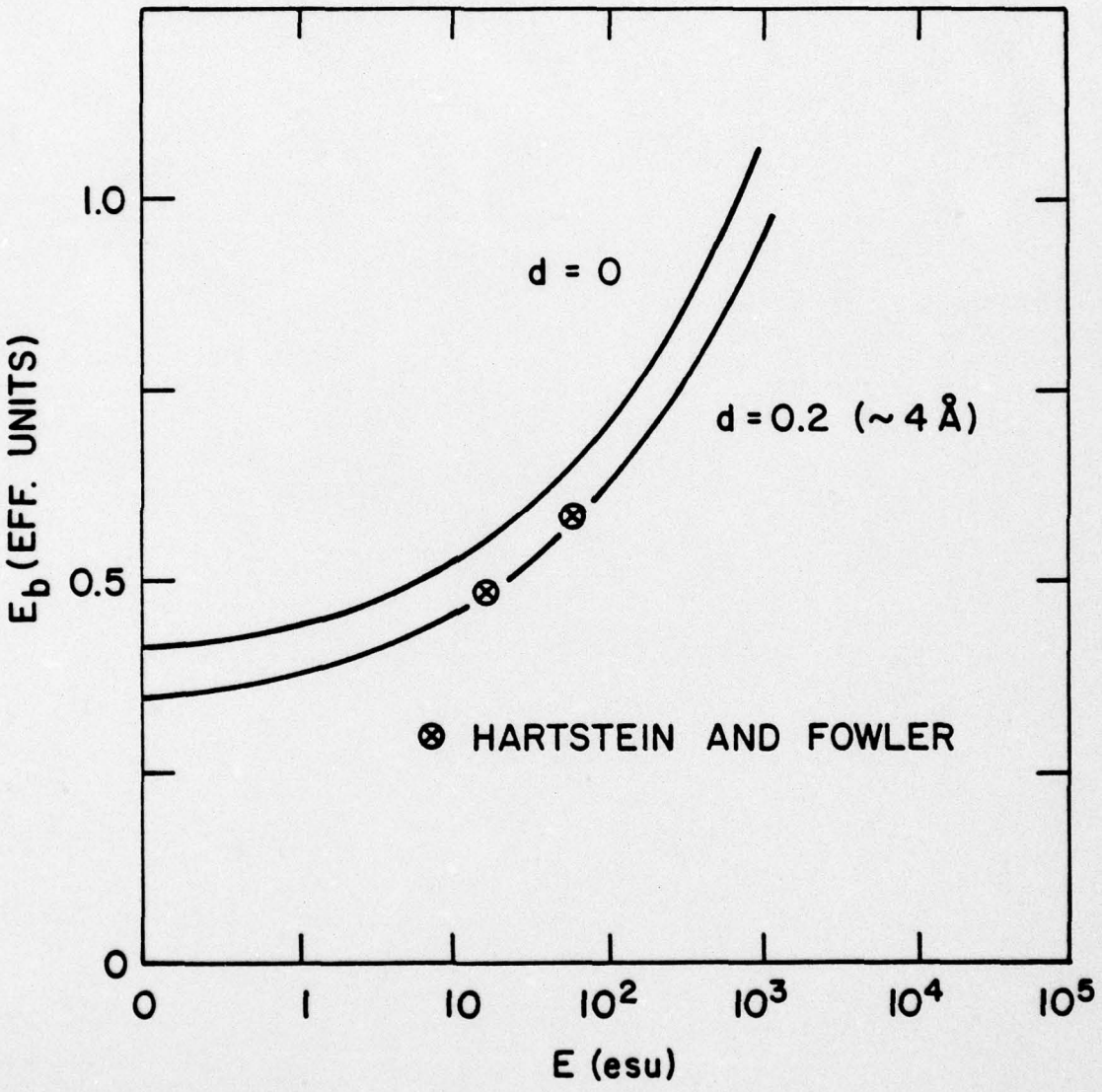
1.0
0.5
0
E_b (EFF. UNITS)
d = 0
d = 0.2 (~ 4 Å)
⊗ HARTSTEIN AND FOWLER
0
1
10
10^2
10^3
10^4
10^5
E (esu)

Fig 6